博士論文

Research on robust control for fusion core plasmas (核融合炉心プラズマのロバスト制御に関する研究)

三善　悠矢
新領域創成科学研究科
先端エネルギー工学専攻

Contents

List of Figures

List of Tables

Chapter 1

Introduction

1.1 Introduction

1.1.1 The nuclear fusion reaction

Recently, many new energy research have been developed in the world. The energy which generates large electricity and doesn't have environmental influence (e.g. doesn't emit CO_2) has been expected. In particular, the development of the alternative energy to the nuclear fission reactor has become urgently wanted because of Fukushima accident. Nuclear fusion reactor is one of such energy. It makes electricity from the nuclear fusion reaction. The fuel of the nuclear fusion reactor can be obtained from water, and the reactor doesn't emit CO_2 and high level radioactive waste. The research has been done in all over the world to realize the nuclear fusion reactor. The typical nuclear fusion reaction are shown from eq. (1.1) to eq. (1.4) [1–3].

$$D + D \rightarrow T(1.01MeV) + p(3.03MeV) \tag{1.1}$$

$$D + D \rightarrow He^3(0.82MeV) + n(2.45MeV) \tag{1.2}$$

$$D + T \rightarrow He^4(3.52MeV) + n(14.06MeV) \tag{1.3}$$

$$D + He^3 \rightarrow He^4(3.67MeV) + p(14.67MeV) \tag{1.4}$$

In this article, DT reaction (eq. (1.3)) is discussed. To construct the commercial reactor, these reactions have to be occurred with high efficiency. The nuclear fusion fuel (i.e. D, T) should become plasma state to make high efficient reaction. J. D. LAWSON established the criterion about the nuclear fusion reactor [4], and the equation (1.5) shows the necessary condition of the fusion core plasma [1],

$$n\tau_e > \frac{12\kappa T}{\eta Q_{NF} < \sigma v >}, \tag{1.5}$$

where n, T, and τ_e are the plasma density, temperature, and confinement time respectively, and η, Q_{NF} and $< \sigma v >$ show the efficient of external heating and the power generation, the fusion power, and the reaction ratio respectively, and κ is Boltzmann constant. Equation (1.5) shows that to get the high efficient nuclear fusion power, high plasma density and the temperature is needed. The dependence of the fusion cross section σ on the kinetic energy and the dependence of the fusion ratio $< \sigma v >$ on the ion temperature are shown in Fig. 1.1 [1, 5–7].

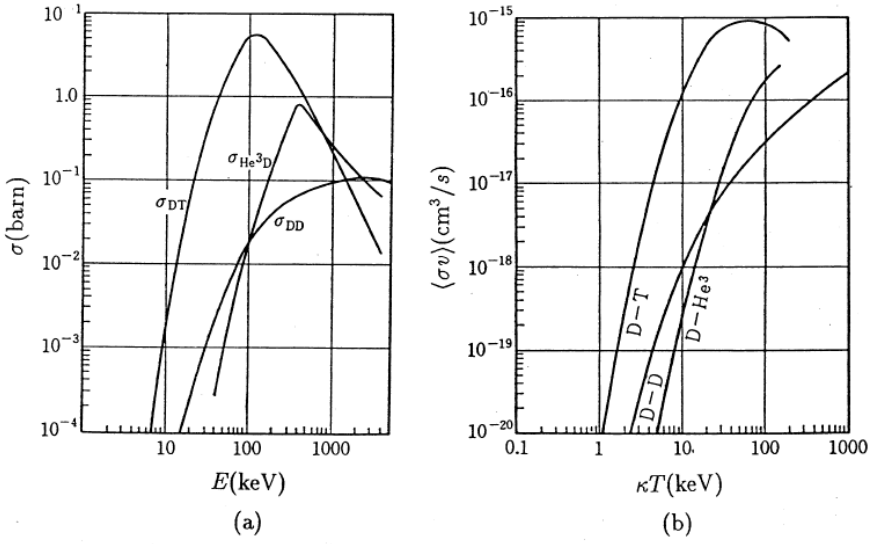

Figure 1.1: (a) The dependence of the fusion cross section on the kinetic energy of the colliding nucleous (b) The dependence of the fusion ratio on the ion temperature [1, 5–7]

In nuclear fusion reactor, the D-T plasma is assuming to be used because of its high reaction ratio, and because D and T can be obtained from the water easily.

1.1.2 The concept of the tokamak fusion reactor

Figure1.2 shows the typical tokamak reactor ITER [8], and the cross section of the tokamak reactor.

The plasma is the aggregate of the charged particles (i.e. electron and ion), thus, each particle moves circle orbit around the magnetic line. Because of this characteristic, the plasma can be trapped with magnetic line. In tokamak reactor, the magnetic line is generated from the TF (Toloidal Field)

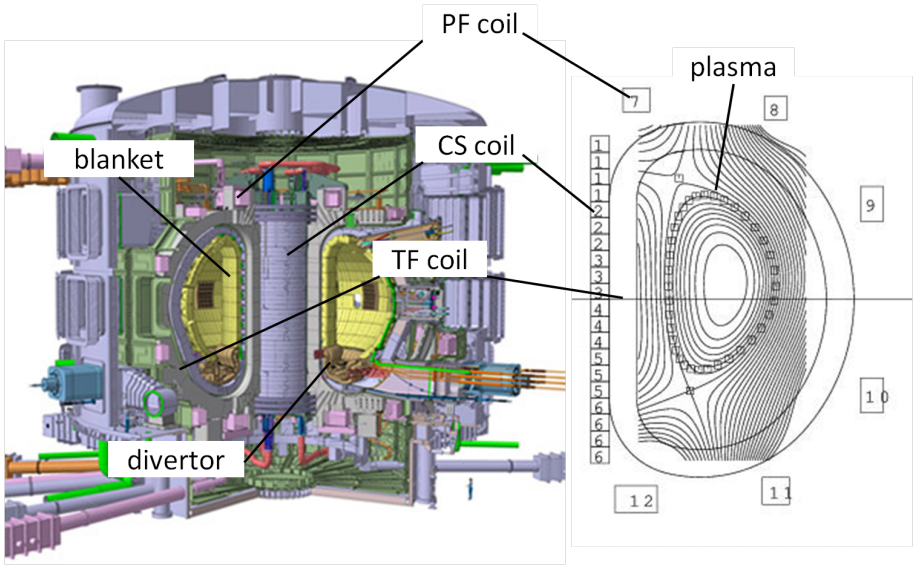

Figure 1.2: ITER [8] and the cross section of the tokamak

coils and the PF (Poloidal Field) coils and the plasma current induced from the CS (Central Solenoid) coil. The plasma is trapped in the center of the reactor, and the fast neutrons is generated from the fusion reaction in the plasma. The kinetic energy of the neutrons are changed to the heat energy in the blanket, and from this heat energy, the electricity is generated.

1.2 Recent fusion research

The beginning of the fusion reactor research is not clear and said to be 1940's. The preliminary study are introduced in ref [9–11]. The tokamak reactor is the mainstream method of the nuclear fusion reactor. The word 'tokamak' is from the Russian words 'Toroidalnaya Kamera and Magnitnaya Katushka', and it means the toroidal chamber and the magnetic coil. ITER is 6m size tokamak experiment machine and it is under construction in France [8, 12]. It is expected to make the 500MW fusion power with the condition that $Q \simeq 10$. Q represents the ratio of the fusion power to the external input power. ITER is also expected to link to the design, and the operation of the Demo or Commercial reactors.

1.2.1 Reactor design

It is quite important to know the relationship between the physical or the engineering parameters and the reactor performance to design the future reactors. The study about this with the simulation code is called reactor design. The simulation codes of the reactor design are classified broadly into two groups. First is called system code, and it calculates the roughly reactor parameter set which satisfy the constraint condition in the plasma physics, reactor engineering and cost. Second is called detailed analysis code, and it calculates the strictly parameter set in each subject. From these reactor design studies, the Demo or the Commercial reactor is designed. In this subsection, the summary of the reactor design is shown [13].

The system code

The system code is used to find the self-consistent design points of the fusion reactor. FUSAC [14–16] is one of the typical system code in Japan. This code has three parts, i.e. the plasma physics part, the engineering part and the cost part. The plasma physics part calculates the plasma parameters including the fusion power based on the ref. [17]. From these parameters, the engineering part calculates the parameters of the TF coils, CS coils, blanket, backing cylinder and so on. Finally, the cost analysis is done in the cost part. The calculation flow is shown in Fig. 1.3.

The engineering design parameters are calculated as the radial build. The radial build represents the size and the location of each component on the radial direction shown as fig 1.4. CREST [18] is designed from the FUSAC analysis. As the similar work, the ARIES team make the their own reactor design with their system code [19], Slim-CS [20] is designed at JAEA and so on.

Coil design

In the tokamak reactor, there are three main coils (CS, TF, PF), and the parameters about the coils should be determined. The size of the CS coil is important factor to determine the reactor size. As written in previous section, CS coil induces the plasma current, but, the NBI or the RF also drive the current. Thus, the size of the CS coil is determined from the ratio of the induced plasma current. Additionally, CS coil is used to keep the plasma equilibrium with the PF coils. The CS coil size have to be designed from these conditions. VECTOR [21] has no CS coil and is designed as quite small size tokamak reactor. The size and the location of the TF coils are determined from the necessary toroidal magnetic field and the strength of

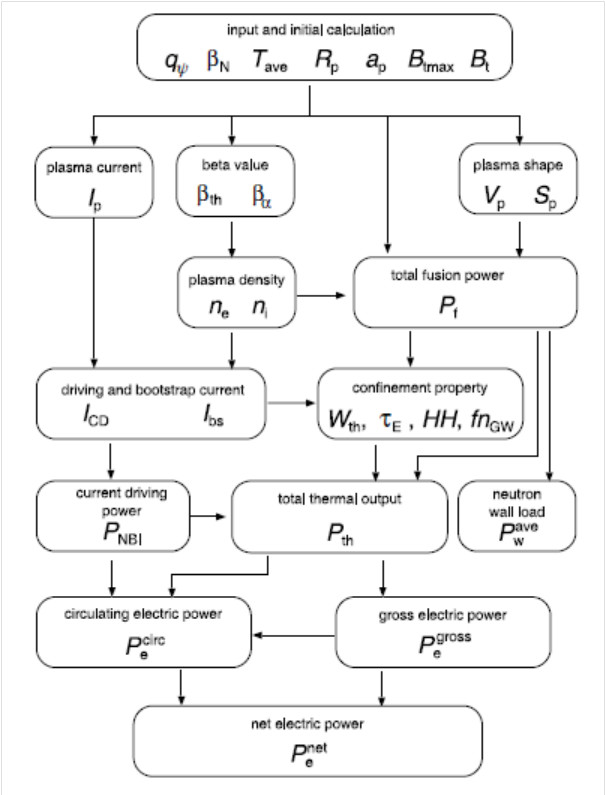

Figure 1.3: The calculation flow of FUSAC [14]

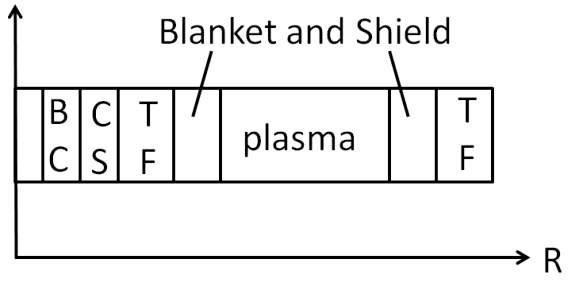

Figure 1.4: The example of the radial build

the TF coil. Considering the TF current, the hoop force, the centripetal force and the inversion force are exerted on the TF coils. SCONE code [22] is the detail analysis code of the TF coil. This code calculates the maximum magnetic field which the coil can generate from the shape of the TF coil with considering the strength of the coil and the condition of the superconducting. The location and the size of the PF coil is determined from the equilibrium analysis. TOSCA [23] code is one of the equilibrium analysis codes. This code solves the Grad-Shafranov equation from the input data, and calculates the necessary PF coil current. Using this code, the optimum position and the size of the PF coils can be determined. In ref. [24], the auto positioning of the PF coils are tried with the integration of the system code and the equilibrium analysis code.

Blanket design

To design the blanket, the following conditions have to be considered,

- it has to withstand the high heat and neutron flux
- it has to breed the enough tritium
- it has to withstand the electromagnetic force
- it has to be attached and detached easily in the maintenance

The first step of the blanket design is to determine the ratio of the breeding, the cooling and the constructional material. After that, the detailed design of the blanket is done. In Slim-CS, the blanket is designed as the separated module form for the easy maintenance.

Divertor design

The divertor have to be designed to withstand the quite high heat flux. In the case of ITER, the fusion power is 500MW and the heat flux of the divertor is $10MW/m^2$, and in the case of the demo or the commercial reactor, it will be higher. Thus, several design concept of the divertor have been researched [25–27].

Integrated design code

In ref. [28], the concept of the integrated design code, which is the integration of the system code and the detailed analysis code is introduced, and in ref. [24], the example of the integration, i.e. the integration of the equilibrium

code and the system code is demonstrated. Using this integrated design code, more detailed and broad parameter surveys may become possible.

1.2.2 The necessity of the control research

To operate the Demo and Commercial reactors, not only the reactor design research but also the research about the plasma control is important issue, and the two big problems have to be considered to control the future plasma. First, the future plasma is MIMO (Multi-Input Multi-Output) system. For example, to keep the electricity supply, the fusion power have to be controlled, or to keep the plasma stability, the plasma current or current profile have to be controlled, and many other parameters should be under controlled to operate the fusion reactor. Additionally, the actuators are not one-to-one correspondence to the controlled parameters, e.g. the typical actuator NBI has the effect to both the fusion power and the plasma current.

Second, because of high heat and neutron flux, the actuators and the diagnostics which can be installed will be limited. To address these problems, what parameters have to be controlled, and what actuators or diagnostics can be installed have to be discussed and determined. The reactor design research is expected to contribute to this discussion. From this discussion, the controller should be designed and in reverse, constraint conditions from the point of view of control engineering will also contribute to this discussion. Figure 1.5 shows the concept of these issues.

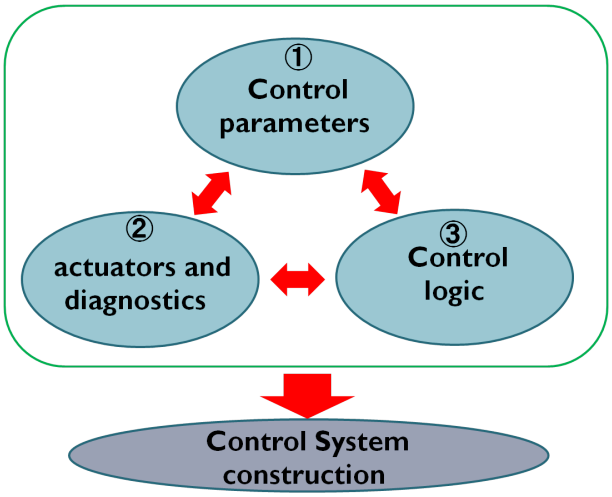

Figure 1.5: The factors of the reactor controller design research [29]

The issue 1 and the issue 2, has been discussed but the conclusion has

not been made and it will vary with the design concept [30–35]. Because of this, the construction of the controller design method that has the broad utility (i.e. the method which can deal flexibly with the control parameters, actuators and diagnostics) will be needed.

1.3 Plasma control research

In this section, the review of some typical previous control researches is shown.

1.3.1 SISO control with classical control theory

In JT-60U, burn control simulation experiments have been done [36, 37]. In the future reactor, D-T reaction will be used, and the alpha particles generated from D-T reaction which have 20 percent of the total fusion power heat the plasma. In this experiment, D-D plasma is used and to simulate the alpha heating in the burning plasma, NB is injected with proportional to the neutron generation ratio from the D-D reaction. With this plasma, the burning plasma control has been simulated. This scheme is shown in Fig. 1.6, and this figure is referred from Fig.1 of ref. [36].

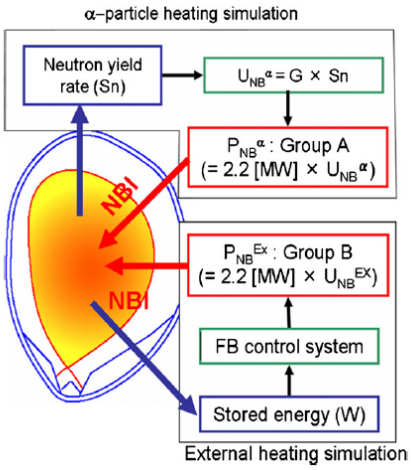

Figure 1.6: Schematic drawing for a burning plasma simulation scheme in JT-60U [36].

The feedback control scheme is applied to the ELMy H-mode plasma (I_p=1.0MA, B_t=2.1T, and q_{95}=4.1) and the reversed shear plasma with the

internal transport barrier (I_p=1.0MA, B_t=3.7T and q_{95}=6.8). In both plasmas, the total stored energy W is controlled by the NBI, and the controller is PD control. The proportional gain and the differential gain are determined from the response characteristics. With this controller, the stored energy is well controlled in both cases.
The PID controller and the method to determine the PID gains from the response characteristics of the system are the quite broadly used in the world. These method can be categorized as classical control theory, and it is for SISO (Single-Input Single-Output) system. Thus, it is not clear that the classical control theory is suitable to the future reactor which is MIMO system.

1.3.2 MIMO control with classical control theory

In JT-60U, the MIMO control (2 inputs and 2 outputs) experiment is also demonstrated by Dr. suzuki [38,39]. For the plasma instability, safety factor profile control is quite important, and from this point of view, minimum safety factor q_{min} is controlled in this experiment. Additionally, the ion temperature gradient (ITG) which has the large effect to the ion transport barrier and plasma confinement is also controlled in this experiment. These 2 parameters are controlled by the NBI and the LHCD. The LHCD is off-axis and it can control q_{min} efficiently, but it has less effect on the plasma heating and the ITG in this experiment. On the other hand, NBI is on-axis perpendicular and it can heat the plasma efficiently and control the ITG, but it has little effect in current drive. Thus, the q_{min} is controlled by LHCD and the ITG is controlled by NBI simultaneously in this experiment. In this case, LHCD is PI controller and the NBI is PID controller, and the gains are determined from the response characteristics of the q_{min} and ITG respectively. These control systems are applied to the ELMy H-mode plasma (I_p=0.8MA, B_t=2.2T, and q_{95}=5.2). In this experiment, the ITG follows the reference value and the q_{min} also follows the reference value with little undershoot. This result is shown in Fig. 1.7, and this figure is referred from Fig. 2 of ref. [38].

In this experiment, MIMO control is demonstrated with classical control theory. Dr. Suzuki suggests that in this case, the actuators are not strongly coupled and the controller which is designed without considering the coupling effect worked fine, and he also suggest that for the future reactor, the controller for the plasma with considering the coupling effect should be designed.

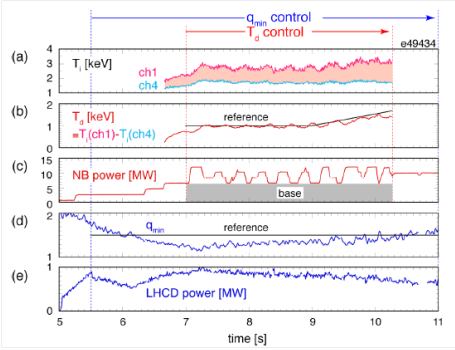

Figure 1.7: Waveforms of discharge for simultaneous real-time control of Td (t=7-10.3 s) and qmin (t=5.5-11 s). (a) Ion temperature at two channels (ch1: r/a 0.3, ch4: r/a 0.57) used by real-time control. Ti measurement was terminated at t 10.3 s due to the stop of diagnostic NB due to interlock on temperature of NB facing tiles. (b) Difference of ion temperature Td (hatched in Fig. 2(a)) and its reference value (Td,ref). (c) total NB heating power controlling Td. Hatched part of the total NB power is the fixed base component. (d) qmin and its reference value (qmin,ref = 1.5). (e) LHCD power controlling qmin [38].

1.3.3 Model based current profile control

Dr. Moreau did the current profile control experiment in JET [42, 43] with the model based controller design method. In this research, 5 points safety factor profile is controlled by the NBI, LHCD and ICRH, this is the 3 inputs 5 outputs MIMO system. In this research, the relationship between the current density profile and the each actuator's deposition is written as the integral equation form, and the controller is designed from the equation. This equation is the function of the time and the radius. In this research, the equation is changed to the function of the time with the singular value decomposition (SVD), and the basis function decomposition. Using these methods, the relationship between the inputs (NBI, LHCD and ICRH) and the outputs (safety factor at each point) can be written. In this experiment, the number of output parameters is larger than that of input parameters. Thus, it is impossible to control all output parameters to any reference values. In this case, the controller is designed to minimize the mean square integral of the error between the reference values and the outputs values. Finally, with this criterion and the relationship of the parameters, the controller is designed as the PI controller. The PI gain is formed 3×5 matrix. With this controller, the safety factor profile is well controlled in this experiment.

The results are shown in Figs. 1.8 and 1.9 [42], and these figures are referred from Figs. 6 and 7 of ref. [42].

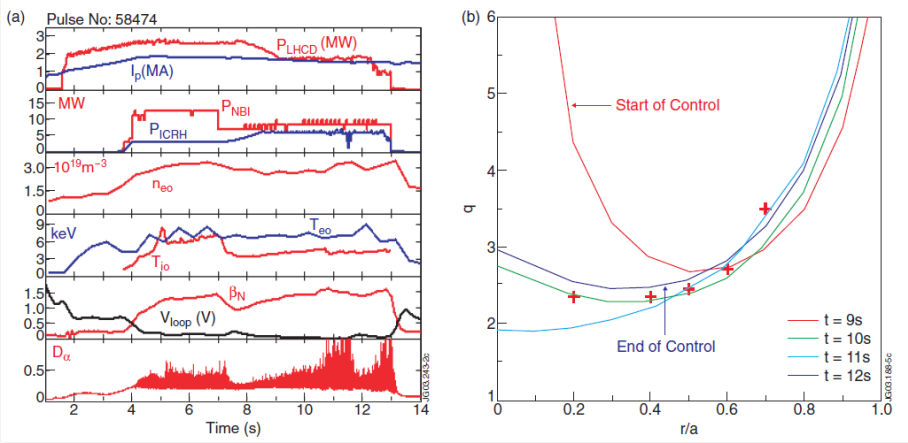

Figure 1.8: (a) Time evolution of the plasma current, Ip, coupled lower hybrid power, PLHCD, ICRH power, PICRH, NBI power, PNBI, central electron density, ne0, and temperature, Te0, central ion temperature, Ti0, surface loop voltage, Vloop, normalized β, β N, and D α emission (pulse #58474, BT = 3 T). (b) Real-time control of the q-profile using LHCD, NBI, and ICRH (pulse #58474, BT = 3T, Ip = 1.8/1.5 MA). The profile is shown at four different times between 7 and 12 s. Pluses represent the five q-set points at r/a = [0.2 0.4 0.5 0.6 0.7] [42].

The current profile control research with other approach is also done in ref. [40,41]. In the future reactor, however, the current profile will not be able to be measured because of the limitation of the diagnostics. Thus, it can be considered that these method can't be applied to the future reactor directly. For this reason, the simulation code which can estimate the unmeasurable parameters will be needed.

1.3.4 The plasma position control with robust control theory

In ref. [44], the plasma position control in TCV is simulated with the robust control theory. The robust control theory is one of the model based control method. The difference between the real system and the physical model of the system is called model error in the robust control theory. In the robust control theory, the effect of the model error is treated as the disturbance

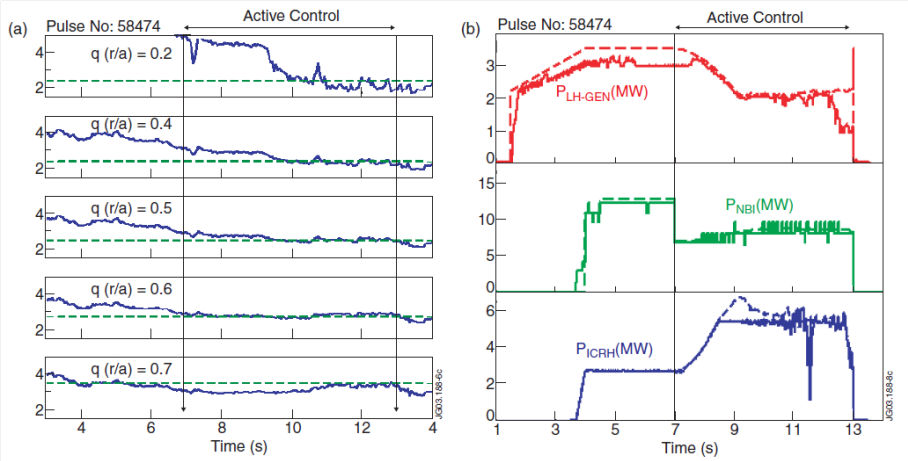

Figure 1.9: (a) Time evolution of the safety factor at the five radii selected for the real-time control experiment of figure 6 (pulse #58474, BT = 3T, Ip = 1.8/1.5 MA). The set point values are indicated with dotted lines. (b) Time evolution of the requested (dotted traces) and delivered (full traces) LHCD, NBI, and ICRH powers during the real-time control experiment of figure 6 (pulse #58474, BT = 3T, Ip = 1.8/1.5 MA). Note that the LHCD request is applied on the generator power, contrary to NBI and ICRH [42].

and the controller is designed to minimize the effect. In this simulation, H-infinity theory which evaluates the effect of the model error as H-infinity norm is used. The detail of the H-infinity theory is shown in chapter 4.
In the model to design the controller, the plasma is assumed as the aggregate of the circular ring current. From this assumption, the equation of motion of the plasma and the PF coils is derived. This equation of motion is changed to the time differential equation form which represents the relationship between the input parameters and the output parameters. The controller is designed from this differential equation, and in this case, the output parameters are plasma current, plasma vertical position, plasma radial position, the outboard field curvature and the inboard field curvature, and the input parameters are plasma current in the 18 PF coils. The typical cross section of the TCV plasma is shown in Fig. 1.10, and this figure is referred from Fig.4 of ref. [44].

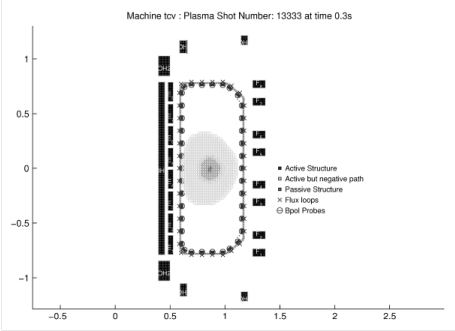

Figure 1.10: TCV equilibrium 13 333 [44].

This is 18 inputs and 5 outputs MIMO system. The controller is tested in the simple simulation code which model is same to the model used to design the controller. After this test simulation, the controller is applied to the nonlinear tokamak simulation code, which can represent the TCV plasma. In this simulation, each parameter can be controlled to the reference value. The controller is designed from the simple model, but the controller can control the parameters in the non-linear tokamak simulation code. This results shows the robust performance of the controller.
In ref. [45], the J-TEXT plasma vertical position control simulation is done and the controller is designed with the μ synthesis theory. The detail of the μ synthesis is shown later. In this simulation, the vertical position is controlled by one vertical field coil. This is SISO system. In this research, the robust controller shows the higher disturbance suppression performance than the traditional PID controller.

1.3.5 Other control researches

In this section, some typical control researched are introduced. Other than those above, in ref. [46, 47, 49], the burning plasma control simulation with the 0-D model is done. In ref. [46], the helical burning plasma control at the unstable operation point simulation is demonstrated, and the controller is designed from the physical model. in ref. [47], the controller is designed with H2 control theory [48] which is one of the robust control theory. In the H2 control theory, the effect of the model error is evaluated as H2 norm. In ref. [49], non-liner stabilizing theory is used.

1.4 The purpose of this research

The controller design from the response characteristics is quite familiar method for the SISO system, but for the MIMO system with the coupling effect, it is not clear that this method is suitable or not. Thus, for the future reactor, the controller concept shown in Fig. 1.11 is suggested in this research.

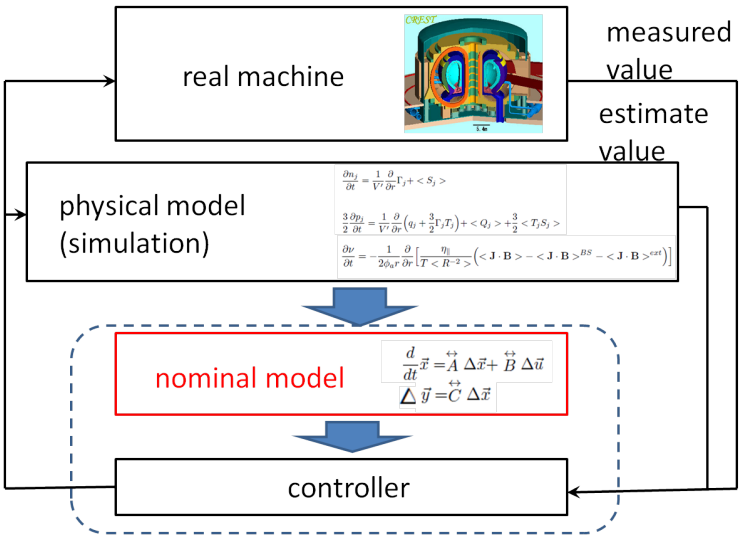

Figure 1.11: The concept of the future reactor controller

Figure 1.11 suggests that in the future reactor, the simulator is used to estimate the unmeasurable parameters (e.g. current profile or safety factor profile), and the controller is designed from the physical model.

In previous researches, the used controller design method is for each experimental machine or situation. In this research, the novelty exists in the

point that the the constructed method can design the controller according to the situation.

In this research, to make the controller design method, the modern control theory and the robust control theory is applied to the fusion reactor, and the method is benchmarked with the plasma control simulation. The modern or the robust control theory is the part of the control engineering theory, and in these theory, the controller is designed from the physical model.

In chapter 1, the review of the tokamak reactor , the control engineering and the previous research are shown. Chapter 2 shows the control simulation of 1 dimensional code. Chapter 3 demonstrates the model based controller design and the MIMO plasma PID control simulation. Chapter 4 shows the example of the robust controller design and the simulation, and shows the comparison of this robust H-infinity controller and the MIMO PID controller. In chapter 5, the concept of plasma profile control and the simulation is shown. Summary and discussion is shown in chapter 6.
There are some nuclear fusion reactor concepts. In this research, Unless otherwise specifically noted, tokamak fusion reactor is discussed.

1.5 The review of the control engineering

In this research, modern control theory and the robust control theory is used. In this section, the review of these control theories and the position of these in control engineering are shown [50–52].

1.5.1 Stability

The control theory is said to be made by J. C. Maxwell [53]. In ref. [53], the motion if the controlled object is expressed into a linear differential equation, and the stability of the system is discussed. In the case that the answer of following differential equation is closer to 0 independently of an initial state, the system is defined asymptotically stable,

$$\frac{d^n y}{dt^n} + a_1 \frac{d^{n-1} y}{dt^{n-1}} + \cdots + a_n y = 0 \tag{1.6}$$

The condition that the system is stable, is shown by Rauth and Hurwitz [54, 55]. Lyapunov also researched about the stability [56]. Equation (1.6) can be written as follows,

$$\dot{\mathbf{x}} = \mathbf{A}\mathbf{x} \tag{1.7}$$

$$\mathbf{x} = \begin{pmatrix} y \\ y' \\ \vdots \\ y^{n-1} \end{pmatrix} \tag{1.8}$$

$$\mathbf{A} = \begin{pmatrix} 0 & 1 & 0 & \cdots & 0 \\ 0 & 0 & 1 & \cdots & 0 \\ \vdots & \vdots & \vdots & \vdots & \vdots \\ -a_n & -a_{n-1} & -a_{n-2} & \cdots & -a_1 \end{pmatrix} \tag{1.9}$$

The condition that the system is stable is that all real part of the eigenvalues of $\mathbf{A}$ is negative. These stable theories are the foundation of the control theory.

1.5.2 Classical control theory

Nyquist and Bode made the base of the classical control theory [57, 58]. In this subsection, some important concept in the classical control theory are introduced.

Transfer function

Defining the output of the system is $y(t)$ and the input is $u(t)$, the general linear system model can be written as follows,

$$\frac{d^n y}{dt^n} + a_1 \frac{d^{n-1} y}{dt^{n-1}} + \cdots + a_n y = \frac{d^m u}{dt^m} + b_1 \frac{d^{m-1} u}{dt^{m-1}} + \cdots + b_m u \tag{1.10}$$

In classical control theory, equation (1.10) is Laplace transformed and expressed as follows (assuming all initial states are 0),

$$(s^n + a_1 s^{n-1} + \cdots + a_n) Y(s) = (s^m + b_1 s^{m-1} + \cdots + b_m) U(s) \tag{1.11}$$

$$G(s) = \frac{Y(s)}{U(s)} = \frac{s^m + b_1 s^{m-1} + \cdots + b_m}{s^n + a_1 s^{n-1} + \cdots + a_n} \tag{1.12}$$

where, $Y(s)$ and $U(s)$ are the Laplace transformation of $y(t)$ and $u(t)$ respectively and $G(s)$ is called transfer function of the system. In the case that $n > m$, the system is called proper. Here, Laplace transformation is defined as follows,

$$Y(s) = \int_0^\infty y(t) e^{-st} dt \tag{1.13}$$

Block diagram

Considering the system expressed as $G(s)$ and the following feed back control,

$$U(s) = K(s)Y(s) \tag{1.14}$$

the total feed back system can be expressed as Fig 1.12.

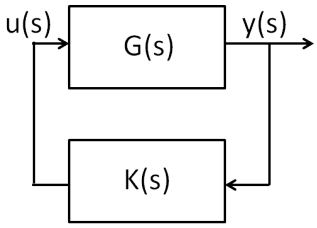

Figure 1.12: The example of the block diagram

This expression is called block diagram. Using the block diagram and the transfer function, the control system can be expressed quite simple form.

Frequency response

In the case that the system is stable and proper, the transfer function can be changed with partial fraction decomposition as follows,

$$\begin{aligned} G(s) &= \frac{s^m + b_1 s^{m-1} + \cdots + b_{m-1}s + b_m}{s^n + a_1 s^{n-1} + \cdots + a_{n-1}s + a_n} \\ &= \frac{(s-z_1)(s-z_2)\cdots(s-z_m)}{(s-p_1)(s-p_2)\cdots(s-p_n)} \\ &= \frac{c_1}{s-p_1} + \frac{c_2}{s-p_2} + \cdots + \frac{c_n}{s-p_n} \end{aligned} \tag{1.15}$$

Considering the sin wave input $X(s) = \mathcal{L}[A\sin(\omega t)] = \frac{A\omega}{s^2+\omega^2}$, the output can be written as follows,

$$\begin{aligned} Y(s) &= G(s) \times A\frac{\omega}{s^2+\omega^2} \\ &= \frac{d_1}{s-p_1} + \cdots + \frac{d_m}{s-p_m} + \frac{k_1}{s-i\omega} + \frac{k_2}{s+i\omega} \end{aligned} \tag{1.16}$$

Here, multiplying the the product of the denominators $(s-p_1)\cdots(s-p_m)(s^2+\omega^2)$, and substituting $s = i\omega, -i\omega$, k_1 and k_2 can be lead as follows,

$$k_1 = \frac{G(i\omega)A}{2i} \tag{1.17}$$

$$k_2 = \frac{G(-i\omega)A}{-2i} \tag{1.18}$$

With the inverse Laplace transformation, the output signal $y(t)$ can be written as follows,

$$y(t) = \mathcal{L}^{-1}[Y(s)] = \sum_{i=1}^{m} d_i e^{p_i t} + k_1 e^{i\omega t} + k_2 e^{-i\omega t} \tag{1.19}$$

Here, $G(s)$ is stable and the first term of the equation is closer to 0. Thus, at the steady state, $y(t)$ can be written as follows,

$$y(t) = k_1 e^{i\omega t} + k_2 e^{-i\omega t} \tag{1.20}$$

Substituting the following expression,

$$G(i\omega) = |G(i\omega)|e^{-i\phi}, \quad G(-i\omega) = |G(i\omega)|e^{i\phi} \tag{1.21}$$

finally, $y(t)$ can be written as follows,

$$\begin{aligned} y(t) &= |G(i\omega)|A\left[\frac{e^{i(\omega t-\phi)}}{2i} - \frac{e^{-i(\omega t-\phi)}}{2i}\right] \\ &= |G(i\omega)|A\sin(\omega t - \phi) \end{aligned} \tag{1.22}$$

This means that the amplitude of the output signal is $|G(i\omega)|$ times of the input signal, and the phase shifts by the argument of $|G(i\omega)|$.

Bode diagram

The frequency response of the linear system is the function of ω, and $|G(i\omega)|$ is called gain, and $arg|G(i\omega)|$ is called phase. The graph representing $20log_{10}|G(i\omega)|[dB]$ and $arg|G(i\omega)|[degree]$on the vertical axis and ω on the horizontal axis is called Bode diagram. The Bode diagram is quite useful to understand the system characteristics. Figure 1.13 shows the example of the bode diagram.

This figure is the bode diagram of the following transfer function,

$$G(s) = \frac{1}{s+1} \tag{1.23}$$

PID control theory

The idea of PID theory is born by Minorsky [59], and Callender made the demo machine [60]. Ziegler and Nichols suggested the method to adjust the PID controller [61]. PID controllers are widely used and its use rate is over

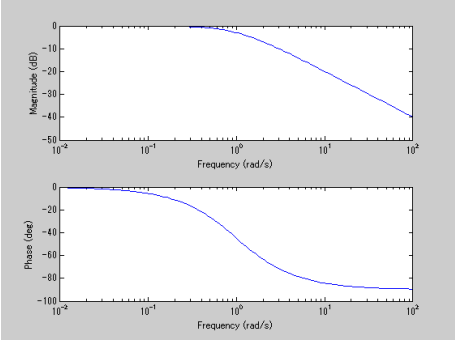

Figure 1.13: The example of the bode diagram

90 percent [62]. PID means proportional, integral and differential, and the PID controller is formed as follows,

$$\begin{aligned} u(t) &= K_p e(t) + K_i \int_0^t e(\tau)d\tau + K_d \frac{d}{dt} e(t) \\ &= K_p \left(e(t) + \frac{1}{T_i} \int_0^t e(\tau)d\tau + T_d \frac{d}{dt} e(t) \right) \end{aligned} \tag{1.24}$$

where, $e(t)$ is the difference between the controlled value and the reference value, K_p, K_i and K_d are called proportional gain, integral gain and differential gain respectively, and T_i and T_d are called integral time and differential time respectively. The PID controller is extremely practical. Using the Ziegler-Nichols' Ultimate Gain method or Ziegler-Nichols' Process Reaction Curve method [61], the PID gain can be adjusted from the response characteristics without the physical model of the system.

Ultimate Gain method

The ultimate gain method is done with the following steps [50, 61, 63]

- Set the system under the P control, with small gain
- Increase the P gain until the output starts oscillating
- Define the P gain at that time as K_c and the oscillating period as T_c
- Adjust the PID gain as table 1.1

Table 1.1: PID gain definition in the ultimate gain method [63]

Controller	P gain	Integration time	Differential time
P	$0.5K_c$	0	0
PI	$0.45K_c$	$0.833T_c$	0
PID	$0.6K_c$	$0.5T_c$	$0.125T_c$

Process Reaction Curve method

In the process reaction curve method, the step response of the system is used [50, 61, 63]. The step response is the output when the input is step signal. The step signal is defined as follows,

$$u(t) = \begin{cases} 0 & (t < t_c) \\ u_c & (t \geq t_c) \end{cases} \tag{1.25}$$

where, u_c and t_c is constant. In most cases, the step output is formed as Fig. 1.14.

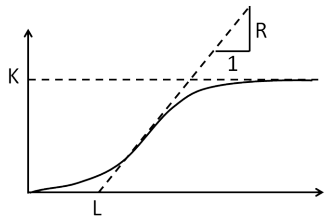

Figure 1.14: The example of the step response

With the parameters L and R, the PID gains are defined as table 1.2

Table 1.2: PID gain definition in the process reaction curve method [63]

Controller	K_pRL	T_i/L	T_d/L
P	1	0	0
PI	0.9	3.33	0
PID	1.2	2	0.5

1.5.3 Modern control theory

With the classical control theory, it is difficult to control the Multi-Input Multi-output system. The modern control system is mainly for the MIMO

system, and it is started from Kalman [64]. In classical control theory, the physical model is used and it is formed as transfer function. In modern control theory, however, they are considered in not frequency region but time region as eq. (1.26) and eq. (1.27),

$$\frac{d}{dt}\mathbf{x} = \mathbf{F}(\mathbf{x}, \mathbf{u}) \tag{1.26}$$

$$\mathbf{y} = \mathbf{G}(\mathbf{x}, \mathbf{u}) \tag{1.27}$$

they are called 'state equation' and $\mathbf{x}, \mathbf{u} and \mathbf{y}$ are called state vector, actuator vector, and output vector respectively. They are written in general form, and in usual, they are linearized and written as the form of eq. (1.28) and eq. (1.29)

$$\frac{d}{dt}\mathbf{x} = \mathbf{A}\mathbf{x} + \mathbf{B}\mathbf{u} \tag{1.28}$$

$$\mathbf{y} = \mathbf{C}\mathbf{x} + \mathbf{D}\mathbf{u} \tag{1.29}$$

the equation (1.28) and equation (1.29) are called LTI (Linear Time Independent) state equation. Using this state equation, the control problem can be dealt as the linear algebra problem.

The answer of the LTI state equation

From the following state equation (the order of $\mathbf{x}$ is n),

$$\frac{d}{dt}\mathbf{x}(t) = \mathbf{A}\mathbf{x}(t) + \mathbf{B}\mathbf{u}(t) \tag{1.30}$$

the answer of this differential equation when $\mathbf{u}(t) = 0$ can be written as follows,

$$\mathbf{x}(t) = e^{\mathbf{A}t}\mathbf{C_0} \tag{1.31}$$

where, $\mathbf{C_0}$ is the n th order vector corresponding to the integral constant, and $e^{\mathbf{A}t}$ is called transition matrix $(n \times n)$. The transition matrix is defined as follows,

$$e^{\mathbf{A}t} = \mathbf{I} + \mathbf{A}\frac{t}{1!} + \mathbf{A}^2\frac{t^2}{2!} + \cdots \mathbf{A}^n\frac{t^n}{n!}\cdots \tag{1.32}$$

$$\frac{d}{dt}e^{\mathbf{A}t} = \mathbf{A}e^{\mathbf{A}t} \tag{1.33}$$

$$e^{\mathbf{A}(t_1+t_2)} = e^{\mathbf{A}t_1}e^{\mathbf{A}t_2} \tag{1.34}$$

$$(e^{\mathbf{A}t})^{-1} = e^{-\mathbf{A}t} \tag{1.35}$$

Assuming that $\mathbf{C_0}$ is the function of time, the equation can written as follows,

$$\begin{aligned} \frac{d}{dt}\mathbf{x}(t) &= \mathbf{A}e^{\mathbf{A}t}\mathbf{C_0}(t) + e^{\mathbf{A}t}\frac{d}{dt}\mathbf{C_0}(t) \\ &= \mathbf{A}\mathbf{x}(t) + \mathbf{B}\mathbf{u}(t) \end{aligned} \tag{1.36}$$

and、

$$\frac{d}{dt}\mathbf{C_0}(t) = e^{-\mathbf{A}t}\mathbf{B}\mathbf{u}(t) \tag{1.37}$$

Finally, with the initial state $\mathbf{x}(0)$, the answer can be written as follows,

$$\mathbf{x}(t) = e^{\mathbf{A}t}\left\{\mathbf{x}(0) + \int_0^t e^{-\mathbf{A}\tau}\mathbf{B}\mathbf{u}(\tau)d\tau\right\} \tag{1.38}$$

Transfer function matrix

the Laplace transformation of the state equation can be written as follows,

$$s\mathbf{X}(s) - \mathbf{x}(0) = \mathbf{A}\mathbf{X}(s) + \mathbf{B}\mathbf{U}(s) \tag{1.39}$$

$$\mathbf{Y}(s) = \mathbf{C}\mathbf{X}(s) + \mathbf{D}\mathbf{U}(s) \tag{1.40}$$

Thus, considering the initial state $\mathbf{x}(0) = 0$, the transfer function matrix can be defined as follows,

$$\mathbf{G}(s) = \mathbf{C}(s\mathbf{I} - \mathbf{A})^{-1}\mathbf{B} + \mathbf{D} \tag{1.41}$$

The block diagram of the transfer function matrix is shown in Fig. 1.15

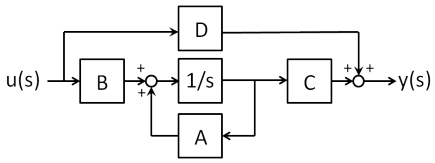

Figure 1.15: The Transfer function of the state equation

Stability

The stability of the system represented by eq. (1.28) and eq. (1.29) can be evaluated with the Lyapunov method [56]. As written in previous section, the condition that the system is stable is that all real part of the eigenvalues

of $\mathbf{A}$ is negative, and such matrix is called stable matrix. Here, matrix $\mathbf{P}(t)$ is defined as follows ($\mathbf{Q} > 0$),

$$\mathbf{P}(t) = \int_0^t e^{\mathbf{A^t}\tau}\mathbf{Q}e^{\mathbf{A}\tau}d\tau \tag{1.42}$$

Thus, the following relationship can be written

$$\begin{aligned}
\mathbf{A^t P}(t) + \mathbf{P}(t)\mathbf{A} &= \int_0^t \left(\mathbf{A^t}e^{\mathbf{A^t}\tau}\mathbf{Q}e^{\mathbf{A}\tau} + e^{\mathbf{A^t}\tau}\mathbf{Q}e^{\mathbf{A}\tau}\mathbf{A}\right)d\tau \\
&= \int_0^t \left(\frac{de^{\mathbf{A^t}\tau}}{d\tau}\mathbf{Q}e^{\mathbf{A}\tau} + e^{\mathbf{A^t}\tau}\mathbf{Q}\frac{de^{\mathbf{A}\tau}}{d\tau}\right)d\tau \\
&= \int_0^t \frac{d}{d\tau}\left(e^{\mathbf{A^t}\tau}\mathbf{Q}e^{\mathbf{A}\tau}\right)d\tau \\
&= e^{\mathbf{A^t}t}\mathbf{Q}e^{\mathbf{A}t} - \mathbf{Q}
\end{aligned} \tag{1.43}$$

When $\mathbf{A}$ is stable, the first term of the right hand side is closer to 0, and $\mathbf{P} = \mathbf{P}(\infty)$ exists. Thus, $\mathbf{P}$ satisfies the following equation,

$$\mathbf{A^t P} + \mathbf{PA} = -\mathbf{Q} \tag{1.44}$$

Equation (1.44) is called Lyapunov equation. When the $\mathbf{A}$ is stable, equation (1.44) has the answer $\mathbf{P} > 0$ to the arbitrary $\mathbf{Q} > 0$. In reverse, when the $\mathbf{P} > 0$ and $\mathbf{Q} > 0$, considering the eigen value of $\mathbf{A}$ is λ, and eigen vector is $\mathbf{x}$, multiplying $\mathbf{x}$ from left and $\overline{\mathbf{x}}$ from right to eq. (1.44), the following equation can be written,

$$(\lambda + \overline{\lambda})\overline{\mathbf{x}}\mathbf{P}\mathbf{x} = -\overline{\mathbf{x}}\mathbf{Q}\mathbf{x} \tag{1.45}$$

In this case, $\lambda + \overline{\lambda}$ is negative because $\mathbf{P} > 0$ and $\mathbf{Q} > 0$. This means the real part of the λ is negative and $\mathbf{A}$ is stable. Thus, the necessary and sufficient condition for the stability of $\mathbf{A}$ is that equation (1.44) has the answer $\mathbf{P} > 0$ to the arbitrary $\mathbf{Q} > 0$.

Similarity transformation

Considering the following transformation,

$$\mathbf{x_2} = \mathbf{T}\mathbf{x} \tag{1.46}$$

equation (1.28) and equation (1.29) can be changed as follows,

$$\frac{d}{dt}\mathbf{x_2} = \mathbf{A'}\mathbf{x} + \mathbf{B'}\mathbf{u} \tag{1.47}$$

$$\mathbf{y} = \mathbf{C}'\mathbf{x_2} + \mathbf{D}'\mathbf{u} \tag{1.48}$$

where $\mathbf{T}$ is regular matrix, and $\mathbf{A}' = \mathbf{TAT}^{-1}$, $\mathbf{B}' = \mathbf{TB}$, $\mathbf{C}' = \mathbf{CT}^{-1}$ and $\mathbf{D}' = \mathbf{D}$. This transformation is called similarity transformation. Here, the transfer function can be written as follows,

$$\begin{aligned}
\mathbf{G}'(s) &= \mathbf{C}'(s\mathbf{I} - \mathbf{A}')^{-1}\mathbf{B}' + \mathbf{D}' \\
&= \mathbf{CT}^{-1}(s\mathbf{I} - \mathbf{TAT}^{-1})^{-1}\mathbf{TB} + \mathbf{D} \\
&= \mathbf{CT}^{-1}(s\mathbf{TT}^{-1} - \mathbf{TAT}^{-1})^{-1}\mathbf{TB} + \mathbf{D} \\
&= \mathbf{CT}^{-1}\left[\mathbf{T}(s\mathbf{I} - \mathbf{A})\mathbf{T}^{-1}\right]^{-1}\mathbf{TB} + \mathbf{D} \\
&= \mathbf{CT}^{-1}\mathbf{T}(s\mathbf{I} - \mathbf{A})^{-1}\mathbf{T}^{-1}\mathbf{TB} + \mathbf{D} \\
&= \mathbf{C}(s\mathbf{I} - \mathbf{A})^{-1}\mathbf{B} + \mathbf{D} \\
&= \mathbf{G}(s)
\end{aligned} \tag{1.49}$$

This means that with the similarity transformation, the transfer function doesn't change, and that the choice of the state vector has the flexibility.

Controllability

In the case that in the system of eq. (1.28) and eq. (1.29), to the arbitrary initial state $\mathbf{x}(0)$, the input $[\mathbf{u}(t);\ (0 < t < T)]$ which makes $\mathbf{x}(T) = 0$ exists at the time $T > 0$, the system eq. (1.28) and eq. (1.29) is called controllable. This has other expression that $(\mathbf{A}, \mathbf{B})$ is controllable. The condition of the controllability can be written as follows,

$$rank\left[\begin{array}{cccc} \mathbf{B} & \mathbf{AB} & \cdots & \mathbf{A}^{n-1}\mathbf{B} \end{array}\right] = n \tag{1.50}$$

where n is the size of $\mathbf{A}$. The equivalent condition is that the following Lyapunov equation has the answer $\mathbf{P} > 0$,

$$\mathbf{PA^t} + \mathbf{AP} = -\mathbf{BB^t} \tag{1.51}$$

Observability

In the case that in the system of eq. (1.28) and eq. (1.29), to the arbitrary time $T > 0$, the initial state $\mathbf{x}(0)$ can be uniquely determined from the input and output date $[u(t), y(t)]$ $(0 < t < T)$, this system is called observable. This has other expression that ($\mathbf{A}$,$\mathbf{C}$) is observable. The condition of the observability can be written as follows,

$$rank\left[\begin{array}{cccc} \mathbf{C^t} & \mathbf{A^tC^t} & \cdots & (\mathbf{A^t})^{n-1}\mathbf{C^t} \end{array}\right] = n \tag{1.52}$$

where n is the size of $\mathbf{A}$. The equivalent condition is that the following Lyapunov equation has the answer $\mathbf{P} > 0$,

$$\mathbf{P}\mathbf{A}^{\mathbf{t}} + \mathbf{A}\mathbf{P} = -\mathbf{C}^{\mathbf{t}}\mathbf{C} \tag{1.53}$$

Zeros and Poles

Considering the following equation,

$$f(s) = \frac{p(s)}{q(s)} \tag{1.54}$$

where $p(s)$ and $q(s)$ are the polynomial equations, the values of s which makes $p(s) = 0$ are called zeros, and $q(s) = 0$ are called poles. Considering the transfer function matrix, the poles of the transfer function can be lead as follows,

$$\begin{aligned} \mathbf{G}(s) &= \mathbf{C}(s\mathbf{I} - \mathbf{A})^{-1}\mathbf{B} + \mathbf{D} \\ &= \frac{1}{det(s\mathbf{I} - \mathbf{A})}\mathbf{C}adj(s\mathbf{I} - \mathbf{A})\mathbf{B} + \mathbf{D} \end{aligned} \tag{1.55}$$

thus, the poles of the transfer function $\mathbf{G}(s)$ are the s values that makes $det(s\mathbf{I} - \mathbf{A}) = 0$, i.e. the eigen values of $\mathbf{A}$.

Pole placement method

The output signals of the transfer function $\mathbf{G}(s)$ is the form of the summation of the exponential functions, and each time constant is same to the pole of $\mathbf{G}(s)$. Thus, poles are quite important parameters to determine the system performance. Considering the following feedback control,

$$\mathbf{u}(t) = -\mathbf{F}\mathbf{x} + \mathbf{u_0} \tag{1.56}$$

the state equation can be written as follows,

$$\begin{aligned} \frac{d}{dt}\mathbf{x} &= \mathbf{A}\mathbf{x} + \mathbf{B}(\mathbf{u_0} - \mathbf{F}\mathbf{x}) \\ &= (\mathbf{A} - \mathbf{B}\mathbf{F})\mathbf{x} + \mathbf{B}\mathbf{u_0} \end{aligned} \tag{1.57}$$

With the feedback control, the poles of the system are changed from the poles of $\mathbf{A}$ to $\mathbf{A} - \mathbf{B}\mathbf{F}$. The method to determine the feedback gain $\mathbf{F}$ to place the poles which satisfy the design specification is called pole placement method [65].

Optimal control

In the optimal control theory, the system performance is evaluated with the evaluate function, and the performance is optimized [66,67]. Considering the following state equation and the evaluate function,

$$\frac{d}{dt}\mathbf{x} = \mathbf{f}(\mathbf{x}, \mathbf{u}) \tag{1.58}$$

$$J = L_0(\mathbf{x}, t_f) + \int_0^{t_f} L(\mathbf{x}, u)dt \tag{1.59}$$

the optimal case is defined that J is minimized. Here, in the interval $[t, t_f]$, the minimum value of J is defined as follows,

$$V(\mathbf{x}, t) \equiv \min_u \left\{ L_0(\mathbf{x}, t_f) + \int_t^{t_f} L(\mathbf{x}, u)d\tau \right\}. \tag{1.60}$$

Dividing the interval $[t, t_f]$ to $[t, \sigma]$ and $[\sigma, t_f]$, $V(\mathbf{x}, t)$ can be written as follows,

$$\begin{aligned} V(\mathbf{x}, t) &\equiv \min_u \left\{ L_0(\mathbf{x}, t_f) + \int_t^{\sigma} L(\mathbf{x}, u)d\tau + \int_{\sigma}^{t_f} L(\mathbf{x}, u)d\tau \right\} \\ &= \min_u \left\{ \int_t^{\sigma} L(\mathbf{x}, u)d\tau + V(\mathbf{x}, \sigma) \right\} \end{aligned} \tag{1.61}$$

Considering $\sigma \to t$, i.e. $(\sigma - t) = \delta t \to 0$, $V(\mathbf{x}, t)$ is written as follows,

$$V(\mathbf{x}, t) \equiv \min_u \lim_{\delta t \to 0} \{ L(\mathbf{x}, t)\delta t + V(\mathbf{x} + \mathbf{f}(\mathbf{x}, \mathbf{u})\delta t, t + \delta t) \} \tag{1.62}$$

In the case that $V(\mathbf{x}, t)$ can be differentiated, the following equation can be written,

$$V(\mathbf{x} + \mathbf{f}(\mathbf{x}, \mathbf{u})\delta t, t + \delta t) = V(\mathbf{x}, t) + \frac{\partial V^t(\mathbf{x}, t)}{\partial \mathbf{x}}\mathbf{f}(\mathbf{x}, \mathbf{u})\delta t + \frac{\partial V(\mathbf{x}, t)}{\partial t}\delta t \tag{1.63}$$

Thus, the following condition can be lead,

$$\min_u \left[\frac{\partial V^t(\mathbf{x}, t)}{\partial \mathbf{x}}\mathbf{f}(\mathbf{x}, \mathbf{u}) + \frac{\partial V(\mathbf{x}, t)}{\partial t} + L(\mathbf{x}, t) \right] = 0 \tag{1.64}$$

From eq. (1.64), optimal input $u(t)$ can be lead. Next considering the following state equation and the evaluate function,

$$\frac{d}{dt}\mathbf{x} = \mathbf{A}\mathbf{x} + \mathbf{B}\mathbf{u} \tag{1.65}$$

$$J = min_u \int_0^\infty \left(\mathbf{x}^t \mathbf{Q} \mathbf{x} + \mathbf{u}^t \mathbf{R} \mathbf{u} \right) dt \tag{1.66}$$

this is called optimal regulator problem. In this case, minimum evaluate function value $V(\mathbf{x}, t)$ is expected to be following form,

$$V(\mathbf{x}, t) = \mathbf{x}^t \mathbf{P}(t) \mathbf{x}. \tag{1.67}$$

Then, assuming the terminal state (i.e. $d/dt = 0$), equation (1.64) can be written as follows,

$$\min_u \{ 2\mathbf{x^t P}(\mathbf{Ax} + \mathbf{Bu}) + \mathbf{x^t Q x} + \mathbf{u}^t \mathbf{R u} \} = 0. \tag{1.68}$$

From the differential of this equation with respect to $\mathbf{u}$, the condition of the optimal $\mathbf{u}$ can be written as follows,

$$2\mathbf{B^t P x} + 2\mathbf{R u} = 0 \tag{1.69}$$

Thus, the optimal $\mathbf{u}$ can be written as follows,

$$\mathbf{u} = -\mathbf{R}^{-1} \mathbf{B^t P x} \tag{1.70}$$

Substituting this to eq. (1.68), the condition that P has to satisfy can be written as follows,

$$\mathbf{A^t P} + \mathbf{PA} - \mathbf{PBR}^{-1} \mathbf{B}^t \mathbf{P} + \mathbf{Q} = 0 \tag{1.71}$$

1.5.4 Robust control theory

The modern control theory can deal the MIMO system, and design the high performance controller theoretically and analytically, but to design the controller, the physical model expressed by the state equation is needed. Additionally, the performance of the modern controller designed from the state equation is ensured theoretically only to the system which satisfies the state equation. Generally, the physics of the system is quite complex and can't be expressed such a simple form. Thus, in most case, the state equation is the extremely roughly approximation of the physics, and it is impossible to check whether the controller is suitable for the system without the experiment or the strictly simulation. The difference between the state equation and the real system is called model error. The postmodern control theory or the robust control theory is the theory for making the controller which performance is ensured to the model error and it is said to be born in 1981 [68–70]. In the robust control theory, the new variable $\mathbf{w}$ and $\mathbf{z}$ are added to the eqs. (1.28) and (1.29) and the system physics are written as follows,

$$\frac{d}{dt}\mathbf{x} = \mathbf{Ax} + \mathbf{B_1 w} + \mathbf{B_2 u} \tag{1.72}$$

$$\mathbf{z} = \mathbf{C_1 x} + \mathbf{D_{11} w} + \mathbf{D_{12} u} \tag{1.73}$$

$$\mathbf{y} = \mathbf{C_2 x} + \mathbf{D_{21} w} + \mathbf{D_{22} u} \tag{1.74}$$

where, $\mathbf{z}$ is the parameters which is wished to be minimized, and $\mathbf{w}$ is a disturbance including the effect of the model error. They are called 'generalized plant'. Using this generalized plant, variable control problems can be dealt.

H_∞ control theory

H_∞ control theory is the typical robust control theory. In this theory, the effect of the model error is evaluated with the H_∞ norm. The H_∞ represents the maximum gain of the system. In this theory, the model error is represented as follows,

$$\mathbf{P_{true}}(s) = \mathbf{P_0}(s) + \mathbf{\Delta}(s) \tag{1.75}$$

or

$$\mathbf{P_{true}}(s) = \mathbf{P_0}(s)(\mathbf{I} + \mathbf{\Delta}(s)) \tag{1.76}$$

where, $\mathbf{P_{true}}$ is the real system, and $\mathbf{P_0}(s)$ is the approximated model (e.g. state equation) which is used to control design, and $\mathbf{\Delta}(s)$ is the model error. $\mathbf{P_0}(s)$ is called nominal model. This concept is also shown in Fig. 1.16. In H_∞ control theory, $\mathbf{\Delta}(s)$ is estimated from the experimental date or the strictly physical model and the effect of the $\mathbf{\Delta}(s)$ is substituted into the $\mathbf{w}$ in eqs. (1.72) to (1.74). The controller is designed to minimize the H_∞ norm of the transfer function from $\mathbf{w}$ to $\mathbf{z}$. The detail is shown in chapter 4.

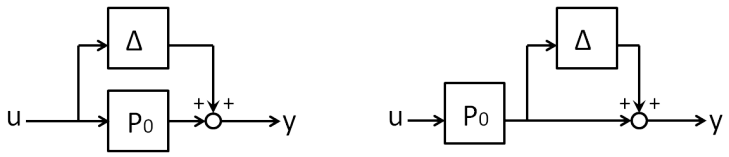

Figure 1.16: The concept of the model error

μ synthesize

In H_∞ control theory, the model error is represented as the form of fig 1.16. In many systems, however, it is difficult to represent the model error as these forms. For example, considering the system shown in Fig. 1.17,

the model error expression of the H_∞ theory is written as follows [71],

$$\mathbf{P_{true}} = \mathbf{P_0} + \mathbf{\Delta_a} \tag{1.77}$$

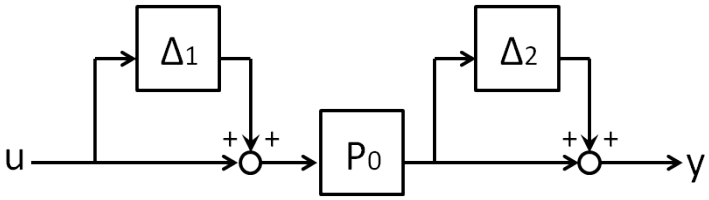

Figure 1.17: The example of the multiple model error

$$\mathbf{\Delta_a} = \mathbf{P_0\Delta_1} + \mathbf{\Delta_2 P_0} + \mathbf{\Delta_2 P_0 \Delta_1}. \tag{1.78}$$

In this case, the model error $\mathbf{\Delta_a}$ seems to be larger than the true model errors $\mathbf{\Delta_1}$ and $\mathbf{\Delta_2}$. To deal the such situation, μ-analysis and synthesize have been developed [72, 73]. In μ-analysis theory, the group of the model errors are expressed as Fig. 1.18.

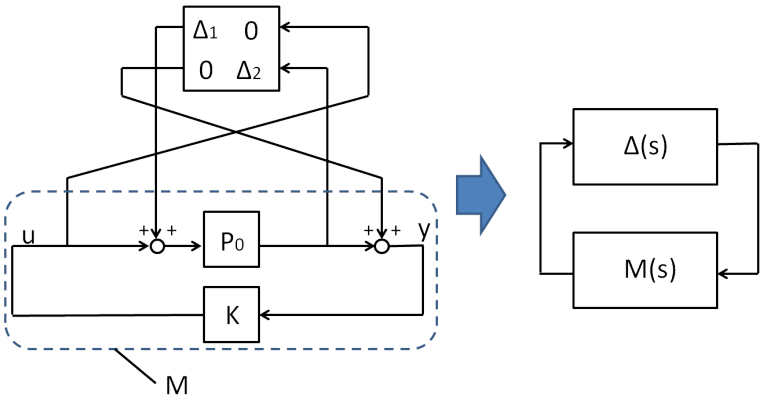

Figure 1.18: The concept of the structured uncertainty

In Fig. 1.18, the general form of $\mathbf{\Delta}$ can be written as follows,

$$\mathbf{\Delta} = \left\{ diag[\delta_1 \mathbf{I_{r1}}, \cdots, \delta_s \mathbf{I_{rs}}, \mathbf{\Delta_1}, \cdots, \mathbf{\Delta_F}] : \delta_i \in C, \mathbf{\Delta_j} \in \mathbf{C}^{m_j \times m_j} \right\} \tag{1.79}$$

where $\delta_i \mathbf{I_{ri}}$ are called repeated scalar block, and $\mathbf{\Delta_i}$ are called full block. This model error expression is called structured uncertainty. Assuming that $\mathbf{\Delta}(s)$ and $\mathbf{M}(s)$ in fig 1.18 are stable, in the case that $det|\mathbf{I} - \mathbf{M\Delta}| = 0$, the system in fig 1.18 is unstable [74]. To consider the smallest $\mathbf{\Delta}$ which makes the system with $\mathbf{M}$ is unstable, the structured singular value μ is defined as follows,

$$\mu_\Delta(\mathbf{M}) = \frac{1}{min\{\bar{\sigma}(\mathbf{\Delta}) : det|\mathbf{I} - \mathbf{M\Delta}| = 0\}} \tag{1.80}$$

Using this μ, the condition that the system is stable for all $\mathbf{\Delta}$ can be written as follows,

$$\mu_{\Delta}\{\mathbf{M}(i\omega)\} < 1 \quad \forall\omega \tag{1.81}$$

The analytical method to find the controller which satisfies this condition have not been found yet, but some practical method have been developed [72]. D-K iteration is the typical μ-controller design method. D-K iteration is done with following steps

- Using the H_∞ control theory, find the controller $\mathbf{K_i}(s)$ which minimize $\|\mathbf{D_i}(s)\mathbf{M}(s)\mathbf{D_i^{-1}}(s)\|_\infty$ ($\mathbf{D_1} = \mathbf{I}$).
- Find the $\mathbf{D_{i+1}}(i\omega)$ for each ω, which minimize $\bar{\sigma}\{\mathbf{D_i}(i\omega)\mathbf{M}(i\omega)\mathbf{D_i^{-1}}(i\omega)\}$, and see the condition $min\{\bar{\sigma}\} < 1; \forall\omega$. If the condition is satisfied, stop, and else if not satisfied, go to next step.
- Approximate each $\mathbf{D_{i+1}}(i\omega)$ with the function $\mathbf{D_{i+1}}(s)$, make $i \to i+1$ and return to step1.

$\mathbf{D}$ is called scaling matrix and formed as follows,

$$\mathbf{D} = diag\{\mathbf{D_1}, \cdots, \mathbf{D_s}, d_1\mathbf{I_{p1}}, \cdots, d_f\mathbf{I_{pf}}\} \tag{1.82}$$

where, $\mathbf{D_i} \in C^{r_i \times r_i} : D_i^* = D_i > 0$ and $d_i \in R : D_i > 0$. The detail of D-K iteration is introduced some textbook [71, 74].

Chapter 2

one dimensional plasma control simulation

2.1 Introduction of this chapter

In ref. [38], the control experiment that the minimum safety factor and the ITG (Ion Temperature Gradient) are controlled by the NBI and LHCD is demonstrated. In this experiment, the tangential NBI has the large effect on the ITG, but not so much on the safety factor, while LHCD has the large effect on the safety factor but not so much on the ITG. Thus, in this case, the parameters can be controlled as two SISO system. References [38, 39] suggests the necessity for the MIMO system control with the coupling.
In this chapter, the control simulation with the 1-D code that the fusion power and the minimum safety factor are controlled by the gas-puff and the NBI is demonstrated. In this case, the parameters have large coupling effect. The part of this chapter is published as ref. [75]

2.2 1-D code

In this simulation, the 1-D code is used. The fundamental equations are follows,

$$\frac{\partial n_j}{\partial t} = \frac{1}{V'}\frac{\partial}{\partial r}\Gamma_j + < S_j > \tag{2.1}$$

$$\frac{3}{2}\frac{\partial p_j}{\partial t} = \frac{1}{V'}\frac{\partial}{\partial r}\left(q_j + \frac{3}{2}\Gamma_j T_j\right) + < Q_j > + \frac{3}{2} < T_j S_j > \tag{2.2}$$

$$S^j(r,t) = S^j_{NBI}(r,t) + S^j_{ntr}(r,t) \tag{2.3}$$

$$\frac{\partial \nu}{\partial t} = -\frac{1}{2\phi_a r}\frac{\partial}{\partial r}\left[\frac{\eta_{\|}}{T < R >^{-2}}\left(< \mathbf{J}\cdot\mathbf{B} > - < \mathbf{J}\cdot\mathbf{B} >^{bs} - < \mathbf{J}\cdot\mathbf{B} >^{ext}\right)\right] \tag{2.4}$$

$$\nu = \frac{d\psi}{d\phi} \tag{2.5}$$

$$\Psi = \frac{1}{2\pi}\int_{\phi_{axis}}^{\psi} B_p d\mathbf{S_p} \tag{2.6}$$

$$\Phi = 2\pi\int_{\phi_{axis}}^{\psi} B_t d\mathbf{S_t} \tag{2.7}$$

Equations (2.1), (2.2) and (2.4) are the equation of continuity, energy conservation law and the poloidal flux diffusion equation respectively. The particle, and hear flux are as follows,

$$\Gamma^j_{ion}(r,t) = V' < |\nabla r|^2 > \left(D_j\frac{\partial n_j(r,t)}{\partial r} + v_j n_j(r,t)\right) \tag{2.8}$$

$$Q_j = V' < |\nabla r|^2 > \left(\chi_j\frac{\partial p_j}{\partial r} + p_j v_j\right) \tag{2.9}$$

where D_j and χ_j are diffusion coefficient. The particle source term is calculated from the neutral particle Bolzman equation as follows,

$$\frac{\partial f_j(\vec{r},\vec{v},t)}{\partial t} + \vec{v}\cdot\nabla f_j(\vec{r},\vec{v},t) = -(\sigma^{ei}+\sigma^{ii})v f_j(\vec{r},\vec{v},t)$$
$$+\sum_k \int d^3v'\sigma^{cx}|\vec{v}-\vec{v'}|\left(f_j(\vec{r},\vec{v'},t)f_k(\vec{r},\vec{v},t) - (f_j(\vec{r},\vec{v'},t)f_k(\vec{r},\vec{v},t)\right) \tag{2.10}$$

the first term of right hand side is the ionization, and the second term is charge exchange reaction. The alpha particle heat source is calculated from the Fokker Plank equation as follows,

$$\tau_s\frac{\partial f^\alpha}{\partial t} = \frac{1}{v^2}\frac{\partial}{\partial v}\left[\frac{\partial}{\partial v}(\hat{A}(v)f^\alpha) + \hat{B}(v)f^\alpha\right] - \frac{\tau_s}{\tau_L^\alpha}f^\alpha + \frac{\tau_s S^\alpha}{4\pi v^2}\delta(v-v_\alpha) \tag{2.11}$$

and

$$\hat{A}(v) = \sum_j \frac{3\sqrt{\pi}}{4}\frac{m_e}{M_\alpha}v_e^3\frac{Z_j^2 n_j \ln\Lambda_j}{n_e\ln\Lambda_e}\frac{1}{2}\frac{v_j}{x_j}\omega(x_j) \tag{2.12}$$

$$\hat{B}(v) = \sum_j \frac{3\sqrt{\pi}}{4}\frac{m_e}{M_\alpha}v_e^3\frac{Z_j^2 n_j \ln\Lambda_j}{n_e\ln\Lambda_e}\left(\left(\frac{M_\alpha}{m_j}+\frac{1}{2x_j^2}\right)\omega(x_j) - \frac{2}{\sqrt{\pi}}x_j e^{-x^2}\right) \tag{2.13}$$

$$\omega(x_j) = \frac{2}{\sqrt{\pi}}\int_0^{x_j} e^{y^2}dy - \frac{2}{\sqrt{\pi}}x_j e^{-x_j^2} \tag{2.14}$$

$$x_j = \frac{v}{v_j}, v_j = \sqrt{\frac{2T_j}{m_j}} \tag{2.15}$$

$$\tau_s^\alpha = \frac{3\pi\sqrt{\pi}\epsilon_0^2 M_\alpha m_e v_e^3}{Z_i^2 e^4 n_e \ln\Lambda_e} \tag{2.16}$$

$$\frac{1}{2}M_\alpha v_\alpha^2 = 3.5MeV. \tag{2.17}$$

The NBI heating and current source is also calculated from Fokker Plank equation.

2.3 Fusion power control

2.3.1 Input parameters

In this simulation, the following input parameters are used,
$R_P = 6.3m, a_P = 1.75m, \kappa = 1.8, \delta = 0.4$
$I_P = 9MA, B_t = 4.76T$
$P_{nbi} = 70MW, E_{nbi} = 1MeV$
where E_{nbi} is the energy of the NBI. The position of the NBI device is $(x, y, z) = (21.70m, 4.80m, 0.00m)$. The diffusion coefficients are as follows,
$D_j = \frac{0.02}{n_e}(10^{20}m^{-3})$
$\chi_j = 0.08\frac{T_e(keV)}{n_e(10^{20}m^{-3})}$

2.3.2 PID control simulation

PID theory

To control the fusion power, PID control theory is used in this simulation. PID theory is one of the most usual feedback control theory, and the actuator value is defined as the linear sum of the proportional, differential and integral value of the error between the reference value and the parameter. In this case, the fusion power is controlled by the gas-puff, and the system is SISO.

Simulation test

With the Ziegler-Nichols ultimate gain method, The gas-puff amount is determined as follows,

$$flxpuf[sec^{-1}] = 0.3\times10^{17}\left(Kp + Ki\int dt + Kd\frac{d}{dt}\right)(dnl\_fb[MW] - dia\_pfus[MW]) \tag{2.18}$$

and

$$K_p = 21, Ki = 1.4, Kd = 65.625 \tag{2.19}$$

Using these gains, the simulation results are shown as follows.

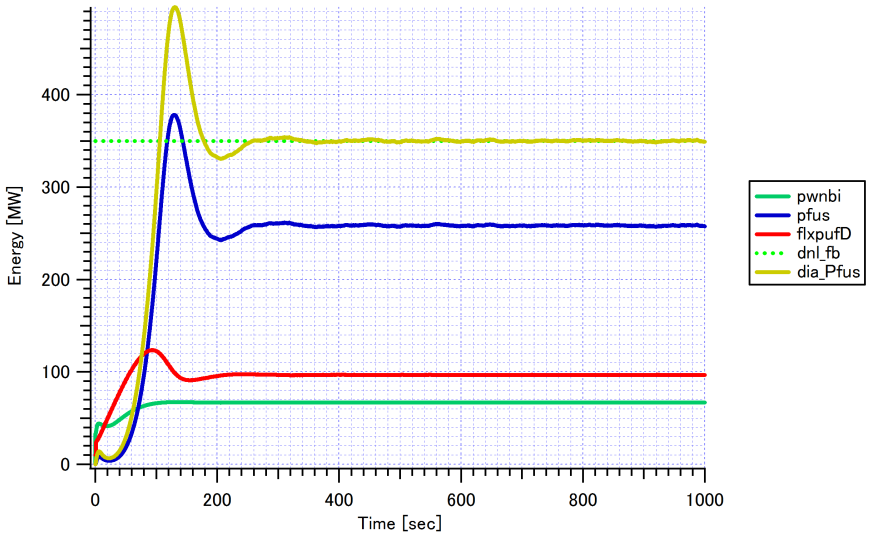

Figure 2.1: The result of the fusion power control test simulation

In Fig. 2.1, $pfus$ is the true fusion power, and dia_pfus represents the measured fusion power which is determined from the line integrated plasma density. The fluxfD is the deuterium gas-puff amount and it is the same value of the tritium gas-puff amount (sec^{-1}) and they are normalized by 10^{19} in Fig. 2.1. The $pwnbi$ is the deposition value from the NBI power. The reference value is dnl_fb and in this simulation, the dia_pfus is controlled to the dnl_fb. Figure 2.1 shows that the overshoot exists and the error between the measured value and the true value of the fusion power is about 100MW. To improve the control performance, the PID gains should be adjusted.
The other parameters in this simulation is shown in Figs. 2.2 to 2.5.

In Fig. 2.2, $qmin$ is the minimum value of the safety factor, and $roqmin$ is the position of $qmin$. The plasma temperature, density and the q profile time dependence are shown in Fig. 2.3 to Fig. 2.5.

Final result of the fusion power control

After some try and error, the PID gains are determined as follows,

$$K_p = 45, Ki = 0.56, Kd = 131.25 \tag{2.20}$$

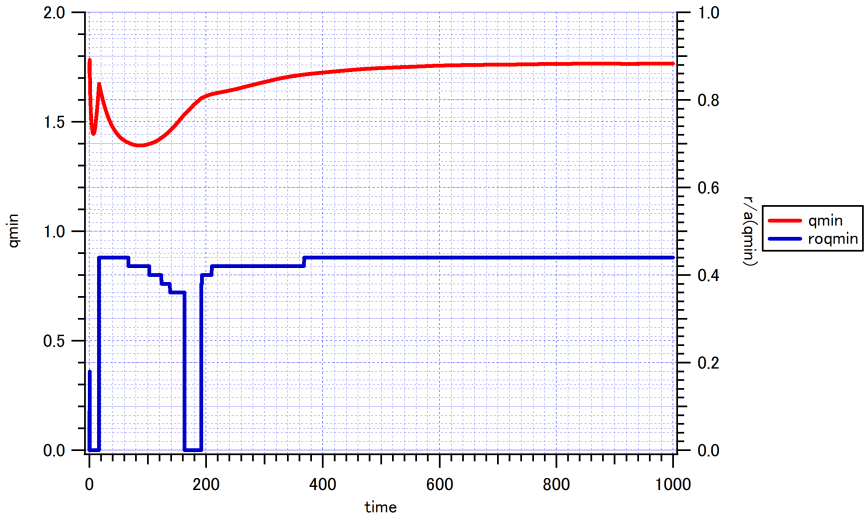

Figure 2.2: The q_{min} time dependence in the test simulation

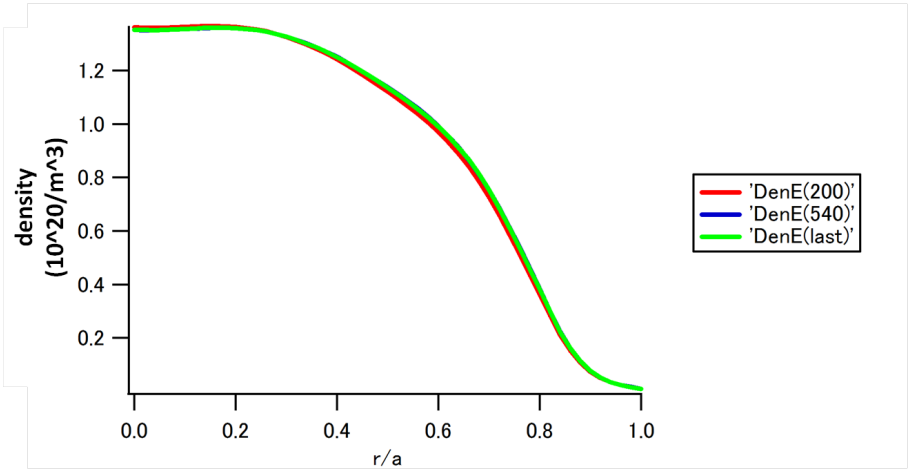

Figure 2.3: The electron density profile in the test simulation

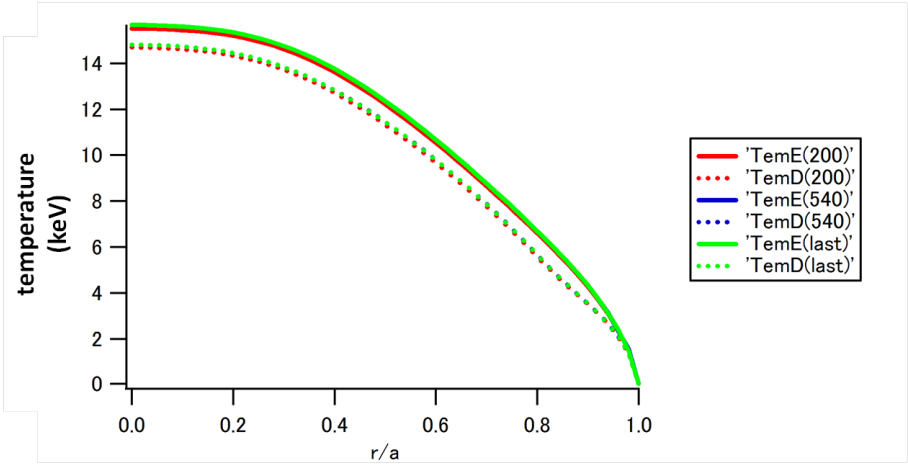

Figure 2.4: The temperature profile in the test simulation

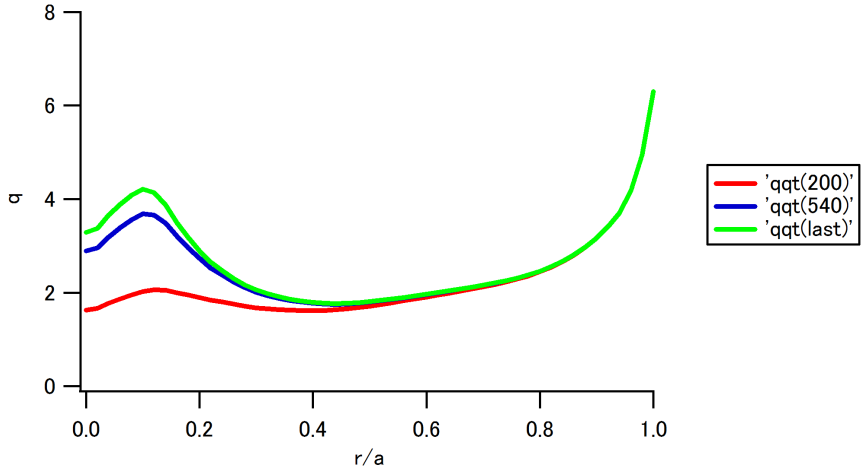

Figure 2.5: The safety factor profile in the test simulation

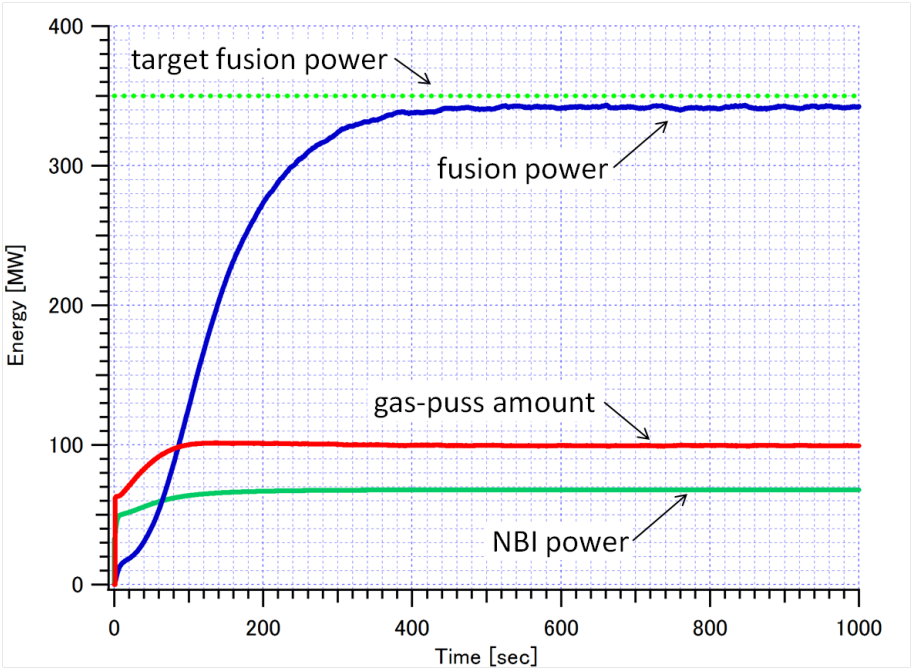

Figure 2.6: The result of the fusion power single control simulation [75]

The simulation results are shown in Fig. 2.6 to Fig. 2.8.

Figure 2.6 shows that in this simulation, the fusion power is kept to 350MW and it means that the state $Q > 5$ can be kept. Figure 2.7 shows that the position of the q_{min} is about $r/a = 0.45$, and current profile is negative shear type. Figure 2.8 shows the current profile at 1000sec, and in this figure, the ohmic current is nearly 0. It means that this simulation represents the steady state operation.

2.4 Minimum q value control

In this section q_{min} is controlled by the NBI. It is also SISO system. In this simulation, the gas-puff amount is kept to $8.0 \times 10^{20}/sec$ and the controller is designed with the same method with last section. Finally, the NBI power is determined as follows,

$$P_{nbi}[MW] = \left(Kp + Ki \int dt + Kd \frac{d}{dt} \right) (q_{min}^{ref} - q_{min}) \tag{2.21}$$

$$K_p = 60, K_i = 1.5, K_d = 600. \tag{2.22}$$

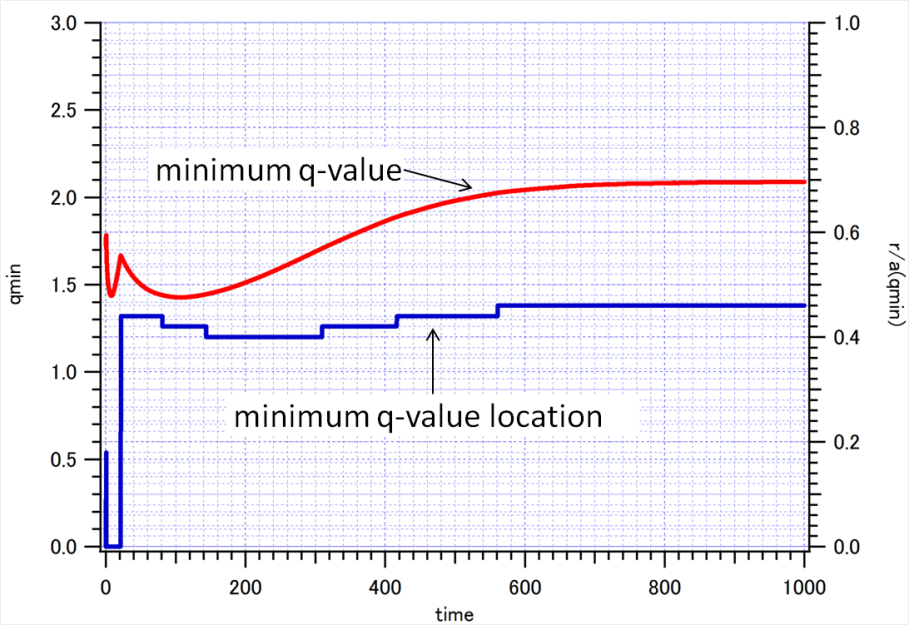

Figure 2.7: The q_{min} time dependence in the fusion power single control simulation [75]

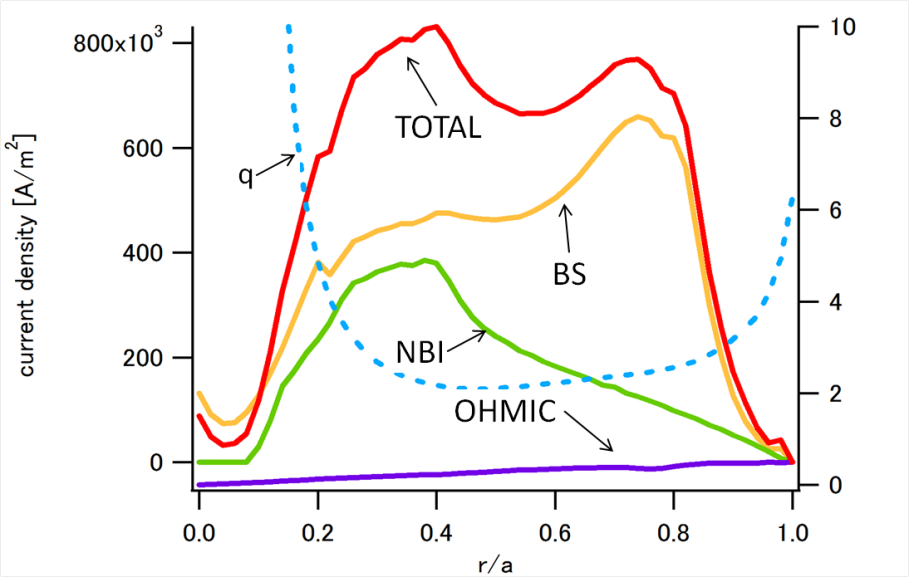

Figure 2.8: The current profile at the steady state in the fusion power single control simulation [75]

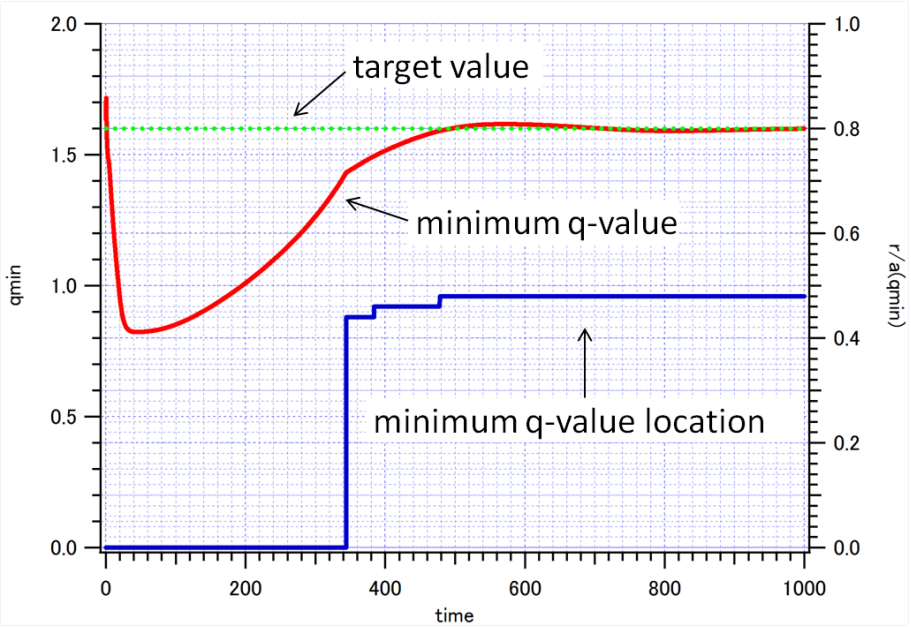

Figure 2.9: The result of the q_{min} single control simulation [75]

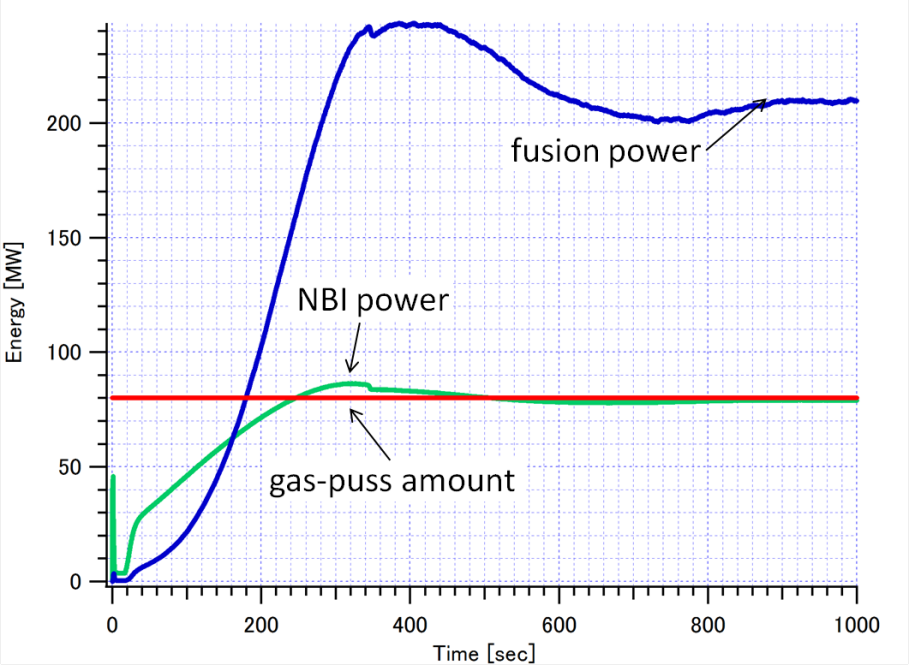

Figure 2.10: The fusion power time dependence in the q_{min} single control simulation [75]

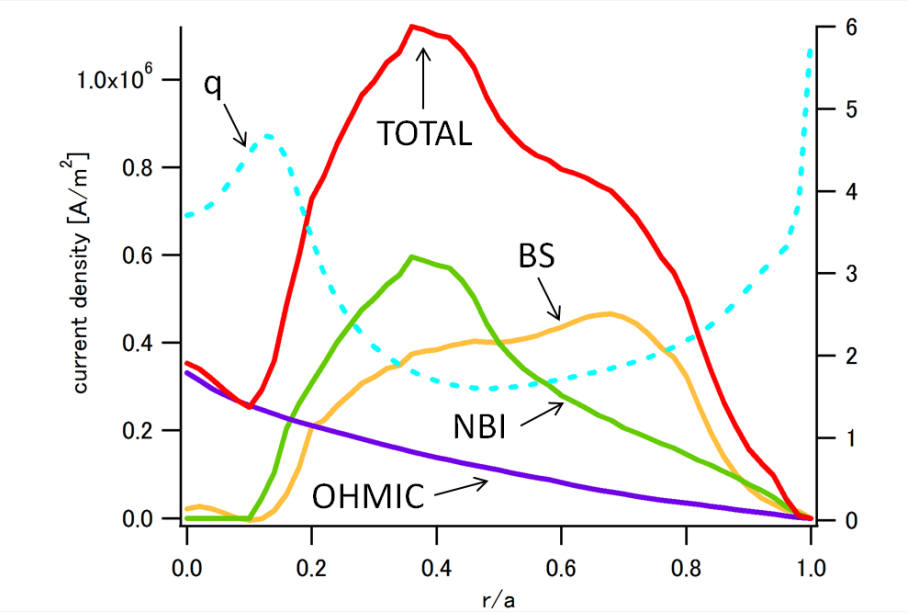

Figure 2.11: The current profile at the steady state in the q_{min} single control simulation [75]

The simulation results are shown in Fig. 2.9 to Fig. 2.11

In Fig. 2.9, the q_{min} can be kept to the reference value, but in Fig 2.10, it is not $Q > 5$ state, and Figure 2.11 shows that the ohmic current is not nearly 0 and shows it is not non-inductive operation.
In Fig. 2.9 and Fig. 2.10, final NBI power is 80MW and $q_{min} = 1.6$, while in Fig. 2.7 and Fig. 2.10, the NBI power is 70MW and the $q_{min} = 2.1$. This is because difference of the bootstrap current ratio. The gas-puff amount has the large effect on the bootstrap current ratio and the q_{min}.

2.5 Simultaneous control simulation

To make the ideal ignition condition, the parameters simultaneous control is needed. In this section, the simulation of the fusion power and the q_{min} control is demonstrated.

2.5.1 The case of only diagonal term

The simultaneous controller can be written as the form of eq. (2.23).

$$\begin{pmatrix} a_{11} & a_{12} \\ a_{21} & a_{22} \end{pmatrix} \begin{pmatrix} P_{fus} - P_{fus}^{ref} \\ q_{min} - q_{min}^{ref} \end{pmatrix} = \begin{pmatrix} P_{puff} \\ P_{nbi} \end{pmatrix} \tag{2.23}$$

In the case that the effect from the gas-puff to the q_{min}, and from the NBI to the fusion power is enough small, only diagonal term of eq.(2.23) have to be considered. The last two controller, however, can't control the fusion power and the q_{min} because of the coupling effect. Thus, the PID gains of NBI (i.e. a_{22} of eq. (2.23)) is re-adjusted with some try and error and finally, the NBI gains are determined to $K_p = 54, K_i = 0.15, K_d = 3560$. Using this controller, the fusion power and the q_{min} are controlled simultaneously. The results are shown later.

$P_{fus}^{ref} = 350MW, q_{min}^{ref} = 1.6$

The results are shown in Fig 2.12 to Fig 2.15.

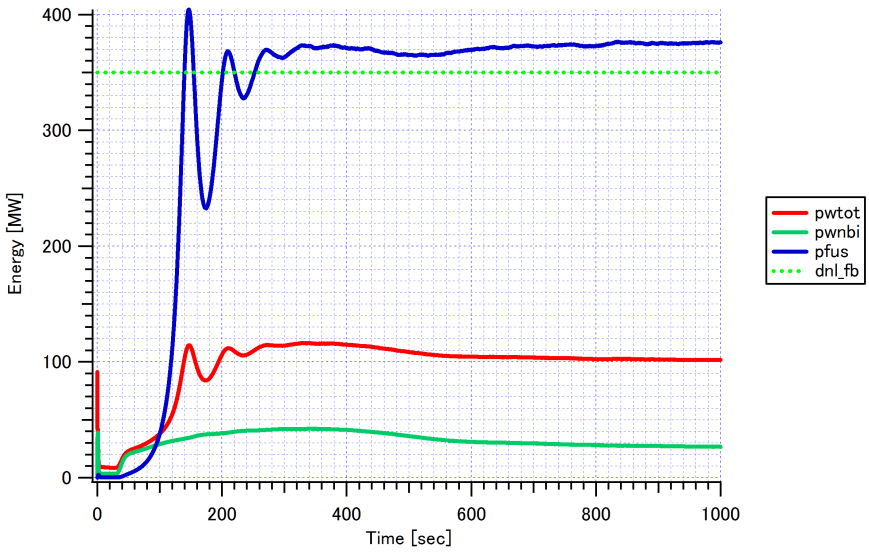

Figure 2.12: The fusion power time dependence in the simultaneous control simulation without the off-diagonal term ($P_{fus}^{ref} = 350MW, q_{min}^{ref} = 1.6$)

In this case, the fusion power and the q_{min} are following to the reference value, but the fusion power oscillates and the current profile is not negative shear type.

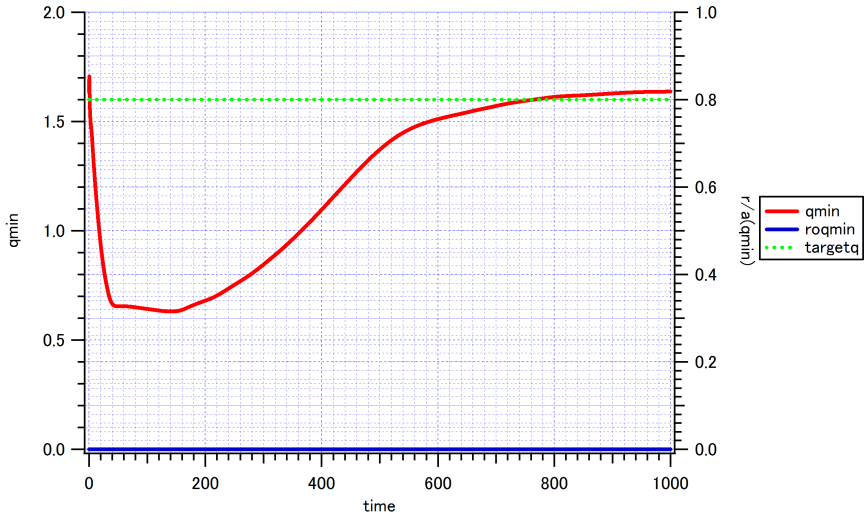

Figure 2.13: The q_{min} time dependence in the simultaneous control simulation without the off-diagonal term ($P_{fus}^{ref} = 350MW, q_{min}^{ref} = 1.6$)

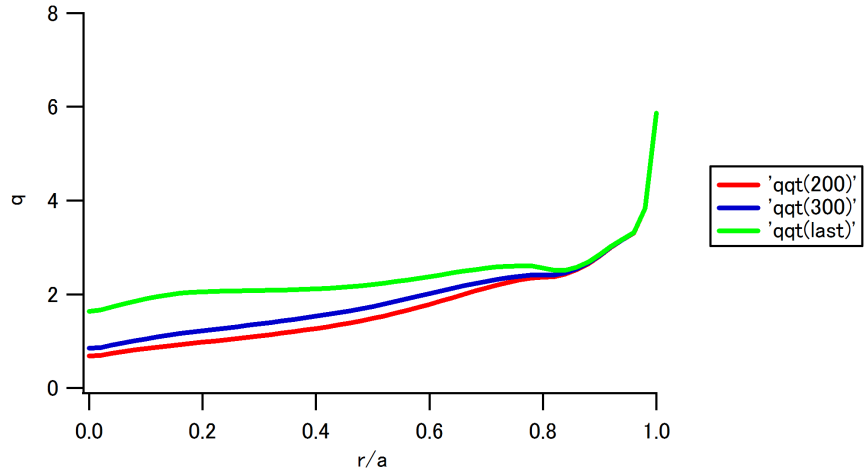

Figure 2.14: The q profile in the simultaneous control simulation without the off-diagonal term ($P_{fus}^{ref} = 350MW, q_{min}^{ref} = 1.6$)

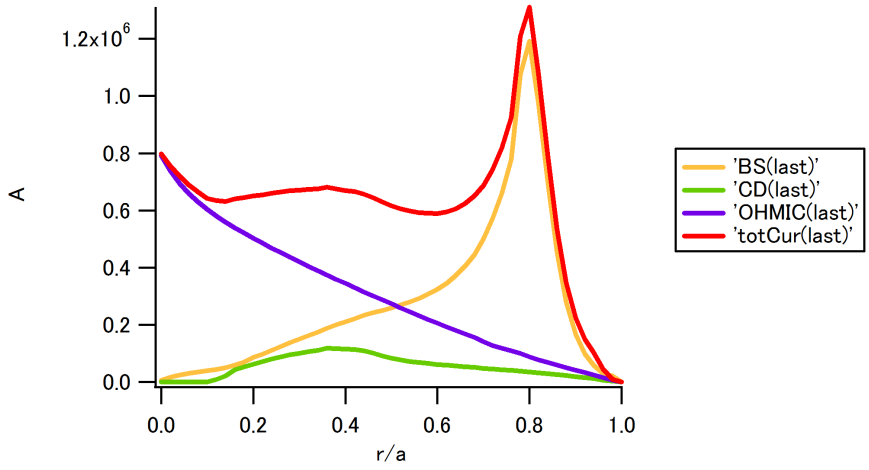

Figure 2.15: The current profile at the steady state in the simultaneous control simulation without the off-diagonal term ($P_{fus}^{ref} = 350MW, q_{min}^{ref} = 1.6$)

$P_{fus}^{ref} = 350MW, q_{min}^{ref} = 1.8$

The results are shown in Fig. 2.16 to Fig. 2.19.

In this case, both of the fusion power and the q_{min} are following near the reference value, but they are kept oscillated. Additionally, the current profile is not negative shear.

2.5.2 The case with the off-diagonal term

Using the controller with only a_{11} and a_{22} of eq. (2.23), the parameter oscillation occurred. To prevent this, the off diagonal term seems to be needed. At first, in this case, a_{21} is added, i.e. to determine the NBI power, not only the PID of q_{min} but also PD of the fusion power is used. The simulation results are shown in Fig. 2.20 to Fig. 2.22.

In this case, both of the fusion power and the q_{min} are controlled to the reference values and they don't oscillate. Figure. 2.20 shows, however, that there are some offset of the fusion power, and Figure 2.22 shows that the current profile is not negative shear and the large ohmic current is needed. There is a possibility that the controller performance becomes higher with a_{12}, but this is future issue.

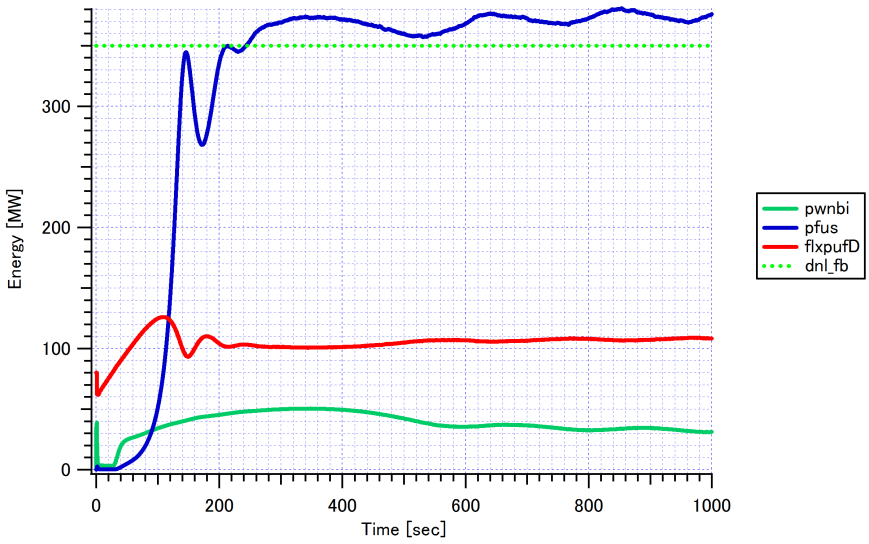

Figure 2.16: The fusion power time dependence in the simultaneous control simulation without the off-diagonal term ($P_{fus}^{ref} = 350MW, q_{min}^{ref} = 1.8$)

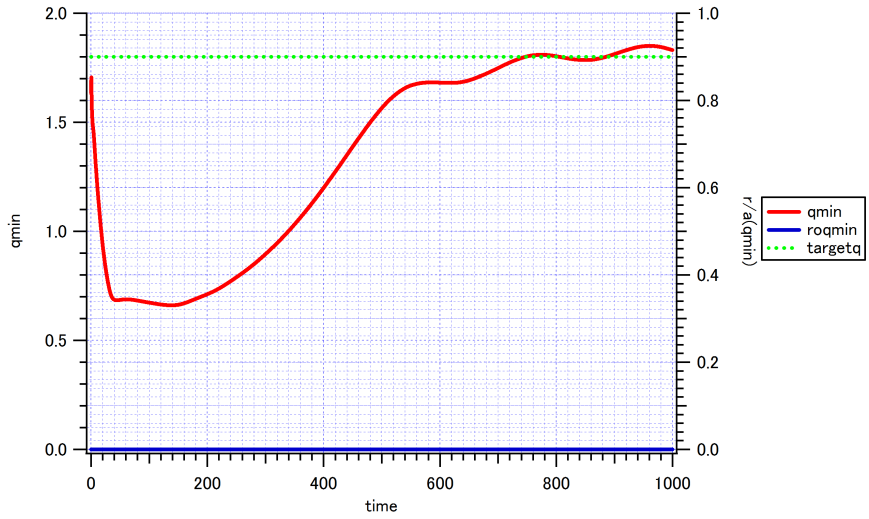

Figure 2.17: The q_{min} time dependence in the simultaneous control simulation without the off-diagonal term ($P_{fus}^{ref} = 350MW, q_{min}^{ref} = 1.8$)

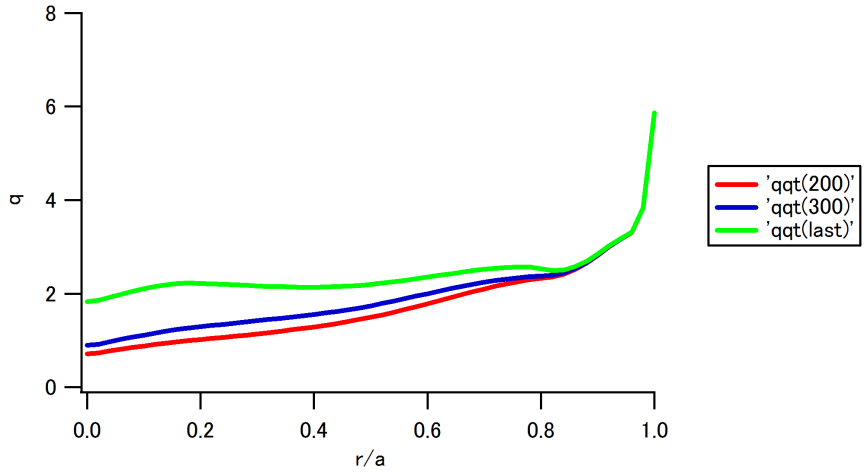

Figure 2.18: The q profile in the simultaneous control simulation without the off-diagonal term ($P_{fus}^{ref} = 350MW, q_{min}^{ref} = 1.8$)

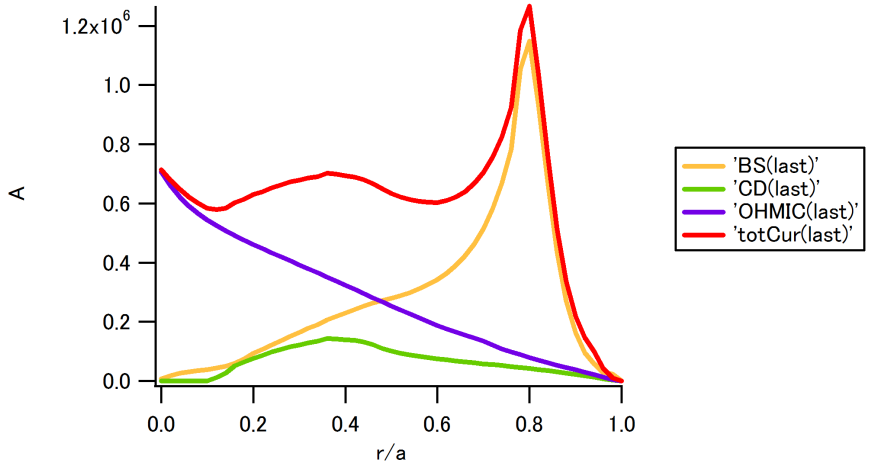

Figure 2.19: The current profile at the steady state in the simultaneous control simulation without the off-diagonal term ($P_{fus}^{ref} = 350MW, q_{min}^{ref} = 1.8$)

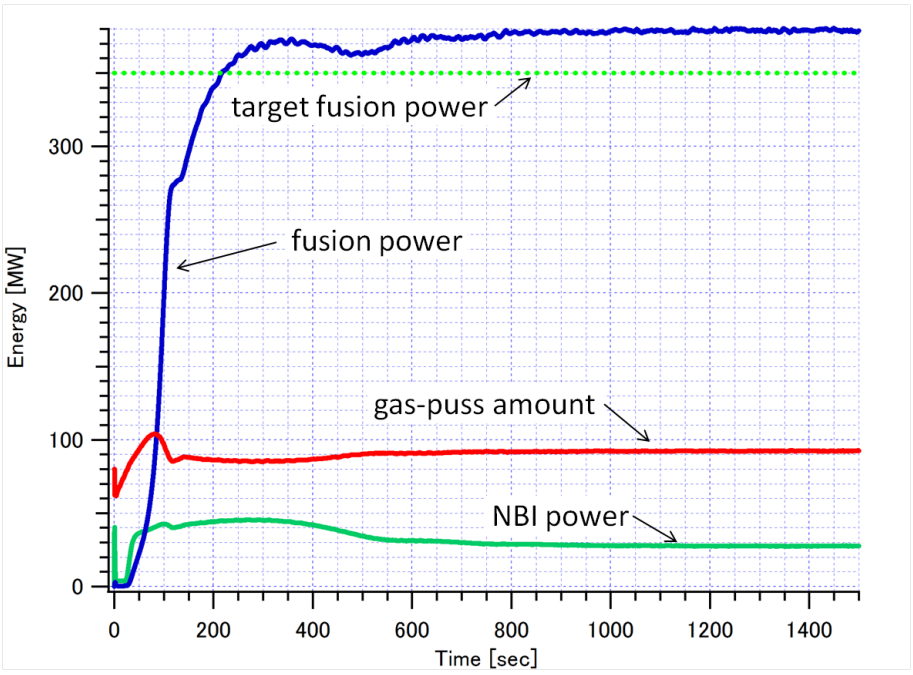

Figure 2.20: The fusion power time dependence in the simultaneous control simulation with the off-diagonal term [75]

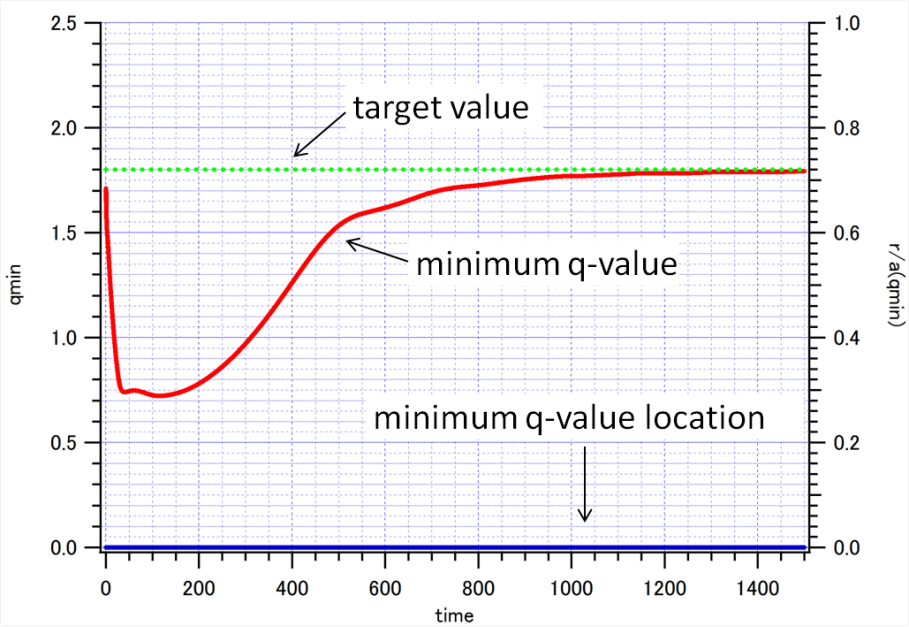

Figure 2.21: The q_{min} time dependence in the simultaneous control simulation with the off-diagonal term [75]

2.6 Summary

For the future reactor, the MIMO controller design is needed. In this chapter, the fusion power and the q_{min} simultaneously control simulation is demonstrated with 1-D code. In this case, the controller is designed from the response characteristics. The results of this simulation show the difficulty of the simultaneous control and the controller design. Especially, the controller design has the high difficulty because of parameters coupling effect. Thus, from the simulation, it seems to be difficult to design the controller from the response characteristics.

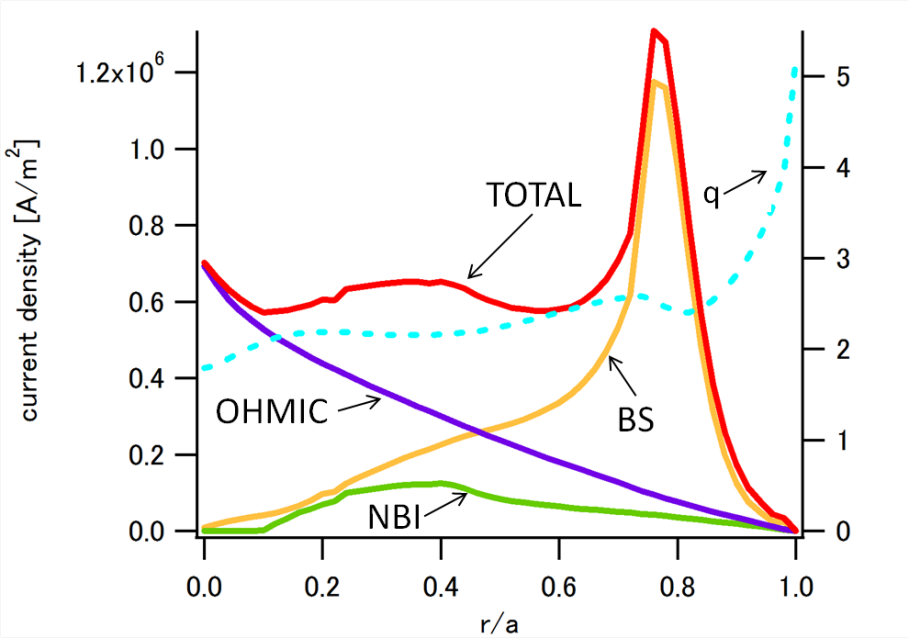

Figure 2.22: The current profile at the steady state in the simultaneous control simulation with the off-diagonal term [75]

Chapter 3

Model based PID control

3.1 Introduction

In previous chapter, the PID controller designed from the response characteristics is used in the 1-D plasma control simulation. From this simulation, the difficulty of the plasma MIMO controller design from the response characteristics is suggested. Thus, this research offer that for the future reactor, the controller should be designed from the physical model. In this chapter, the 0-D plasma MIMO control simulation with the model based PID controller is demonstrated. The part of this chapter is published in as. [29].

3.2 0-D plasma model

To design the controller from the physical model is usual method in the control engineering, and it is called modern control theory. In modern control theory, the physical model is written as the form of time differential equation, and this is called state equation. In this section, the plasma state equation is introduced from the plasma physics [1–3].

3.2.1 Energy equation

For simplification, following approximation is used.

$$2n_D = 2n_T = n_e \equiv n \tag{3.1}$$

$$T_D = T_T = T_e \equiv T \tag{3.2}$$

and

$$W = \frac{3}{2}n_D T_D + \frac{3}{2}n_T T_T + \frac{3}{2}n_e T_e = 3nT \tag{3.3}$$

$$p = p_D + p_T + p_e = 2nT \tag{3.4}$$

From the equations, energy conservation law can be written as follows,

$$\frac{3}{2}\frac{\partial p}{\partial t} + \frac{3}{2}\nabla \cdot p\vec{v} + p\nabla \cdot \vec{v} + \nabla \cdot \vec{q} = S \tag{3.5}$$

This equation is time and space differential equation, thus, to get the state equation, the volume integral of this equation is needed. First, the term of $\vec{q}$ is the heat diffusion and this is defined as follows,

$$\frac{1}{V}\int_V \nabla \vec{q} d\vec{r} = \frac{1}{V}\int_S \vec{q} d\vec{S} \equiv \frac{W}{\tau_e}. \tag{3.6}$$

Second, from the following relation,

$$\nabla p\vec{v} = p\nabla \cdot \vec{v} + \vec{v} \cdot \nabla p \tag{3.7}$$

the following equation can be gotten.

$$\frac{3}{2}\nabla \cdot p\vec{v} + p\nabla \cdot \vec{v} = \frac{5}{2}\nabla \cdot p\vec{v} - \vec{v} \cdot \nabla p \tag{3.8}$$

The integration of this term is written as follows,

$$\int_V \nabla \cdot p\vec{v} d\vec{r} = \int_S p\vec{v} \cdot \vec{n} dS \tag{3.9}$$

and at the surface, $\vec{v} \cdot \vec{n} = 0$, thus, this term is equal to zero, and $\vec{v} \cdot \nabla p$ can be approximated to zero [2]. Finally, the volume integration can be written as follows.

$$\frac{dW}{dt} + \frac{W}{\tau_e} = S_e \tag{3.10}$$

The source term S_e is discussed later.

3.2.2 Density equation

This is from the following continuous equation,

$$\frac{\partial n}{\partial t} + \nabla \cdot (n\vec{v}) = S_p \tag{3.11}$$

Defining the particle confinement time as follows,

$$\frac{1}{V}\int_V \nabla \cdot (n\vec{v}) d\vec{r} = \frac{1}{V}\int_S n\vec{v} d\vec{S} \equiv \frac{n}{\tau_p} \tag{3.12}$$

the volume integral can be written as follows,

$$\frac{dn}{dt} + \frac{n}{\tau_p} = S_p \tag{3.13}$$

Current equation

The differential equation of the plasma current can be written from the torus circuit equation. The circuit equation is written as follows,

$$L_p \frac{d}{dt} I_p = -R_p(I_p - I_{CD}) - \frac{d}{dt}\Phi_{CS} \tag{3.14}$$

where, L_p, R_p, I_{CD} and Φ_{CS} are the plasma inductance, plasma resistance, driven current and the CS coil flux respectively. From this equation, the plasma current equation can be written as follows,

$$\frac{d}{dt} I_p = -\frac{I_p - I_{CD}}{\tau_j} + I_{ind} \tag{3.15}$$

where I_{CD} is the induced current.

3.2.3 Source term

In this case, the source term and loss term are determined as follows [16],

$$I_{BS} = C_{bs}\epsilon^{0.5}\beta_p I[MA] \tag{3.16}$$

$$I_{NBI} = \frac{\gamma}{n_{20}R} P_{NBI}[MW] \tag{3.17}$$

$$S_p = N_{puff} \tag{3.18}$$

$$L_p = \frac{n^2}{2} < \sigma v > V \tag{3.19}$$

$$S_\alpha = \frac{E_\alpha}{4} n^2 < \sigma v > V \tag{3.20}$$

$$S_B = C_B n_{20}^2 T_{10}^{1/2} V \tag{3.21}$$

$$S_h = P_{NBI} \tag{3.22}$$

and

$$T = \frac{W}{3N} \tag{3.23}$$

3.3 First PID control simulation

3.3.1 State equation

From the previous section, the plasma 0-D state equation can be written as follows,

$$\begin{aligned}\frac{d}{dt}\begin{pmatrix} I \\ N \\ W \end{pmatrix} &= \begin{pmatrix} -\frac{I}{\tau_j} + \frac{1}{\tau_j}\left(C_{bs}\epsilon^{0.5}\beta_p I + \frac{\gamma}{n_{20}R}P_{NBI}\right) + \dot{I}_{ind} \\ -\frac{N}{\tau_p} - \frac{n^2}{2} < \sigma v > V + N_{puff} \\ -\frac{W}{\tau_e} + \frac{E_\alpha}{4}n^2 < \sigma v > V - C_B n_{20}^2 T_{10}^{1/2} V + P_{NBI} \end{pmatrix} \\ &= \vec{F}(\vec{x}, \vec{u}) \end{aligned} \tag{3.24}$$

The output vector, state vector and actuator vector are as follows,

$$\vec{y} = \begin{pmatrix} I_p \\ P_{fus} \\ n_e \end{pmatrix} = \begin{pmatrix} I_p \\ \frac{E_\alpha N^2}{V} < \sigma v > \\ \frac{N}{V} \end{pmatrix} = \vec{G}(\vec{x}) \tag{3.25}$$

$$\vec{x} = \begin{pmatrix} I_p \\ N \\ W \end{pmatrix} \tag{3.26}$$

$$\vec{u} = \begin{pmatrix} \dot{I}_{ind} \\ P_{NBI} \\ N_{puff} \end{pmatrix} \tag{3.27}$$

The parameters are as follows [76],

$$\gamma = 0.25, C_{bs} = 0.782, C_b = 0.032 \tag{3.28}$$

$$\tau_p = 1sec, \tau_j = 100sec \tag{3.29}$$

$$\beta_p = 0.7, B_T = 5.3T \tag{3.30}$$

$$R = 6.2m, a = 2.0m, \kappa = 1.7 \tag{3.31}$$

$$V = 830m^3, A_i = 2.5 \tag{3.32}$$

$$\begin{aligned}\tau_e &= HH \times 0.0562 A_i^{0.19} R_p^{1.39} a^{0.58} \kappa^{0.78} B_T^{0.15} I_P^{0.93} n_{19}^{0.41} P_{tot}^{-0.69} \\ &= HH \times 2.453 I_P^{0.93} n_{19}^{0.41} P_{tot}^{-0.69} \end{aligned} \tag{3.33}$$

This state equation is nonlinear, and linearization is needed. Assuming the reference value equals to the equilibrium value, the linearized state equation can be written as follows,

$$\frac{d}{dt}\Delta\mathbf{x} = \mathbf{A}\Delta\mathbf{x} + \mathbf{B}\Delta\mathbf{u} \tag{3.34}$$

$$\Delta\mathbf{y} = \mathbf{C}\Delta\mathbf{x} \tag{3.35}$$

$$\Delta\mathbf{k} = \mathbf{k} - \mathbf{k_{ref}}\ (\mathbf{k} = \mathbf{x}, \mathbf{u}, \mathbf{y}) \tag{3.36}$$

$$\mathbf{F}(\mathbf{x_{ref}}, \mathbf{u_{ref}}) = 0 \tag{3.37}$$

$$\mathbf{y_{ref}} = \mathbf{G}(\mathbf{x_{ref}}) \tag{3.38}$$

$$\mathbf{A} = \left.\frac{\partial \mathbf{F}(\mathbf{x}, \mathbf{u})}{\partial \mathbf{x}}\right|_{\mathbf{x}=\mathbf{x_{ref}}, \mathbf{u}=\mathbf{u_{ref}}} \tag{3.39}$$

$$\mathbf{B} = \left.\frac{\partial \mathbf{F}(\mathbf{x}, \mathbf{u})}{\partial \mathbf{u}}\right|_{\mathbf{x}=\mathbf{x_{ref}}, \mathbf{u}=\mathbf{u_{ref}}} \tag{3.40}$$

$$\mathbf{C} = \left.\frac{\partial \mathbf{G}(\mathbf{x})}{\partial \mathbf{x}}\right|_{\mathbf{x}=\mathbf{x_{ref}}} \tag{3.41}$$

The controller is designed from this linear state equation.

3.3.2 Controller design

To control the $\mathbf{y}$ to the $\mathbf{y_{ref}}$, the $\Delta\mathbf{y}$ have to be zero. In this case, the $\Delta\mathbf{y}$ is required to be moving as follows,

$$\frac{d}{dt}\Delta\mathbf{y} = -\mathbf{K}\Delta\mathbf{y} \tag{3.42}$$

where $\mathbf{K}$ is determined as follows,

$$\mathbf{K} = \begin{pmatrix} 0.01 & 0 & 0 \\ 0 & 1 & 0 \\ 0 & 0 & 1 \end{pmatrix} \tag{3.43}$$

Each diagonal term is determined near the inverse of each parameter's time constant to make the each reference error of the parameter decays to zero with these time constant. to The time differential of the $\Delta\mathbf{y}$ also can be written as follows,

$$\frac{d}{dt}\Delta\mathbf{y} = \frac{d}{dt}\mathbf{C}\Delta\mathbf{x} = \mathbf{C}\frac{d}{dt}\Delta\mathbf{x} \tag{3.44}$$

and

$$\frac{d}{dt}\Delta\mathbf{y} = \mathbf{CA}\Delta\mathbf{x} + \mathbf{CB}\Delta\mathbf{u} \tag{3.45}$$

and

$$\frac{d}{dt}\Delta\mathbf{y} = \mathbf{CAC}^{-1}\Delta\mathbf{y} + \mathbf{CB}\Delta\mathbf{u} \tag{3.46}$$

From eqs. (3.42) and (3.46), the necessary actuator value can be gotten as follows,

$$\Delta\mathbf{u} = (\mathbf{CB})^{-1}\left(\mathbf{K} + \mathbf{CAC}^{-1}\right)(\mathbf{y} - \mathbf{y_{ref}}) \tag{3.47}$$

This is just a proportional controller.
Only with the P control, the reference error or the effect of the disturbance can't be canceled out. Because of this, the integral and differential term should be added. In this case, the following controller is used.

$$\begin{aligned}\Delta\mathbf{u} = (\mathbf{CB})^{-1}\left(\mathbf{K} + \mathbf{CAC}^{-1}\right)(\mathbf{y} - \mathbf{y}_{ref}) - \\ (\mathbf{CB})^{-1}\mathbf{K}_2\int_0^t(\mathbf{y} - \mathbf{y}_{ref})d\tau - \\ (\mathbf{CB})^{-1}\mathbf{K}_3\frac{d}{dt}(\mathbf{y} - \mathbf{y}_{ref}),\end{aligned} \tag{3.48}$$

where

$$\mathbf{K}_2 = \begin{pmatrix} 0.001 & 0 & 0 \\ 0 & 0.1 & 0 \\ 0 & 0 & 0.1 \end{pmatrix}, \tag{3.49}$$

$$\mathbf{K}_3 = \begin{pmatrix} 1.5\times10^{-4} & 0 & 0 \\ 0 & 0.015 & 0 \\ 0 & 0 & 0.015 \end{pmatrix}. \tag{3.50}$$

The $\mathbf{K}_2$ and the $\mathbf{K}_3$ are determined to make the integral, and the differential terms comparable to the proportional term. In this case, $\mathbf{A}, \mathbf{B}$ and $\mathbf{C}$ in eq. (3.48) are the differential value of eq. (3.24) at the reference point. Thus, they depend on the reference values, i.e. the PID gains in eq. (3.48) changes when the target values change in the operation.

3.3.3 Result

In this simulation, the time dependence of eq. (3.24) is solved with the software MATLAB/SIMULINK [77], the actuator value is determined as eq. (3.48). The result is shown in Figs. 3.1 and 3.2

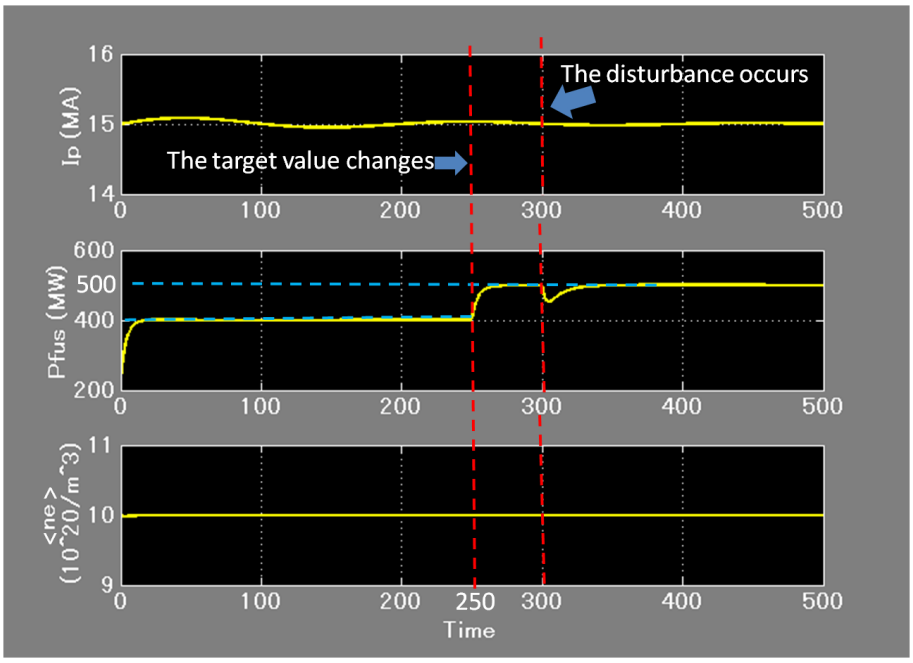

Figure 3.1: The time evaluation of the plasma current I_p, the fusion power P_{fus} and the plasma electron density $< n_e >$. I_p and $< n_e >$ is kept in the constant target value. P_{fus} follows the target value from $400MW$ to $500MW$ at 250sec and is recovered from the disturbance at 300sec [29].

In this simulation, the initial value of $\mathbf{y_{ref}}$ and $\mathbf{x}$ are as follows,

$$\mathbf{y} = \begin{pmatrix} I_p \\ P_{fus} \\ < n_e > \end{pmatrix} = \begin{pmatrix} 15MA \\ 400MW \\ 1.0 \times 10^{20}/m^3 \end{pmatrix}. \tag{3.51}$$

$$\mathbf{x} = \begin{pmatrix} I_p \\ N \\ W \end{pmatrix} = \begin{pmatrix} 15MA \\ 8.3 \times 10^{23} \\ 300MJ \end{pmatrix}. \tag{3.52}$$

During t=0sec to 250sec, each parameter is kept to the reference value. At t=250sec, the fusion power reference is changed to 500MW, then, the fusion power follows to the new reference value smoothly, and the plasma current and the density are kept constant. In this case, the NBI power changed from 66MW to 87MW, and to keep the current, the ohmic current is changed. The gas-puff also changed to keep the density.

At t=300sec, the HH factor changed from 1 to 0.95. At this time, the fusion power decreased around 10 percent, and recovered to the reference

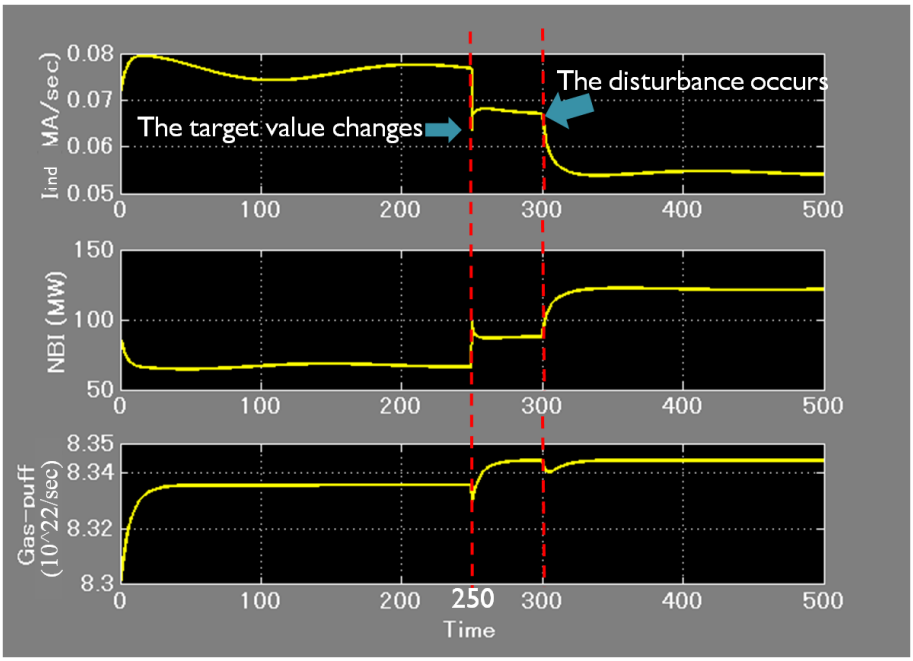

Figure 3.2: The time evaluation of the induced current $\dot{I}_{cs}$, the NBI power and the gas-puff amount. The NBI power changes to take the fusion power to the target value at 250sec and 300sec, at the same time, other two actuators changes to keep the I_p and $< n_e >$ constant [29].

value within a time of 40 sec. At the same time, the actuators changed to keep the other parameters constant.

3.3.4 Summary of this section

With the 0-D plasma model, 3-input(i.e. the ohmic current, the NBI and the gas-puff) 3-output(i.e. the plasma current, the fusion power and the plasma density) control simulation is demonstrated. In spite of this system has the large coupling effect, the fusion power can be controlled independently, and this simulation shows that the high target following performance and the disturbance inhibiting performance. This result suggests the effectiveness of the modern control theory to the plasma control.

In this simulation, however, the model and the method of the controller design has the room of improvement. The improved model, and the controller is discussed in next section.

3.4 PI control simulation with the pole assignment method

3.4.1 Model improvement

The previous simulation is to confirm the effectiveness of the modern control theory, thus the simulation model is quite simple form, and in future, the simulation with the strictly model or the experiment with the controller designed from the modern control theory is needed. In this subsection, as the preparation, equation (3.24) is changed to more strictly model. In this case, τ_j, C_B, C_{bs}, γ is re-adjusted to the ITER, and τ_p is changed to the proportional value of the τ_e.

The current diffusion time

The τ_j can be lead from the following circuit equation,

$$L_p \frac{dI_p}{dt} = -R_p I_p \tag{3.53}$$

where L_p and R_p are the plasma inductance and the plasma resistance respectively. From this equation, τ_j can be written as follows,

$$\tau_j = L_p / R_p \tag{3.54}$$

The plasma resistivity can be written as follows [1, 2],

$$\eta = 1.65 \times 10^{-9} ln\Lambda Z_{eff} (T_e[keV])^{-1.5} \tag{3.55}$$

and each parameter is defined as follows [76],

$$< T_e >= 8.8keV \tag{3.56}$$

$$Z_{eff} = 1.66 \tag{3.57}$$

$$ln\Lambda = 20. \tag{3.58}$$

From these parameters, η is gotten as follows,

$$\eta = 2.098 \times 10^{-9} [\Omega m] \tag{3.59}$$

With the parameters $R = 6.2m, a = 2m$ and $\kappa = 1.6$, finally, plasma resistance can be lead as follows,

$$R_p = 3.516 \times 10^{-9} [\Omega] \tag{3.60}$$

The plasma inductance is written as follows,

$$L_p = \mu_0 R \left(ln \frac{8R}{a} + \frac{l_i}{2} - 2 \right) \tag{3.61}$$

where l_i is internal inductance, and in this case, defined as $l_i = 0.84$, and L_p is lead as follows,

$$L_p = 1.271 \times 10^{-5}[H] \tag{3.62}$$

Finally, τ_j can be written as follows,

$$\tau_j = 3615[sec] \tag{3.63}$$

The NBI current drive efficiency

The γ is derived from refs. [16, 78]. Assuming the D beam, the A_b and the Z_b is defined $A_b = 2, Z_b = 1$, and each parameter can be lead as follows,

$$E_{crit} = 0.1 \times A_b T_1 0 = 0.176[keV] \tag{3.64}$$

$$G = \left(1.55 + \frac{0.85}{Z_{eff}} \right) \left(\frac{\epsilon}{2} \right)^{0.5} - \left(0.2 + \frac{1.55}{Z_{eff}} \right) \left(\frac{\epsilon}{2} \right) = 0.645 \tag{3.65}$$

$$F = 1.0 - \frac{Z_b}{Z_{eff}} (1 - G) = 0.786, \tag{3.66}$$

where ϵ is the inverse of the aspect ratio. Assuming $E_b = 1[MeV]$, the following parameters can be written as

$$x = \left(\frac{E_b}{E_{crit}} \right)^{0.5} = 2.384 \tag{3.67}$$

$$y = \frac{12 Z_{eff}}{5 A_b} = 1.992 \tag{3.68}$$

$$J = \frac{x^2}{4 + 3y + x^2 (x + 1.39 + 0.61 y^{0.7})} = 0.153 \tag{3.69}$$

and with the definition that $R_{tang} = R$,$n_{20L} = 1$,

$$d_b = 2R \left((1 + \frac{a}{R})^2 - \left(\frac{R_{tang}}{R} \right)^2 \right)^{0.5} = 10.73 \tag{3.70}$$

$$f_{sb} = exp \left(-(n_{20L} d_b) \left(\frac{0.775}{E_b} \right)^{0.78} \right) = 1.514 \times 10^{-4} \tag{3.71}$$

can be lead. Finally, with the profile parameter $\alpha_n = 0.5, \alpha_T = 1.0$, the γ can be written as follows,

$$A_{db} = 0.11(1 - 0.35\alpha_n + 0.14\alpha_n^2) \times (1 - 0.21\alpha_T)(1 - 0.2E_b + 0.09E_b^2) = 0.0665 \tag{3.72}$$

$$\gamma = 5 \times A_{db} T_{10}(1 - f_{sb}) \frac{R_{tang}}{R} \times \frac{J}{0.2} F = 0.176 \tag{3.73}$$

The ratio of the boot strap current

The new model of boot strap current is from 'ITER Physics design guideline', and it is as follows,

$$I_{BS} = C_{BS}(\epsilon^{0.5}\beta_p^*)^{1.3} I_p \tag{3.74}$$

$$C_{BS} = 1.32 - 0.235\left(\frac{q_{95}}{q_0}\right) + 0.0185\left(\frac{q_{95}}{q_0}\right)^2 = 0.7815 \tag{3.75}$$

in this equation, from ref. [76], $q_{95}/q_0 = 3$ is used. The β_p^* can be written as follows [78],

$$\beta_p^* = \beta_T \left(\frac{B_T}{B_a}\right)^2 \tag{3.76}$$

$$B_a = \frac{\mu_0 I_p}{2\pi a_p \kappa^{0.5}} \tag{3.77}$$

$$B_T = 5.3 \tag{3.78}$$

$$\beta_t = \beta_{th} + \beta_\alpha \tag{3.79}$$

$$\beta_{th} = \frac{(n_e + n_i)T_e[eV]}{B_T^2/2\mu_0} \tag{3.80}$$

$$\beta_\alpha = f_\alpha \beta_{th} \tag{3.81}$$

$$f_\alpha = 0.029(f_D + f_T)(T_e[keV] - 3.7) \tag{3.82}$$

Bremsstrahlung radiation

C_B is defined as follows

$$C_B = \frac{0.16 Z_{eff}(1 + \alpha_n)^{1.5} \times (1 + \alpha_n + \alpha_T)^{0.5}}{1 + 2\alpha_n + 0.5\alpha_T} = 0.031 \tag{3.83}$$

The particle confinement time

Considering the particle recycling, the τ_p is defined as follows,

$$\tau_p = \alpha \tau_e \tag{3.84}$$

where α is the proportional constant.

3.4.2 PI controller design

The method to define the P gain in section 3.3 is near the pole assignment method [65], and the I and D gain is not determined theoretically. In this section, with the pole assignment method, both the P and I gain is determined. From the new model and the following equation point,

$$\mathbf{y} = \begin{pmatrix} 14.9452MA \\ 400.0611MW \\ 10.0611 \times 10^{19}/m^3 \end{pmatrix} \mathbf{x} = \begin{pmatrix} 14.9452MA \\ 8.3507 \times 10^{22} \\ 363.9389MW \end{pmatrix} \mathbf{u} = \begin{pmatrix} 0.0026MA/sec \\ 69.9981MW \\ 0.3632 \times 10^{22}/sec \end{pmatrix} \tag{3.85}$$

the linearized state equation formed as follows can be gotten,

$$\frac{d}{dt}\Delta\mathbf{y} = \mathbf{A}'\Delta\mathbf{y} + \mathbf{B}'\Delta\mathbf{u} \tag{3.86}$$

$$\mathbf{A}' = \mathbf{CAC}^{-1},\ \mathbf{B}' = \mathbf{CB} \tag{3.87}$$

From eq. (3.86), the following extended state equation can be written,

$$\frac{d}{dt}\begin{pmatrix} \Delta\mathbf{y} \\ \int \Delta\mathbf{y}dt \end{pmatrix} = \begin{pmatrix} \mathbf{A}' & 0 \\ \mathbf{I} & 0 \end{pmatrix}\begin{pmatrix} \Delta\mathbf{y} \\ \int \Delta\mathbf{y}dt \end{pmatrix} + \begin{pmatrix} \mathbf{B}' \\ 0 \end{pmatrix}\mathbf{u} \tag{3.88}$$

Considering the PI control, $\mathbf{u}$ can be written as follows,

$$\mathbf{u} = \begin{pmatrix} -\mathbf{K_p} & -\mathbf{K_i} \end{pmatrix}\begin{pmatrix} \Delta\mathbf{y} \\ \int \Delta\mathbf{y}dt \end{pmatrix} \tag{3.89}$$

Using the actuator eq. (3.89), equation (3.88) can be written as follows,

$$\begin{pmatrix} \Delta\mathbf{y} \\ \int \Delta\mathbf{y}dt \end{pmatrix} = \begin{pmatrix} \mathbf{A}' - \mathbf{B}'\mathbf{K_p} & -\mathbf{B}'\mathbf{K_i} \\ \mathbf{I} & 0 \end{pmatrix}\begin{pmatrix} \Delta\mathbf{y} \\ \int \Delta\mathbf{y}dt \end{pmatrix} \tag{3.90}$$

The solution of eq. (3.90) is linear sum of the exponential functions which time constant equal to the eigen value of the coefficient matrix of eq. (3.90). These time constant is called 'pole'. From the requirement of the 'pole', $\mathbf{K_p}$ and $\mathbf{K_i}$ can be gotten. The algorithm of the pole assignment method is shown in ref. [65]. In this case, to make the high target following performance, with try and error, following pole is used,

$$pole = \begin{pmatrix} -1 & -1 & -1 & -0.1 & -0.1 & -0.1 \end{pmatrix}^t \tag{3.91}$$

and the $\mathbf{K_p}$ and the $\mathbf{K_i}$ are determined as follows,

$$\mathbf{K_p} = \begin{pmatrix} 1.0994 & 0 & -0.0003 \\ 28.6635 & 1.0115 & 35.3735 \\ 0.0658 & 0.0011 & 0.9568 \end{pmatrix},\ \mathbf{K_i} = \begin{pmatrix} 0.1 & 0 & 0 \\ 0 & 0.1094 & 2.9683 \\ 0 & 0.0002 & 0.0877 \end{pmatrix} \tag{3.92}$$

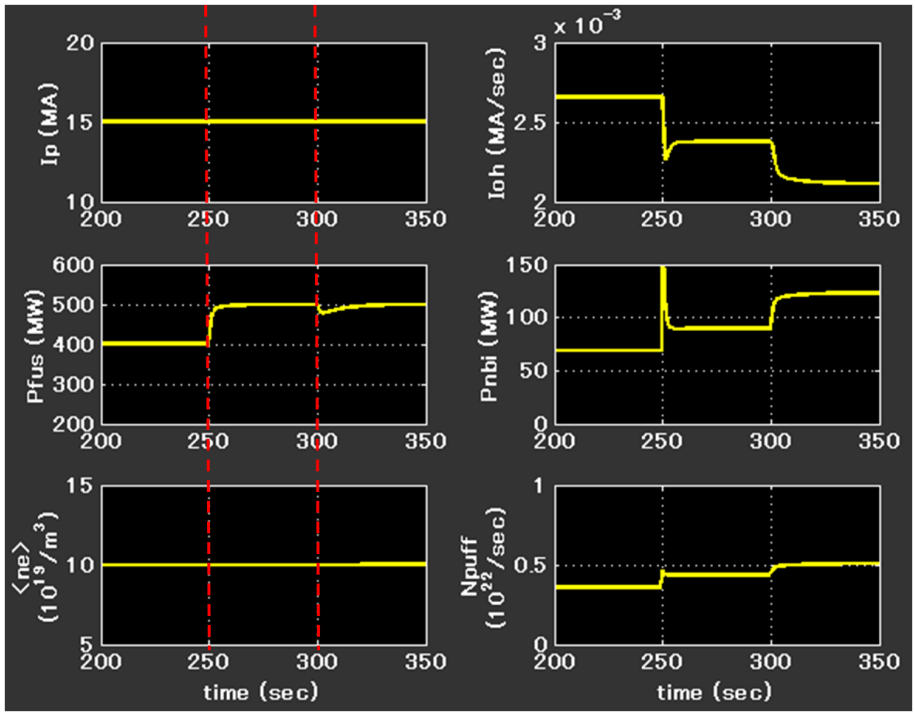

Figure 3.3: The result of the PI control simulation

3.4.3 Result

The simulation result is shown in Fig 3.3. The higher target following performance and the disturbance inhibiting performance than the previous section is shown.

3.5 Summary

In this chapter, the 3 inputs and 3 outputs plasma control simulation is demonstrated with the 0-D plasma model. In this simulation, the controller is designed from the physical model with the modern control theory. The controller is well worked in 0-D plasma model, and this results suggests the effectivity of the modern control theory for the plasma operation. To check the performance of the controller in the more strictly simulation, or the experiment is the future work.

Chapter 4

H infinity control

4.1 Introduction

In the previous chapter, the model based controller design, and the plasma MIMO control simulation is demonstrated. The model, however, doesn't represent the real plasma strictly. Thus, the model error between the real plasma and the controller model exists. The plasma physics is extremely complex and the model error will be large. For this reason, the controller should be designed taking the model error into consideration.

The robust control theory is to minimize the effect of the model error. In this chapter, the typical robust control theory 'H-infinity theory' is used.

4.2 The concept of the H-infinity theory

In H-infinity control theory, the extended state equation as follows is used [51, 74, 79, 80],

$$\frac{d}{dt}\mathbf{x} = \mathbf{A}\mathbf{x} + \mathbf{B_1}\mathbf{w} + \mathbf{B_2}\mathbf{u} \tag{4.1}$$

$$\mathbf{z} = \mathbf{C_1}\mathbf{x} + \mathbf{D_{11}}\mathbf{w} + \mathbf{D_{12}}\mathbf{u} \tag{4.2}$$

$$\mathbf{y} = \mathbf{C_2}\mathbf{x} + \mathbf{D_{21}}\mathbf{w} + \mathbf{D_{22}}\mathbf{u} \tag{4.3}$$

where $\mathbf{z}$ is the value which should be minimize, e.g. the reference error or the actuator value, and $\mathbf{w}$ is the uncontrollable input, e.g. the effect of the model error or the disturbance. This extended state equation can be changed the form of transfer function as follows,

$$\begin{pmatrix} \mathbf{z} \\ \mathbf{y} \end{pmatrix} = \begin{pmatrix} \mathbf{G_{11}}(s) & \mathbf{G_{12}}(s) \\ \mathbf{G_{21}}(s) & \mathbf{G_{22}}(s) \end{pmatrix} \begin{pmatrix} \mathbf{w} \\ \mathbf{u} \end{pmatrix} \tag{4.4}$$

This extended state equation and the transfer function are called 'generalized plant'. Considering the feedback control as $\mathbf{u} = \mathbf{K}(s)\mathbf{y}$, the transfer function from $\mathbf{w}$ to $\mathbf{z}$ can be written as follows,

$$\mathbf{\Phi}(s) = \mathbf{G_{11}}(s) + \mathbf{G_{12}}(s)\mathbf{K}(s)(\mathbf{I} - \mathbf{G_{22}}(s)\mathbf{K}(s))^{-1}\mathbf{G_{21}}(s) \tag{4.5}$$

In H-infinity theory, the controller $\mathbf{K}(s)$ is designed to minimize the 'size' of $\mathbf{\Phi}(s)$ and the 'size' is evaluated as 'H-infinity norm'. The definition of H-infinity norm is shown as follows,

$$\| \overset{\leftrightarrow}{F}(s)\|_\infty = \sup_\omega \sigma\left(\overset{\leftrightarrow}{F}(i\omega)\right) \tag{4.6}$$

This means the maximum gain of the transfer function.

4.3 The theory to solve the H-infinity control problem

The theory to get the H-infinity controller is quite complex. In this section, the summarize of the theory is introduced [51].

4.3.1 Chain-scattering representation

In the case that $\mathbf{G_{21}}$ has the inverse, eq. (4.4) can be changed as follows,

$$\begin{aligned}\begin{pmatrix}\mathbf{z}\\ \mathbf{w}\end{pmatrix} &= \begin{pmatrix}\mathbf{G_{12}} - \mathbf{G_{11}}{\mathbf{G_{21}}}^{-1}\mathbf{G_{22}} & \mathbf{G_{11}}{\mathbf{G_{21}}}^{-1}\\ -{\mathbf{G_{21}}}^{-1}\mathbf{G_{22}} & {\mathbf{G_{21}}}^{-1}\end{pmatrix}\begin{pmatrix}\mathbf{u}\\ \mathbf{y}\end{pmatrix}\\ &= \mathbf{\Sigma}(s)\begin{pmatrix}\mathbf{u}\\ \mathbf{y}\end{pmatrix} = CHAIN(\mathbf{G})\begin{pmatrix}\mathbf{u}\\ \mathbf{y}\end{pmatrix}\end{aligned} \tag{4.7}$$

This $CHAIN(\mathbf{G})$ is called chain-scattering matrix. This transformation is shown in Fig. 4.1.

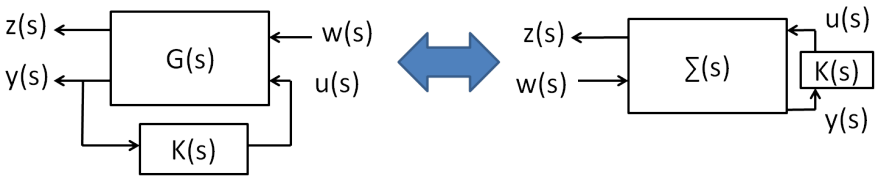

Figure 4.1: The concept of the chain-scattering representation

Using this chain-scattering representation, the star product can be written in simple form. The star product of $\mathbf{G}$ and $\mathbf{U}$ is defined as follows,

$$\begin{pmatrix} \mathbf{G_{11}} & \mathbf{G_{12}} \\ \mathbf{G_{21}} & \mathbf{G_{22}} \end{pmatrix} \otimes \begin{pmatrix} \mathbf{U_{11}} & \mathbf{U_{12}} \\ \mathbf{U_{21}} & \mathbf{U_{22}} \end{pmatrix}$$
$$= \begin{pmatrix} \mathbf{G_{11}} + \mathbf{G_{12}}\mathbf{U_{11}}(\mathbf{I} - \mathbf{G_{22}}\mathbf{U_{11}})^{-1}\mathbf{G_{21}} & \mathbf{G_{12}}(\mathbf{I} - \mathbf{U_{11}}\mathbf{G_{22}})^{-1}\mathbf{U_{12}} \\ \mathbf{U_{21}}(\mathbf{I} - \mathbf{G_{22}}\mathbf{U_{11}})^{-1}\mathbf{G_{21}} & \mathbf{U_{22}} + \mathbf{U_{21}}(\mathbf{I} - \mathbf{G_{22}}\mathbf{U_{11}})^{-1}\mathbf{G_{22}}\mathbf{U_{12}} \end{pmatrix} \quad (4.8)$$

The meaning of the star product is shown in Fig. 4.2.

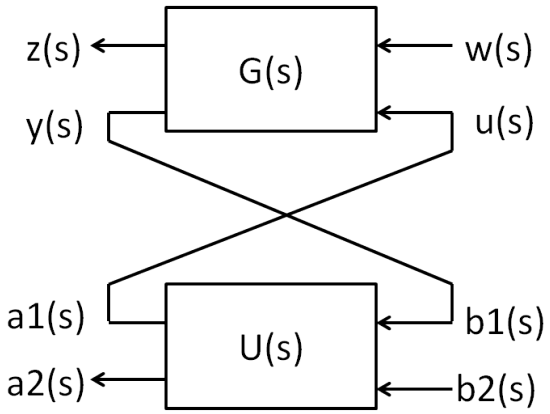

Figure 4.2: The concept of the star product

With the chain-scattering representation, the star product can be written as follows,

$$CHAIN(\mathbf{G} \otimes \mathbf{U}) = CHAIN(\mathbf{G}) \cdot CHAIN(\mathbf{U}) \quad (4.9)$$

This equation represents Fig. 4.3.

4.3.2 J-lossless matrix

Figure 4.4 shows the concept of the solution of the H-infinity control problem.

In Fig. 4.4, $\mathbf{\Theta}(s)$ is called J-lossless matrix. J-lossless matrix is the chain-scattering representation of the lossless matrix. The lossless matrix is defined as follows,

Lossless matrix

In the case that the matrix $\mathbf{S}(s)$ satisfies the following conditions, $\mathbf{S}(s)$ is called lossless matrix.

$$\mathbf{I} - \mathbf{S}^t(-s)\mathbf{S}(s) = 0, \quad \forall s \quad (4.10)$$

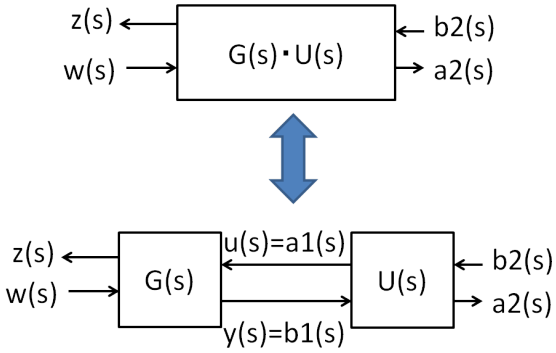

Figure 4.3: The chain-scattering representation of the star product

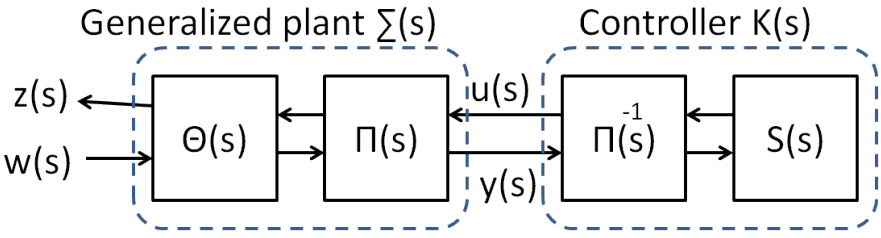

Figure 4.4: The concept of the H-infinity controller

$$\mathbf{I} - \mathbf{S}^*(s)\mathbf{S}(s) \geq 0, \quad \forall Re[s] \geq 0 \tag{4.11}$$

This means that the gain of the lossless matrix is 1.
In fig 4.4, $\mathbf{S}(s)$ is called bounded matrix, and this is defined as follows,

Bounded matrix

In the case that the matrix $\mathbf{S}(s)$ is stable, and satisfies the following condition, $\mathbf{S}(s)$ is called bounded matrix.

$$\mathbf{S}^*(s)\mathbf{S}(s) \leq \mathbf{I}, \quad \forall Re[s] \geq 0 \tag{4.12}$$

Figure 4.4 means that in the case that the chain-scattering representation of the generalized plant $\mathbf{\Sigma}(s)$ can be divided with the J-lossless matrix $\mathbf{\Theta}(S)$ as follows,

$$\mathbf{\Sigma}(s) = \mathbf{\Theta}(s)\mathbf{\Pi}(s) \tag{4.13}$$

the chain scattering representation of the H-infinity controller can be written with the arbitrary bounded matrix $\mathbf{S}(s)$ as follows,

$$\mathbf{K}(s) = \mathbf{\Pi}^{-1}(s)\mathbf{S}(s). \tag{4.14}$$

Thus, the H-infinity controller problem equals to find the suitable J-lossless matrix.

4.3.3 J-lossless conjugation

To find the suitable J-lossless matrix, the J-lossless stabilizing conjugator and the J-lossless anti-stabilizing conjugator are defined as follows,

J-lossless stabilizing conjugator

With the matrix $\mathbf{G}(s)$, in the case that the J-lossless matrix $\mathbf{\Theta}(s)$ satisfies the following conditions,

- $\mathbf{G(s)\Theta}(s)$ is stable
- The order of the $\mathbf{\Theta}(s)$ equals the number of the unstable poles of the $\mathbf{G}(s)$

the $\mathbf{\Theta}(s)$ is called J-lossless stabilizing conjugator of the $\mathbf{G}(s)$, and the operation to multiply the $\mathbf{\Theta}(s)$ is called J-lossless stabilizing conjugation.

J-lossless anti-stabilizing conjugator

With the matrix $\mathbf{G}(s)$, in the case that the J-lossless matrix $\mathbf{\Theta}(s)$ satisfies the following conditions,

- $\mathbf{G(s)\Theta}(s)$ is unstable
- The order of the $\mathbf{\Theta}(s)$ equals the number of the stable poles of the $\mathbf{G}(s)$

the $\mathbf{\Theta}(s)$ is called J-lossless anti-stabilizing conjugator of the $\mathbf{G}(s)$, and the operation to multiply the $\mathbf{\Theta}(s)$ is called J-lossless anti-stabilizing conjugation.

The condition of the J-lossless conjugator exists

The conditions that the system $\mathbf{G}(s) = \mathbf{D} + \mathbf{C}(s\mathbf{I} - \mathbf{A})^{-1}\mathbf{B}$ has the J-lossless (anti-) stable conjugator are as follows,

- The riccati equation

$$\mathbf{XA} + \mathbf{A}^t\mathbf{X} - \mathbf{XBJB}^t\mathbf{X} = 0 \tag{4.15}$$

  has the solution $\mathbf{X} \geq 0$, and

$$\hat{\mathbf{A}} = \mathbf{A} - \mathbf{BJB}^t\mathbf{X} \tag{4.16}$$

  is (anti-) stable.

In this case, the J-lossless (anti-) stable conjugator $\mathbf{\Theta}(s)$ is written as follows,

$$\mathbf{\Theta}(s) = (\mathbf{I} - \mathbf{JB}^t(s\mathbf{I} + \mathbf{A}^t)^{-1}\mathbf{XB})\mathbf{D_c} \tag{4.17}$$

where $\mathbf{D_c}$ is arbitrary J-unitary matrix. The J-unitary matrix is the matrix which satisfies the following equation,

$$\mathbf{D_c}^t(-s)\mathbf{JD_c}(s) = \mathbf{J}, \quad \forall s \tag{4.18}$$

and $\mathbf{J}$ is as follows,

$$\mathbf{J} = \begin{pmatrix} \mathbf{I} & 0 \\ 0 & -\mathbf{I} \end{pmatrix} \tag{4.19}$$

4.3.4 J-lossless dividing

Using the J-lossless conjugator, the J-lossless matrix which can divide the generalized plant $\mathbf{G}(s)$ can be found. With the J-lossless anti-stabilizing conjugator $\mathbf{\Theta}_+(s)$ of the $\mathbf{G}^t(-s)\mathbf{J}$, and the J-lossless stabilizing conjugator $\mathbf{\Theta}_-(s)$ of the $\{\mathbf{J}(\Theta_+^t(-s)\mathbf{JG}(s))\}^{-1}$, $\mathbf{G}(s)$ can be divided as follows,

$$\mathbf{G}(s) = \mathbf{\Theta}_+(s)\mathbf{\Theta}_-(s)\mathbf{\Pi}(s) = \mathbf{\Theta}(s)\mathbf{\Pi}(s) \tag{4.20}$$

4.3.5 The condition of the H-infinity control problem can be solved

To find the H-infinity controller, the J-lossless matrix which can divide the generalized plant have to be found, and to find the J-lossless matrix, 2 J-lossless conjugator are needed. To get the J-lossless conjugator, one riccati equation have to be solved. Thus, to get the H-infinity controller, 2 riccati equation have to be solved. The detail theory of the riccati equation is introduced in ref. [81].

In the case that the system of eqs. (4.1) to (4.3) satisfies the following conditions, the system is called standard plant.

- $(\mathbf{A}, \mathbf{B_2})$ can be stabilized, and $(\mathbf{C_2}, \mathbf{A})$ can be measured
- $rank\mathbf{D_{12}} = p$(full rank), $rank\mathbf{D_{21}} = q$(full rank), and

$$rank \begin{pmatrix} \mathbf{A} - i\omega\mathbf{I} & \mathbf{B_2} \\ \mathbf{C_1} & \mathbf{D_{12}} \end{pmatrix} = n + p, \quad \forall\omega \tag{4.21}$$

$$rank \begin{pmatrix} \mathbf{A} - i\omega\mathbf{I} & \mathbf{B_1} \\ \mathbf{C_2} & \mathbf{D_{21}} \end{pmatrix} = n + q, \quad \forall\omega \tag{4.22}$$

In the case that the system is the standard plant, the conditions that the H-infinity controller exist can be written as follows,

- $\gamma^2\mathbf{I_r} - \mathbf{D_{11}}^t(\mathbf{I_m} - \mathbf{D_{12}}(\mathbf{D_{12}}^t\mathbf{D_{12}})^{-1}\mathbf{D_{12}}^t)\mathbf{D_{11}} > 0$
- $\gamma^2\mathbf{I_m} - \mathbf{D_{11}}^t(\mathbf{I_r} - \mathbf{D_{21}}^t(\mathbf{D_{21}}\mathbf{D_{21}}^t)^{-1}\mathbf{D_{21}})\mathbf{D_{11}} > 0$
- The riccati equation

  $$\mathbf{XA} + \mathbf{A}^t\mathbf{X} - (\mathbf{C_z}^t\mathbf{D_z} + \mathbf{XB})(\mathbf{D_z}^t\mathbf{J}_\gamma\mathbf{D_z})^{-1}(\mathbf{D_z}^t\mathbf{C_z} + \mathbf{B}^t\mathbf{X}) + \mathbf{C_z}^t\mathbf{C_z} = 0 \tag{4.23}$$

  has the solution $\mathbf{X} \geq 0$ and the matrix

  $$\mathbf{A_F} = \mathbf{A} + \mathbf{BF} \tag{4.24}$$

  is stable, where

  $$\mathbf{F} = -(\mathbf{D_z}^t\mathbf{J}_\gamma\mathbf{D_z})^{-1}(\mathbf{D_z}^t\mathbf{C_z} + \mathbf{B}^t\mathbf{X}) \tag{4.25}$$

- The riccati equation

  $$\mathbf{YA}^t + \mathbf{AY} - (\mathbf{B_w}\mathbf{D_w}^t + \mathbf{YC}^t)(\mathbf{D_w}\mathbf{J}'_\gamma\mathbf{D_w}^t)^{-1}(\mathbf{D_w}\mathbf{B_w}^t + \mathbf{BY}) + \mathbf{B_w}\mathbf{B_w}^t = 0 \tag{4.26}$$

has the solution $\mathbf{Y} \geq 0$ and the matrix

$$\mathbf{A_L} = \mathbf{A} + \mathbf{LC} \tag{4.27}$$

is stable, where

$$\mathbf{L} = -(\mathbf{B_w}\mathbf{D_w}^t + \mathbf{Y}\mathbf{C}^t)(\mathbf{D_w}\mathbf{J}'_\gamma\mathbf{D_w}^t)^{-1} \tag{4.28}$$

- $\lambda_{max}(\mathbf{XY}) < \gamma^2$

  where,

$$\mathbf{C_z} = \begin{pmatrix} \mathbf{C_1} \\ 0 \end{pmatrix} \tag{4.29}$$

$$\mathbf{D_z} = \begin{pmatrix} \mathbf{D_{11}} & \mathbf{D_{12}} \\ \mathbf{I_r} & 0 \end{pmatrix} \tag{4.30}$$

$$\mathbf{B_w} = \begin{pmatrix} \mathbf{B_1} & 0 \end{pmatrix} \tag{4.31}$$

$$\mathbf{D_w} = \begin{pmatrix} \mathbf{D_{11}} & \mathbf{I_m} \\ \mathbf{D_{21}} & 0 \end{pmatrix} \tag{4.32}$$

$$\mathbf{J}_\gamma = \begin{pmatrix} \mathbf{I_m} & 0 \\ 0 & -\gamma^2\mathbf{I_r} \end{pmatrix} \tag{4.33}$$

$$\mathbf{J}'_\gamma = \begin{pmatrix} \mathbf{I_r} & 0 \\ 0 & -\gamma^2\mathbf{I_m} \end{pmatrix} \tag{4.34}$$

In the case that these conditions are satisfied, the controller can be written as follows,

$$\frac{d\mathbf{x_k}}{dt} = (\mathbf{A} + \mathbf{BF})\mathbf{x_k} + \mathbf{U}((\mathbf{B_2} + \mathbf{L_z}\mathbf{D_{12}})\xi - \mathbf{L_y}\eta) \tag{4.35}$$

$$\mathbf{u} = \mathbf{F_u}\mathbf{x_k} + \xi \tag{4.36}$$

$$\eta = \mathbf{y} - (\mathbf{C_2} + \mathbf{D_{21}}\mathbf{F_w})\mathbf{x_k} \tag{4.37}$$

$$\mathbf{U} = (\mathbf{I} - \gamma^{-2}\mathbf{YX})^{-1} \tag{4.38}$$

$$\xi = \mathbf{H}(\mathbf{S})\eta \tag{4.39}$$

$$\mathbf{H}(\mathbf{S}) = -(\mathbf{V_{21}}\mathbf{S} + \mathbf{V_{22}})(\mathbf{V_{11}}\mathbf{S} + \mathbf{V_{12}})^{-1} \tag{4.40}$$

$$\mathbf{V} = \begin{pmatrix} \mathbf{V_{11}} & \mathbf{V_{12}} \\ \mathbf{V_{21}} & \mathbf{V_{22}} \end{pmatrix} \tag{4.41}$$

$$\mathbf{F} = \begin{pmatrix} \mathbf{F_w} \\ \mathbf{F_u} \end{pmatrix} \tag{4.42}$$

$$\mathbf{L} = \begin{pmatrix} \mathbf{L_z} & \mathbf{L_y} \end{pmatrix} \tag{4.43}$$

where, $\mathbf{S}$ is the arbitrary transfer function which satisfies $\|\mathbf{S}\|_\infty < 1$ and $\mathbf{V}$ is the conversion matrix which satisfies the following equation,

$$-\mathbf{V}^t \mathbf{D_u}^t (\mathbf{D_w} \mathbf{J}'_\gamma \mathbf{D_w}^t)^{-1} \mathbf{D_u} \mathbf{V} = \mathbf{J_{pq}} \tag{4.44}$$

4.4 Mixture sensitivity function problem

Considering the control of fusion reactor, both of the servo performance (i.e. the target following performance) and the robust performance (i.e. the effect of the model error mitigation performance) are needed.

4.4.1 Sensitivity function

Figure 4.5 shows the closed loop system, where $\mathbf{K}$ is controller, $\mathbf{P}$ is the nominal model (i.e. the model for the controller design) and $\mathbf{\Delta}$ is the model error.

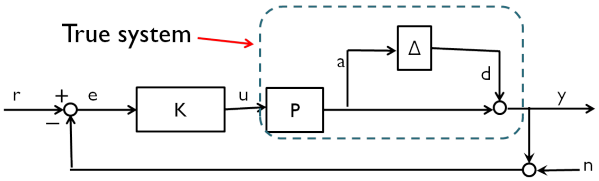

Figure 4.5: The system with the model error

To get the high servo performance, the H-infinity norm of the transfer function from $\mathbf{r}$ to $\mathbf{e}$ should be minimized. This transfer function is formed as follows,

$$\mathbf{S}(s) = (\mathbf{I} + \mathbf{PK})^{-1}. \tag{4.45}$$

This equation is called 'sensitivity function'.

4.4.2 Complementary sensitivity function

Figure 4.5 can be changed to Fig. 4.6.

In Fig. 4.6, $\mathbf{T}$ is written as follows,

$$\mathbf{T}(s) = (\mathbf{I} + \mathbf{PK})^{-1}\mathbf{PK} \tag{4.46}$$

This is called 'complementary sensitivity function'. In the case that $|\mathbf{\Delta T}|_\infty < 1$, the effect of the model error (i.e. the signals from $\mathbf{\Delta}$) is converged to 0.

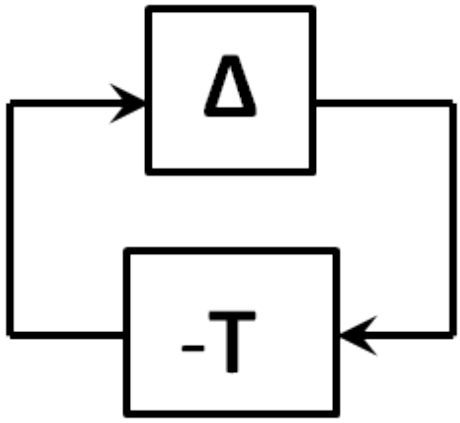

Figure 4.6: The concept of the small gain theory

This is called 'small gain theory'. For the reason of this, to get the high robust performance, the H-infinity norm of $\mathbf{T}$ have to be small.

4.4.3 Mixture sensitivity problem

To get the high servo performance, $\mathbf{S}(s)$ have to be small, and to get the high robust performance, $\mathbf{T}(s)$ have to be small. They have, however, the trade-off relationship as follows,

$$\mathbf{S}(s) + \mathbf{T}(s) = 1 \tag{4.47}$$

Equation (4.47) means that it is impossible to minimize both of $\mathbf{S}(s)$ and $\mathbf{T}(s)$ at the same frequency band. Thus, using the weight function, to minimize the $\mathbf{S}(s)$ at some frequency band, and to minimize the $\mathbf{T}(s)$ at other frequency band are the usual method to tackle this problem. In most case, the servo performance is required at the low frequency, and the effect of the model error becomes large at the high frequency. Thus, with the low-pass weight function $\mathbf{W_s}(s)$ and the high-pass weight function $\mathbf{W_t}(s)$, the controller is designed to satisfy the following condition,

$$\left| \begin{array}{c} \mathbf{W_s}(s)\mathbf{S}(s) \\ \mathbf{W_t}(s)\mathbf{T}(s) \end{array} \right|_\infty < \gamma \tag{4.48}$$

where γ represent the performance of the controller.

4.5 Robust servo controller design

In the mixture sensitivity problem, the figure of the generalized plant is shown in Fig. 4.7.

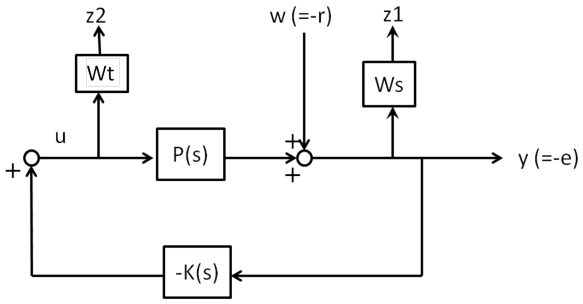

Figure 4.7: The block diagram of the robust servo problem

To converge the reference error to 0, the controller has to have the integrator, i.e. 0 pole. The controller $\mathbf{K}(s)$ has the same pole of $\mathbf{W_s}(s)$. Thus, to design the robust servo controller, $\mathbf{W_s}(s)$ has to have the 0 pole. It is, however, not standard H-infinity problem. In this research the controller is designed with the Dr. Mita's method [74, 82, 83]. This is one of the methods of solving the un-standard H-infinity problem. Other methods have been researched [84–86]

4.5.1 Weight function selection

To converge the reference error, $W_s(s)$ is determined to has the integrator as follows,

$$\mathbf{W}_s = \begin{pmatrix} 1/s & 0 & 0 \\ 0 & 1/s & 0 \\ 0 & 0 & 1/s \end{pmatrix}. \tag{4.49}$$

In the case that $\mathbf{\Delta}$ can be estimated from the experiment or the strictly simulation, $\mathbf{W_t}(s)$ is determined from $\mathbf{\Delta}$. In this simulation, $\mathbf{W_t}(s)$ is designed from some try and error and not from $\mathbf{\Delta}$. The estimation of Δ is the future work. In this case, the following $\mathbf{W_t}(s)$ is used.

$$\mathbf{W}_t = \begin{pmatrix} \frac{5s}{s+100} & 0 & 0 \\ 0 & \frac{0.1s}{s+300} & 0 \\ 0 & 0 & \frac{5s}{s+100} \end{pmatrix} \tag{4.50}$$

This is designed to make the H-infinity problem has the solution, and to suppress the actuator values to the low values.

The theoretical method of determine the weight function have been researched [87–90].

4.5.2 Controller design

Solving the two riccati equations

In Fig. 4.7, $\mathbf{P}(s)$ is the nominal plant, and it is written with the coefficient matrix of the linearized state equation as follows,

$$\mathbf{P}(s) = \mathbf{C_0}(s\mathbf{I} - \mathbf{A_0})^{-1}\mathbf{B_0} \tag{4.51}$$

The $\mathbf{W_s}(s)$ and the $\mathbf{W_t}(s)$ also can be written as follows,

$$\mathbf{W_s}(s) = \mathbf{C_s}(s\mathbf{I} - \mathbf{A_s})^{-1}\mathbf{B_s} \tag{4.52}$$

$$\mathbf{W_t}(s) = \mathbf{C_t}(s\mathbf{I} - \mathbf{A_t})^{-1}\mathbf{B_t} + \mathbf{D_t} \tag{4.53}$$

$$\mathbf{A}_s = \mathbf{D}_s = 0 \tag{4.54}$$

$$\mathbf{B}_s = \mathbf{C}_s = \mathbf{I} \tag{4.55}$$

$$\mathbf{A}_t = \begin{pmatrix} -100 & 0 & 0 \\ 0 & -300 & 0 \\ 0 & 0 & -100 \end{pmatrix} \tag{4.56}$$

$$\mathbf{D}_t = \begin{pmatrix} 5 & 0 & 0 \\ 0 & 0.1 & 0 \\ 0 & 0 & 5 \end{pmatrix} \tag{4.57}$$

$$\mathbf{B}_t = \mathbf{I} \tag{4.58}$$

$$\mathbf{C}_t = \mathbf{A}_t\mathbf{D}_t \tag{4.59}$$

Finally, the generalized plant can be written as the following form,

$$\dot{\mathbf{x}} = \begin{pmatrix} 0 & 0 & \mathbf{B}_s\mathbf{C}_0 \\ 0 & \mathbf{A}_t & 0 \\ 0 & 0 & \mathbf{A}_0 \end{pmatrix}\mathbf{x} + \begin{pmatrix} \mathbf{B}_s \\ 0 \\ 0 \end{pmatrix}\mathbf{w} + \begin{pmatrix} 0 \\ \mathbf{B}_t \\ \mathbf{B}_0 \end{pmatrix}\mathbf{u} \tag{4.60}$$

$$\mathbf{z} = \begin{pmatrix} \mathbf{C}_s & 0 & 0 \\ 0 & \mathbf{C}_t & 0 \end{pmatrix}\mathbf{x} + \begin{pmatrix} 0 \\ 0 \end{pmatrix}\mathbf{w} + \begin{pmatrix} 0 \\ \mathbf{D}_t \end{pmatrix}\mathbf{u} \tag{4.61}$$

$$\mathbf{y} = \begin{pmatrix} 0 & 0 & \mathbf{C}_0 \end{pmatrix}\mathbf{x} + \mathbf{I}\mathbf{w} + (0)\,\mathbf{u} \tag{4.62}$$

To solve the H-infinity control problem, the following variables are defined from the generalized plant.

$$\mathbf{A} = \begin{pmatrix} 0 & 0 & \mathbf{B}_s\mathbf{C}_0 \\ 0 & \mathbf{A}_t & 0 \\ 0 & 0 & \mathbf{A}_0 \end{pmatrix} \tag{4.63}$$

$$\mathbf{B}_1 = \begin{pmatrix} \mathbf{B}_s \\ 0 \\ 0 \end{pmatrix} \tag{4.64}$$

$$\mathbf{B}_2 = \begin{pmatrix} 0 \\ \mathbf{B}_t \\ \mathbf{B}_0 \end{pmatrix} \tag{4.65}$$

$$\mathbf{C}_1 = \begin{pmatrix} \mathbf{C}_s & 0 & 0 \\ 0 & \mathbf{C}_t & 0 \end{pmatrix} \tag{4.66}$$

$$\mathbf{C}_2 = \begin{pmatrix} 0 & 0 & \mathbf{C}_0 \end{pmatrix} \tag{4.67}$$

$$\mathbf{D}_{12} = \begin{pmatrix} 0 \\ \mathbf{D}_t \end{pmatrix} \tag{4.68}$$

$$\mathbf{D}_{21} = \mathbf{I} \tag{4.69}$$

$$\mathbf{D}_{11} = \mathbf{D}_{22} = 0 \tag{4.70}$$

and

$$\mathbf{D}_{12}^{\dagger} = \begin{pmatrix} 0 & \mathbf{D}_t^{-1} \end{pmatrix} \tag{4.71}$$

$$\mathbf{D}_{12}^{\perp} = \begin{pmatrix} \mathbf{I} & 0 \end{pmatrix} \tag{4.72}$$

$$\mathbf{D}_{21}^{\dagger} = \mathbf{I} \tag{4.73}$$

$$\mathbf{D}_{21}^{\perp} = 0 \tag{4.74}$$

From these variables, the first riccati equation is written as follows,

$$\mathbf{A}\mathbf{X} + \mathbf{X}\mathbf{A}^T - \mathbf{X}\tilde{\mathbf{B}}\mathbf{R}^{-1}\tilde{\mathbf{B}}^T\mathbf{X} + \mathbf{Q} = 0 \tag{4.75}$$

where

$$\tilde{\mathbf{B}} = \begin{pmatrix} \mathbf{B}_1/\gamma & \mathbf{B}_2\mathbf{D}_t^{-1} \end{pmatrix} \tag{4.76}$$

$$\mathbf{R} = \begin{pmatrix} -\mathbf{I} & 0 \\ 0 & \mathbf{I} \end{pmatrix} \tag{4.77}$$

$$\mathbf{Q} = (\mathbf{D}_{12}^{\perp}\mathbf{C}_1)^T(\mathbf{D}_{12}^{\perp}\mathbf{C}_1) \tag{4.78}$$

and in this case, $\gamma = 0.5$. The answer of this equation is as follows,

$$\mathbf{X} = 1.0e+03 \times \begin{pmatrix} 0.0127 & -0.0000 & -0.0004 & 0.1208 & -0.0000 \\ -0.0000 & 0.0001 & 0.0000 & -0.0000 & 0.0001 \\ -0.0004 & 0.0000 & 0.0045 & -0.0038 & 0.0002 \\ 0.1208 & -0.0000 & -0.0038 & 1.2665 & -0.0002 \\ -0.0000 & 0.0001 & 0.0002 & -0.0002 & 0.0003 \\ -0.0036 & -0.0008 & 0.0416 & -0.0348 & -0.0001 \\ 0.0061 & 0.0000 & -0.0002 & 0.0602 & 0.0000 \\ -0.0002 & -0.0003 & 0.0018 & -0.0016 & -0.0003 \\ -0.0000 & 0.0000 & 0.0000 & -0.0000 & 0.0000 \end{pmatrix}$$
$$\begin{pmatrix} -0.0036 & 0.0061 & -0.0002 & -0.0000 \\ -0.0008 & 0.0000 & -0.0003 & 0.0000 \\ 0.0416 & -0.0002 & 0.0018 & 0.0000 \\ -0.0348 & 0.0602 & -0.0016 & -0.0000 \\ -0.0001 & 0.0000 & -0.0003 & 0.0000 \\ 0.5127 & -0.0018 & 0.0227 & -0.0003 \\ -0.0018 & 0.0030 & -0.0001 & 0.0000 \\ 0.0227 & -0.0001 & 0.0017 & -0.0001 \\ -0.0003 & 0.0000 & -0.0001 & 0.0000 \end{pmatrix} \tag{4.79}$$

The second riccati equation is written as follows,

$$\mathbf{Y}(\mathbf{A}-\mathbf{B}_1\mathbf{D}_{21}^{\dagger}\mathbf{C}_2)^T+(\mathbf{A}-\mathbf{B}_1\mathbf{D}_{21}^{\dagger}\mathbf{C}_2)\mathbf{Y}+\mathbf{Y}(\mathbf{C}_1^T\mathbf{C}_1/\gamma^2-\mathbf{C}_2^T\mathbf{C}_2)\mathbf{Y} = 0 \tag{4.80}$$

This equation has no stable answer, thus, the quasi-stable answer have to be used and lead from following method.

First, finding the matrix $\mathbf{U}$ which satisfies the following condition,

$$\mathbf{U}(\mathbf{A} - \mathbf{B}_1\mathbf{D}_{21}^{\dagger}\mathbf{C}_2) = \mathbf{A}_q\mathbf{U} \tag{4.81}$$

$$\mathbf{U}\mathbf{B}_1\mathbf{D}_{21}^{\perp} = 0 \tag{4.82}$$

$$\mathbf{U}\mathbf{B}_2 = 0 \tag{4.83}$$

in this case, $\mathbf{A_q} = 0$ and $\mathbf{U}$ can be determined as follows,

$$\mathbf{U} = \begin{pmatrix} \mathbf{I} & 0 & 0 \end{pmatrix} \tag{4.84}$$

With the $\mathbf{U}$ and the suitable co-basis matrix $\mathbf{H}$, the regular matrix $\mathbf{T}$ can be defined as follows,

$$\mathbf{T} = \begin{pmatrix} \mathbf{H} \\ \mathbf{U} \end{pmatrix} = \begin{pmatrix} 0 & 0 & \mathbf{I} \\ 0 & \mathbf{I} & 0 \\ \mathbf{I} & 0 & 0 \end{pmatrix} \tag{4.85}$$

In this case, $\mathbf{T}^{-1} = \mathbf{T}^T = \mathbf{T}$. With $\mathbf{T}$, following variable transformation can be done,

$$\tilde{\mathbf{A}} = \mathbf{T}^{-1}(\mathbf{A} - \mathbf{B}_1\mathbf{D}_{21}^{\dagger}\mathbf{C}_2)\mathbf{T} = \begin{pmatrix} \mathbf{A}_0 & 0 & 0 \\ 0 & \mathbf{A}_t & 0 \\ 0 & 0 & 0 \end{pmatrix} \tag{4.86}$$

$$\mathbf{A}_1 = \begin{pmatrix} \mathbf{A}_0 & 0 \\ 0 & \mathbf{A}_t \end{pmatrix} \tag{4.87}$$

$$\tilde{\mathbf{C}}_1 = \mathbf{T}^{-1}\mathbf{C}_1^T = \begin{pmatrix} 0 & 0 \\ 0 & \mathbf{C}_t^T \\ \mathbf{C}_s^T & 0 \end{pmatrix} \tag{4.88}$$

$$\mathbf{C}_{11} = \begin{pmatrix} 0 & 0 \\ 0 & \mathbf{C}_t^T \end{pmatrix} \tag{4.89}$$

$$\tilde{C}_2 = \mathbf{T}^{-1}\mathbf{C}_2^T = \begin{pmatrix} \mathbf{C}_0^T \\ 0 \\ 0 \end{pmatrix} \tag{4.90}$$

$$\mathbf{C}_{22} = \begin{pmatrix} \mathbf{C}_0^T \\ 0 \end{pmatrix} \tag{4.91}$$

$$\tilde{\mathbf{Y}} = \mathbf{T}^T\mathbf{Y}\mathbf{T} \tag{4.92}$$

Then, multiplying $\mathbf{T}^t$ from left and multiplying $\mathbf{T}$ from right to eq. (4.80), following riccati equation can be lead.

$$\tilde{\mathbf{Y}}\tilde{\mathbf{A}}^T + \tilde{\mathbf{A}}\tilde{\mathbf{Y}} + \tilde{\mathbf{Y}}(\tilde{\mathbf{C}}_1\tilde{\mathbf{C}}_1^T/\gamma^2 - \tilde{\mathbf{C}}_2\tilde{\mathbf{C}}_2^T)\tilde{\mathbf{Y}} = 0 \tag{4.93}$$

The answer of this equation can be written as the following form,

$$\tilde{\mathbf{Y}} = \begin{pmatrix} \mathbf{Y}_1 & 0 \\ 0 & 0 \end{pmatrix} \tag{4.94}$$

where $\mathbf{Y_1}$ is 6×6 matrix. Finally, following lower order riccati equation can be gotten,

$$\mathbf{Y}_1\mathbf{A}_1^T + \mathbf{A}_1\mathbf{Y}_1 - \mathbf{Y}_1\begin{pmatrix} \mathbf{C}_{11}/\gamma & \mathbf{C}_{22} \end{pmatrix}\begin{pmatrix} -\mathbf{I} & 0 \\ 0 & \mathbf{I} \end{pmatrix}\begin{pmatrix} \mathbf{C}_{11}/\gamma & \mathbf{C}_{22} \end{pmatrix}^T\mathbf{Y}_1 = 0 \tag{4.95}$$

In this case, finally the $\mathbf{Y}$ becomes as follows,

$$\mathbf{Y} = 0 \tag{4.96}$$

Controller design

With $\mathbf{X}, \mathbf{Y}$ from the previous subsection, the following variables are defined.

$$\mathbf{E}_{12} = \mathbf{D}_{12}^T\mathbf{D}_{12} \tag{4.97}$$

$$\mathbf{E}_{21} = \mathbf{D}_{21}\mathbf{D}_{21}^T \tag{4.98}$$

and

$$\mathbf{Z} = (\mathbf{I} - \mathbf{YX})^{-1} \tag{4.99}$$

$$\mathbf{L}_\infty = -\mathbf{B}_1\mathbf{D}_{21}^\dagger - \mathbf{Y}\mathbf{C}_2^T\mathbf{E}_{21}^{-1} \tag{4.100}$$

$$\mathbf{F}_\infty = -\mathbf{D}_{12}^\dagger\mathbf{C}_1 - \mathbf{E}_{12}^{-1}\mathbf{B}_2^T\mathbf{X} \tag{4.101}$$

$$\hat{\mathbf{C}}_2 = \mathbf{C}_2 + \mathbf{D}_{21}\mathbf{B}_1^T\mathbf{X} \tag{4.102}$$

$$\hat{\mathbf{B}}_2 = \mathbf{B}_2 + \mathbf{Y}\mathbf{C}_1^T\mathbf{D}_{12} \tag{4.103}$$

$$\hat{\mathbf{A}} = \mathbf{A} + \mathbf{B}_1\mathbf{B}_1^T\mathbf{X} + \mathbf{B}_2\mathbf{F}_\infty + \mathbf{Z}\mathbf{L}_\infty\hat{\mathbf{C}}_2 \tag{4.104}$$

In this research, the central solution is used, and the answer is written as follows,

$$-\mathbf{K}(s) = -\mathbf{F}_\infty(s\mathbf{I} - \hat{\mathbf{A}})^{-1}\mathbf{Z}\mathbf{L}_\infty \tag{4.105}$$

Finally, as the form of the state equation, the controller is designed as follows,

$$\dot{\mathbf{x}}_k = \hat{\mathbf{A}}\mathbf{x} + \mathbf{Z}\mathbf{L}_\infty(\mathbf{r} - \mathbf{y}) \tag{4.106}$$

$$\mathbf{u} = \mathbf{F}_\infty\mathbf{x}_k \tag{4.107}$$

and

$$\hat{\mathbf{A}} = \begin{pmatrix} 0 & 0 & 0 & 0 & 0 \\ 0 & 0 & 0 & 0 & 0 \\ 0 & 0 & 0 & 0 & 0 \\ -5.0766 & -0.0026 & -0.0521 & -53.0950 & -0.0008 \\ 1.0700 & -10.2211 & -25.2942 & -1.2812 & -27.6691 \\ 0.0511 & 0.0387 & -1.9509 & 0.1999 & 0.0077 \\ -5.0766 & -0.0027 & -0.0523 & 46.9049 & 0.0013 \\ 0.0494 & 0.0549 & -1.9109 & 0.2019 & -0.4235 \\ 0.3317 & -3.1686 & -7.8412 & -0.3972 & 84.4228 \end{pmatrix}$$

$$\begin{pmatrix} 0 & 0 & 0 & 0 \\ 0 & 0 & 0 & 0 \\ 0 & 0 & 0 & 0 \\ 0.2045 & -2.5360 & 0.0018 & -0.0019 \\ -0.4424 & -2.1633 & 29.9877 & -4.1031 \\ -23.9901 & 0.0065 & -1.2449 & 0.0070 \\ 0.2045 & -2.5364 & 0.0020 & -0.0019 \\ 76.0106 & 0.0303 & -1.2919 & 0.0121 \\ -0.1371 & 8.2151 & 12.2580 & -1.4474 \end{pmatrix} \tag{4.108}$$

$$\mathbf{ZL}_\infty = \begin{pmatrix} -1 & 0 & 0 \\ 0 & -1 & 0 \\ 0 & 0 & -1 \\ 0 & 0 & 0 \\ 0 & 0 & 0 \\ 0 & 0 & 0 \\ 0 & 0 & 0 \\ 0 & 0 & 0 \\ 0 & 0 & 0 \end{pmatrix} \tag{4.109}$$

$$\mathbf{F}_\infty = \begin{pmatrix} -5.0766 & -0.0026 & -0.0521 & 46.9050 & -0.0008 \\ 1.0700 & -10.2211 & -25.2942 & -1.2812 & 272.3309 \\ 0.0511 & 0.0387 & -1.9509 & 0.1999 & 0.0077 \\ 0.2045 & -2.5360 & 0.0018 & -0.0019 \\ -0.4424 & -2.1633 & 29.9877 & -4.1031 \\ 76.0099 & 0.0065 & -1.2449 & 0.0070 \end{pmatrix} \tag{4.110}$$

4.6 Simulation result

The condition of the simulation is same to the simulation in chapter 3, and the results are shown in Fig. 4.8 and Fig. 4.9.

In Fig. 4.8, the higher robust and servo performance are shown than chapter 3. Figure 4.9 shows, however, that at the time that the reference value changes or the disturbance occurred, the actuators get the severe request. In this case, the request of the NBI power is over 700MW but the limitation of the NBI is set to 150MW.

In this simulation, the controller is designed from the linearized model of 0-D plasma model, but the time development of the parameters are solved from the nonlinear model. Thus, this result shows the robustness of the controller.

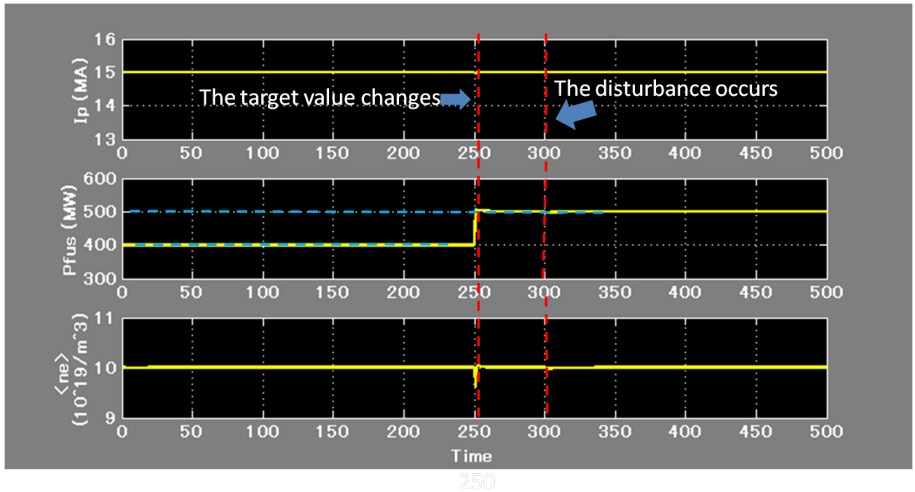

Figure 4.8: The result of the H_∞ robust servo simulation (controlled parameters)

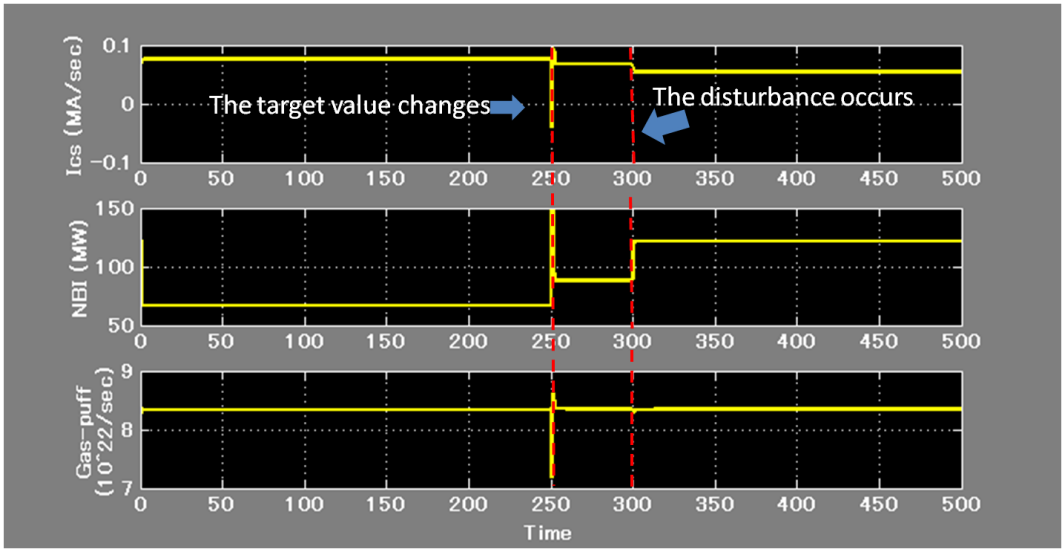

Figure 4.9: The result of the H_∞ robust servo simulation (actuators)

4.7 Comparison of the H-infinity and PI controller

4.7.1 The simulation conditions

To compare the performance of the H-infinity controller and the PI controller, the following 96 simulations with the PI and H-infinity controller are done.

- The limit of the NBI power = 150MW, 100MW, 85MW, 70MW
- $\alpha = \tau_p/\tau_e = 5$, 10 , 20
- The reference value of the $Pfus$ changes from 400MW to 320MW and 480 MW
- The reference value of the $< ne >$ changes from $1.0 \times 10^{20}/m^3$ to $0.8 \times 10^{20}/m^3$ and $1.2 \times 10^{20}/m^3$
- HH factor changes from 1 to 0.9 and 1.1
- α changes from each value to its 0.8 and 1.2 times value

In each simulation, the H-infinity controller designed in section 4.5 is used, and the following PI controller is used.

$$\mathbf{K_p} = \begin{pmatrix} 2.0010 & 0 & -0.0003 \\ 28.6635 & 7.4989 & 35.3735 \\ 0.0658 & 0.0011 & 1.7599 \end{pmatrix} \tag{4.111}$$

$$\mathbf{K_i} = \begin{pmatrix} 0.0011 & 0 & 0 \\ 0 & 1.3273 & 2.9683 \\ 0 & 0.0002 & 0.0170 \end{pmatrix} \tag{4.112}$$

In this case, the pole of the system is as follows,

$$pole = (\ -7.2530 \quad -2.0011 \quad -1.9949 \quad -0.0005 \quad -0.1771 \quad -0.0094\ )^t \tag{4.113}$$

This PI controller is re-designed from the controller in chapter 3 to conform the diagonal low frequency component of the PI controller's bode diagram to that of H-infinity controller shown as Fig. 4.10. In Fig. 4.10, the blue line represents the H_∞ controller and the green line represents the MIMO PI controller, and the parts surrounded by the red circle show the diagonal bode diagrams(i.e. the bode diagram from the reference error of I_p to the I_{oh}, the P_{fus} to the P_{nbi} and the $< ne >$ to the N_{puff}) of both controllers are same in the low frequency band.

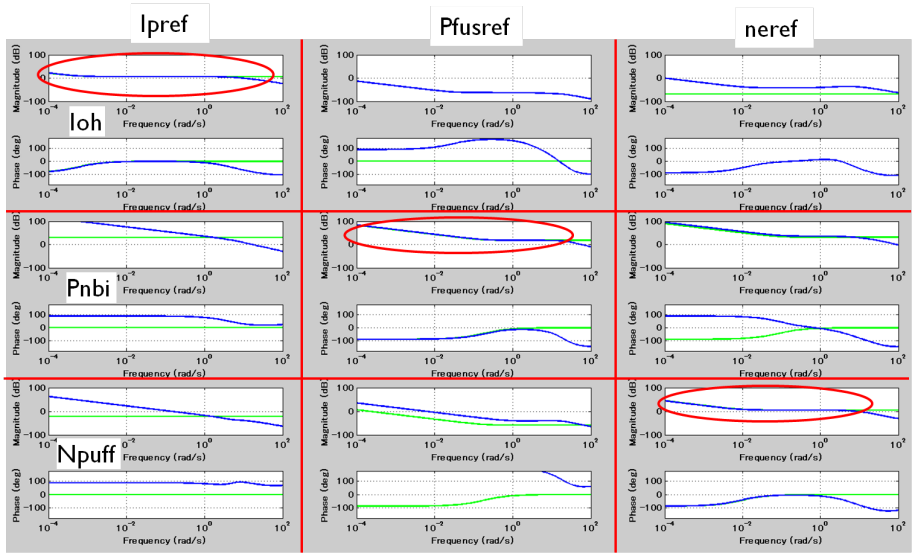

Figure 4.10: The bode diagram of the PI (green line) and the H-infinity (blue line) controller

4.7.2 Simulation results

In the cases of $\alpha = 5, 10, 20$, the behavior of the controllers are not difference, thus, only the results of the case that $\alpha = 10$ are shown in this subsection.

The case with the change of the $Pfus$ reference

Figure 4.11 shows the $NBI_{lim} = 150MW$ and P_{fus}^{ref} increases pattern simulation. Both with the H-infinity controller and the PI controller, P_{fus} follows the new reference value, and the following time is about 1 sec. The NBI_{lim} decrease, the following time becomes longer. Figure 4.12 shows the $NBI_{lim} = 85MW$ case simulation. This shows that the following time is about 15sec, and the perturbation of the density in the case of the H-infinity controller is larger than that of the PI controller.

Figure 4.13 shows the $NBI_{lim} = 150MW$ and P_{fus}^{ref} decreases pattern simulation. The controller behavior in the other NBI_{lim} case, are not difference from this case. In this case, both of PI and H-infinity controller make the NBI power to 0 and the P_{fus} decrease as the same time constant and the perturbation of the density in the case of the H-infinity controller is larger than that of the PI controller.

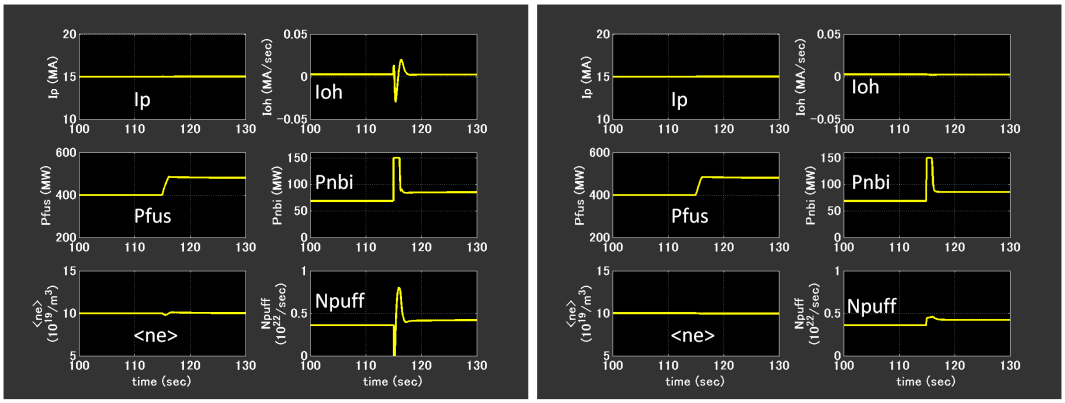

Figure 4.11: The case that $NBI_{lim} = 150MW and P_{fus}^{ref}$ increases

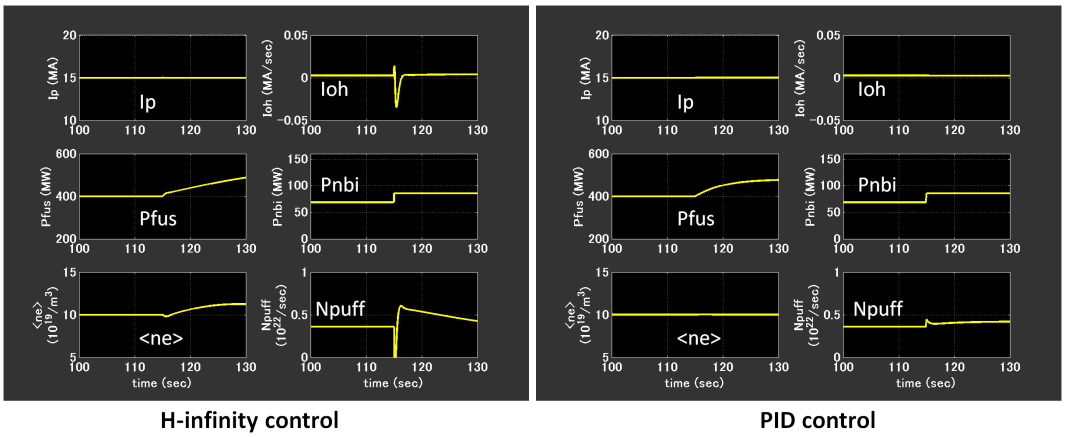

Figure 4.12: The case that $NBI_{lim} = 85MW and P_{fus}^{ref}$ increases

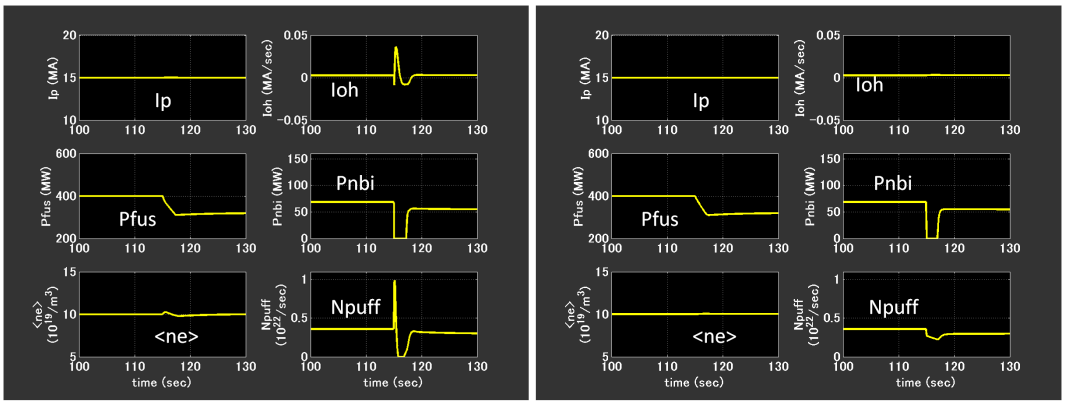

Figure 4.13: The case that $NBI_{lim} = 150MW and P_{fus}^{ref}$ decreases

The case with the change of the $< ne >$ reference value

Figure 4.14 shows that the case of $NBI_{lim} = 150MW$ and the reference value of $< ne >$ increases. Both of the PI and the H-infinity control, $< ne >$ changes to the reference value at about 1sec. In this case, the NBI power increases to keep the temperature constant. Thus, the NBI_{lim} decrease, the fusion power changes. Figure 4.15 shows that the case of $NBI_{lim} = 70MW$. In Fig. 4.15, in the case of PI controller, the fusion power undershoots and recovers about 15sec, while H-infinity controller, the parameters are not controlled.

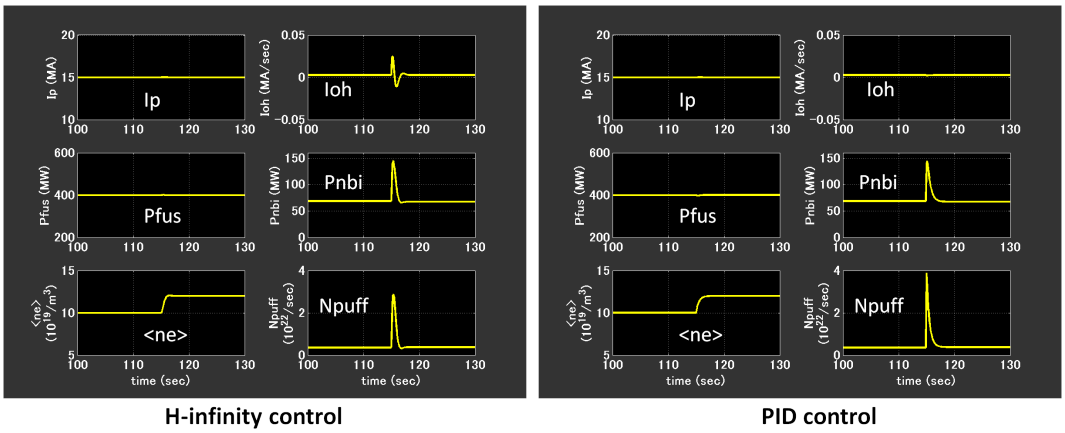

Figure 4.14: The case that $NBI_{lim} = 150MW and < ne >^{ref}$ increases

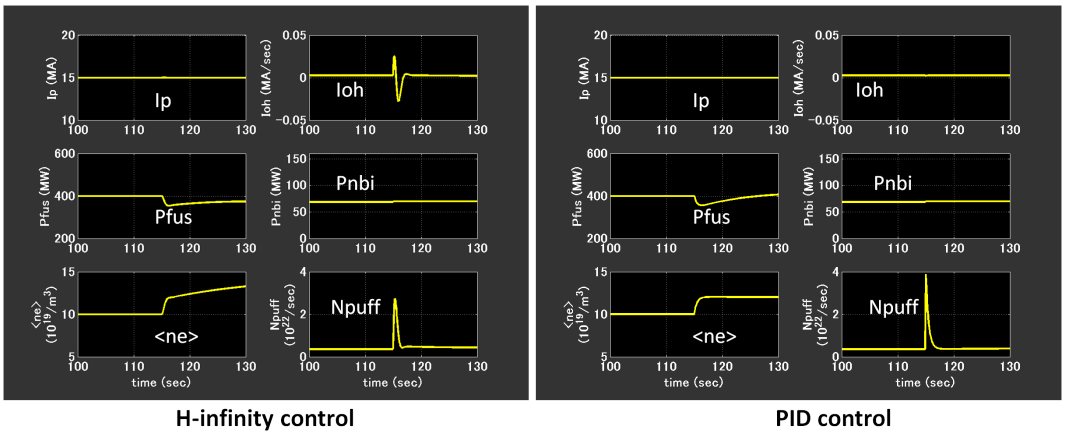

Figure 4.15: The case that $NBI_{lim} = 70MW$ and $< ne >^{ref}$ increases

Figure 4.16 shows that the case of $NBI_{lim} = 150MW$ and the reference value of $< ne >$ decreases. In both cases, the N_{puff} becomes 0 and $< ne >$ decreases at the same time constant.

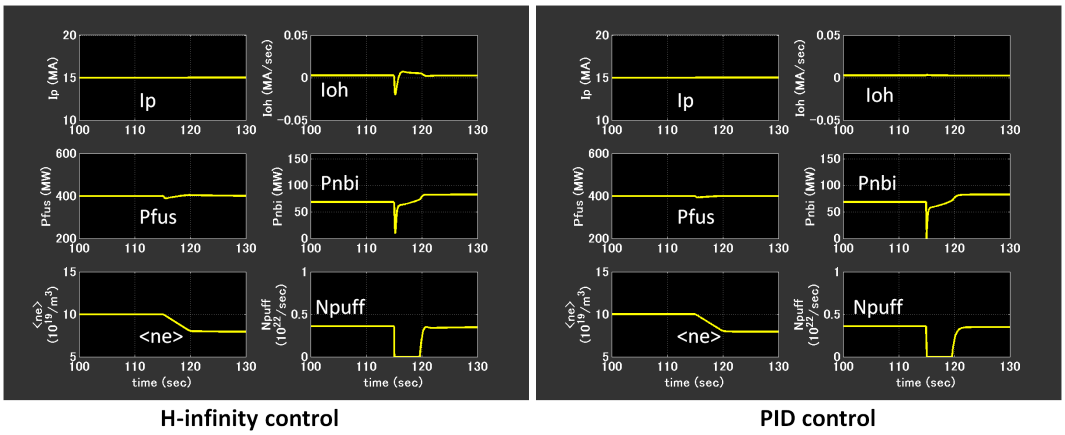

Figure 4.16: The case that $NBI_{lim} = 150MW$ and $< ne >^{ref}$ decreases

HH change case

Figure 4.17 shows the case that HH decreases, and Figure 4.18 shows the case that HH increases. In both case, each parameter is kept constant.

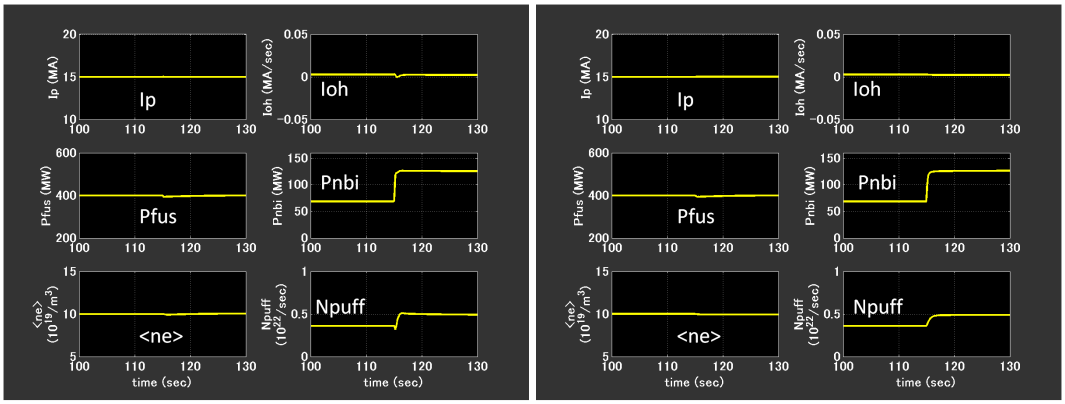

Figure 4.17: The case that $NBI_{lim} = 150MW$, HH decreases

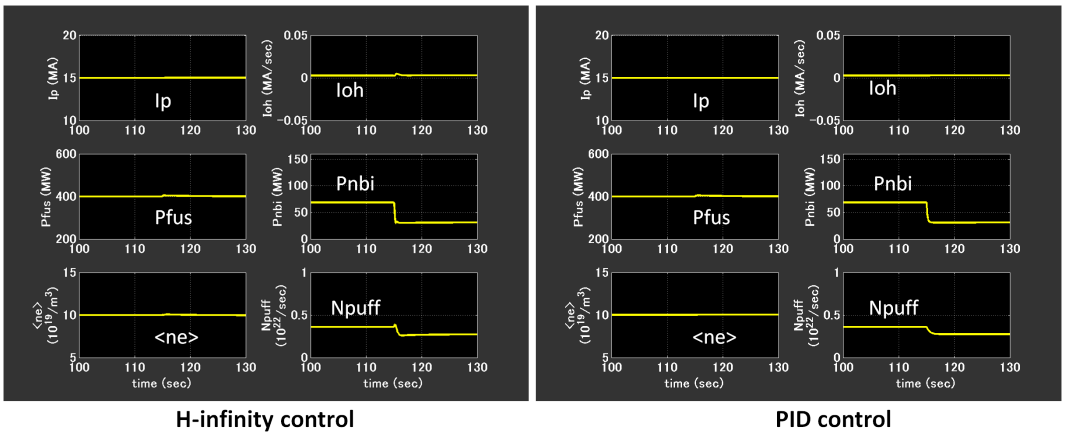

Figure 4.18: The case that $NBI_{lim} = 150MW$, HH increases

α change case

Figure 4.19 shows the case that α decreases, and Figure 4.20 shows the case that α increases. In both case, each parameter is kept constant.

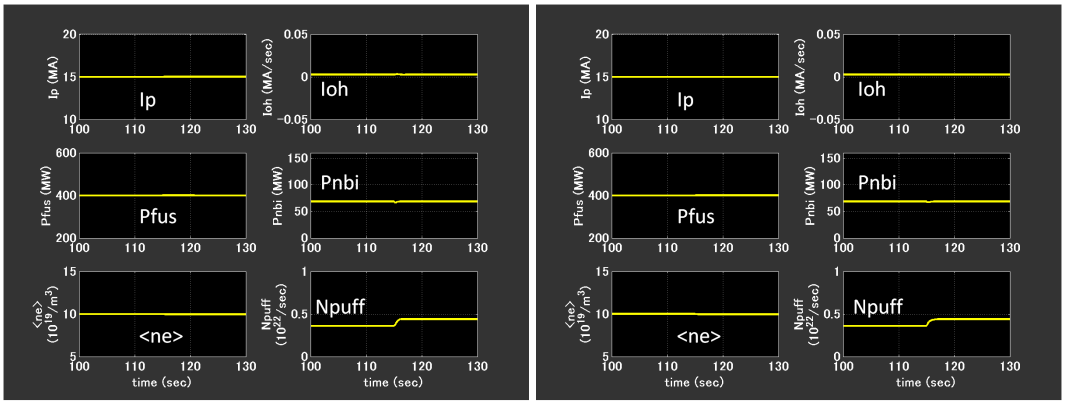

Figure 4.19: The case that $NBI_{lim} = 150MW$, α decreases

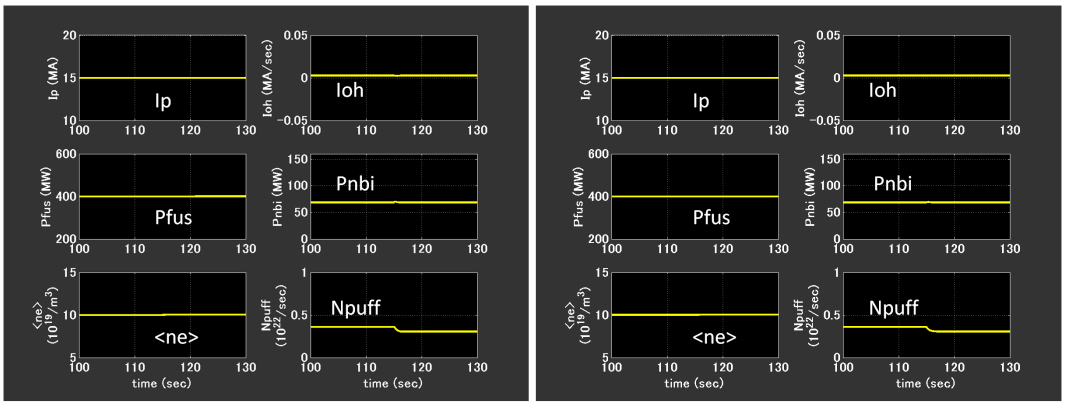

Figure 4.20: The case that $NBI_{lim} = 150MW$, α increases

4.7.3 discussion

In this comparison, both controllers have almost same performance, and against the actuator limitation, the PI controller seems to be more robust than H-infinity controller. This results suggests that the PI controller may

have enough performance to control the reactor and that the suitable feed back gain can be designed from the H-infinity theory. The H-infinity controller, however, is not designed from the estimation of the model error, thus, more high performance or the more suitable H-infinity controller may be able to be designed.

4.8 Summary

In this chapter, the H-infinity robust servo theory is used and the plasma control simulation is done with the 0-D plasma model. In this simulation, the higher robust and servo performance is demonstrated than in chapter 3. Additionally, with the MIMO PI controller which is re-designed from the H-infinity controller shows the same performance. These results suggests the effectivity of the H-infinity theory for the plasma control and the controller design. The H-infinity controller design with the estimated model error is the future work.

Chapter 5

Profile control

5.1 Introduction

In chapter 3 and chapter 4, the 0-D plasma parameter control is demonstrated. Additionally, for the future reactor, the profile control will be needed. To do so, 1-D differential equation (i.e. the equation of the time and the space) has to be re-written to the 0-D state equation. In this chapter, the state equation modeling for the profile control, and the controller design is discussed.

5.2 Basic policy

The modeling is started from the diffusion equation which represents the parameter's time and space evolution. In this research, assuming the profile with well known function, the space term is vanished. The two methods are discussed in this chapter. The first method is from considering the diffusion equation as follow,

$$\frac{\partial}{\partial t} f(r,t) = -D\nabla \cdot (\nabla f(r,t)) + S(r,t) \tag{5.1}$$

where f, S, D are the controlled parameter, the source term and the diffusion coefficient. With the assumption that

$$f(r,t) = f_0(t)g(r) \tag{5.2}$$

where $g(r)$ is the well known function, eq. (5.1) can be changed as follows,

$$g(r)\frac{d}{dt} f_0(t) = -Df_0(t)\nabla \cdot (\nabla g(r)) + S(r,t). \tag{5.3}$$

Integrating this equation with r, the time differential equation of $f_0(t)$ can be lead, and the profile can be represent with $f_0(t)$ and $g(r)$. This method is quite simple and easy. The controller designed from this method, however, can only one profile parameter. For example, the controller can control only q_{min}, and can not control q_{min} and its location simultaneously.

The second method is also started from eq. (5.1). Using the profile form assumption and basis functions $g_k(r)$, equation (5.1) can be divided approximately as follows,

$$\sum_{k=0}^{n} \frac{d}{dt} f_k(t) g_k(r) = \sum_{k=0}^{n} D_k f_k(t) g_k(r) + \sum_{k=0}^{n} S_k(t) g_k(r) \tag{5.4}$$

Because of $g_k(r)$ are the basis function, each profile parameter's time differential equation can be gotten as follows,

$$\frac{d}{dt} f_k(t) = D_k f_k(t) + S_k(t) \ (k = 0 \cdots n) \tag{5.5}$$

The controller designed from this method, can control the multiple profile parameters, but it will be hard work to find the general suitable basis functions. In this chapter, the current profile (q profile) control is discussed. In refs. [42,43], the similar method is used. In these research, the basis functions are determined from the machine experimental data.

5.3 Modeling for the current

5.3.1 Modeling for the diffusion equation

To make the current diffusion equation, start from the generalized Ohm's low and Maxwell equation.

$$\mathbf{E} = \eta(\mathbf{j} - \mathbf{j}_{ni}) \tag{5.6}$$

$$\nabla \times \mathbf{B} = \mu_0 \mathbf{j} \tag{5.7}$$

$$\frac{\partial \mathbf{B}}{\partial t} = -\nabla \times \mathbf{E} \tag{5.8}$$

where $\mathbf{j}_{ni}$ is non-inductive current. Additionally, from these equations,

$$\mathbf{B} = \nabla \times \mathbf{A} \tag{5.9}$$

$$\mathbf{E} = -\frac{\partial \mathbf{A}}{\partial t} \tag{5.10}$$

the following equation can be written.

$$\mathbf{j} = \frac{\mathbf{E}}{\eta} + \mathbf{j}_{ni} = \nabla \times \nabla \times \mathbf{A} \tag{5.11}$$

Using the cylindrical coordinate and assuming that the current is only toroidal direction and the function of minor radius, the following equation can be written,

$$j(r,t) = \frac{E(r,t)}{\eta(r,t)} + j_{ni}(r,t) = -\frac{1}{\mu_0}\frac{1}{r}\frac{\partial}{\partial r}\left(r\frac{\partial A_\phi}{\partial r}\right) \tag{5.12}$$

Additionally, following relationship is used.

$$\Phi(r) = \int_S \mathbf{B} d\mathbf{S} = \int_S \nabla \times \mathbf{A} d\mathbf{S} = \int_C \mathbf{A} d\mathbf{l} \simeq 2\pi R A_\phi(r) \tag{5.13}$$

$$2\pi R E = V_{loop} = -\frac{\partial \Phi}{\partial t} \tag{5.14}$$

From these equations, following magnetic flux diffusion equation can be written.

$$-\frac{1}{\eta(r,t)}\frac{\partial \Phi}{\partial t} + 2\pi R j_{ni}(r,t) = -\frac{1}{\mu_0}\frac{1}{r}\frac{\partial}{\partial r}\left(r\frac{\partial \Phi}{\partial r}\right) \tag{5.15}$$

Here, the total flux is the summation of the plasma flux and the CS coil's flux as follows,

$$\Phi(r,t) = \Phi_{CS}(t) + \Phi_p(r,t) \tag{5.16}$$

Finally, the diffusion equation can be written as follows,

$$\frac{\partial \Phi_p}{\partial t} = \frac{\eta}{\mu_0}\frac{1}{r}\frac{\partial}{\partial r}\left(r\frac{\partial \Phi_p}{\partial r}\right) + 2\pi R \eta j_{ni} - \dot{\Phi}_{CS} \tag{5.17}$$

This equation equals to the following circuit equation,

$$\frac{\partial \Phi_p}{\partial t} = -2\pi R \eta (j - j_{ni}) - \dot{\Phi}_{CS} \tag{5.18}$$

In this research, the non-inductive current is assumed as follows,

$$j_{ni} = j_{bs} + j_{nbi} + j_{RF} \tag{5.19}$$

where, J_{bs}, j_{NBI}, j_{RF} are bootstrap current, NBI current, RF current respectively.

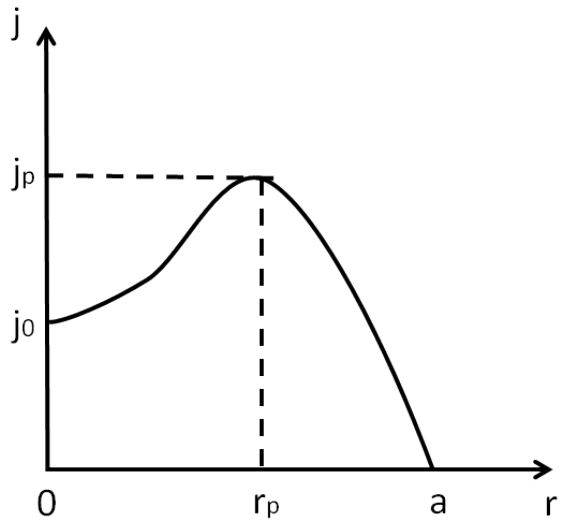

Figure 5.1: The assumption of the current profile

5.3.2 The assumption of the current profile

To represent the flux profile with the equation, the assumption of the current profile is used. Assuming the current profile as Fig. 5.1, and the profile is represented with 4th order equation.

Assuming the following conditions,

$$j(r_p, t) = j_p(t) \tag{5.20}$$

$$j(0, t) = j_0(t) \tag{5.21}$$

$$j(a, t) = 0 \tag{5.22}$$

$$\frac{\partial}{\partial r} j(0, t) = 0 \tag{5.23}$$

$$\frac{\partial}{\partial r} j(r_p, t) = 0 \tag{5.24}$$

the current profile can be written as follows,

$$j(r, t) = -kr^4 + \left(2kr_p - \frac{2(j_p - j_0)}{r_p^3}\right) r^3 - \left(kr_p^2 - \frac{3(j_p - j_0)}{r_p^2}\right) r^2 + j_0 \tag{5.25}$$

where,

$$k = \frac{1}{a^4 - 2r_p a^3 + r_p^2 a^2} \left(-\frac{2(j_p - j_0)}{r_p^3} a^3 + \frac{3(j_p - j_0)}{r_p^2} a^2 + j_0\right). \tag{5.26}$$

Using the following variable transformation,

$$j_p = (c_j + 1)j_0 \tag{5.27}$$

$$r_p = c_p a \tag{5.28}$$

the current profile is written as follows,

$$\begin{aligned} j(r,t) &= \frac{j_0}{(1-c_p)^2}\left\{-\frac{c_p^3 + 3c_j c_p - 2c_j}{a^4 c_p^3} r^4 + \frac{2(c_p^4 + 2c_j c_p^2 - c_j)}{a^3 c_p^3} r^3 \right. \\ &- \left. \frac{c_p^4 + 4c_j c_p - 3c_j}{a^2 c_p^2} r^2 + (1-c_p)^2 \right\} \end{aligned} \tag{5.29}$$

Finally using the normalized variable $\rho = r/a$, the following function can be lead,

$$\begin{aligned} j(\rho,t) &= j_0[MA/m^2]\left(-\frac{c_p^3 + 3c_j c_p - 2c_j}{c_p^3(1-c_p)^2}\rho^4 + \frac{2c_p^4 + 4c_j c_p^2 - 2c_j}{c_p^3(1-c_p)^2}\rho^3 \right. \\ &- \left. \frac{c_p^4 + 4c_j c_p - 3c_j}{c_p^2(1-c_p)^2}\rho^2 + 1\right) \\ &= j_0[MA/m^2](c_{j1}\rho^4 + c_{j2}\rho^3 + c_{j3}\rho^2 + 1) \end{aligned} \tag{5.30}$$

and

$$c_{j3} = -(1 + c_{j1} + c_{j2}) \tag{5.31}$$

The variables c_j, r_p, j_0 can be changed to c_{j1}, c_{j2}, j_0.

5.3.3 Change of the circuit equation

To make the state equation, equation (5.18) is changed from the current profile equation.

Flux form

From Biot-Savart law, the magnetic flux passing through the $Z = 0$ and minor radius r circle made by the plasma current is written as follows,

$$\begin{aligned} \Phi_p(r) &= \int_0^a \int_0^{2\pi} \mu_0 \kappa j(r') r' \sqrt{(R_0 + r' cos\theta)(R_0 - r)} \\ &\times \left\{\left(\frac{2}{k} - k\right) K(k) - \frac{2}{k} E(k)\right\} d\theta dr' \end{aligned} \tag{5.32}$$

where, $K(k), E(k)$ are first and second complete elliptic integral, and

$$k^2 = \frac{4(R_0 + r'cos\theta)(R_0 - r)}{(2R_0 - r + r'cos\theta)^2 + r'sin^2\theta} \tag{5.33}$$

Using the large aspect approximation, this equation can be changed as follows,

$$\Phi_p(r) \simeq \int_0^a \int_0^{2\pi} \mu_0 \kappa j(r') r' R_0 \left\{ ln\left(\frac{8R_0}{\delta}\right) - 2 \right\} d\theta dr' \tag{5.34}$$

$$\delta = \sqrt{r^2 + r'^2 + 2rr'cos\theta} \tag{5.35}$$

adn also changed to as follows,

$$\Phi_p(r) \simeq \mu_0 R_0 \left(ln\left(\frac{8R_0}{a}\right) - 2 \right) I_p(t) - \kappa\mu_0 R_0 \int_0^a \int_0^{2\pi} j(r') r' ln\left(\frac{\delta}{a}\right) d\theta dr' \tag{5.36}$$

The first term of this equation is the function of t, and second term is the function of t and r. Second term can be changed as follows,

$$Second\, term = \kappa\mu_0 R_0 a^2 \int_0^1 \int_0^{2\pi} j(\rho') \rho' ln(\delta_\rho) d\theta d\rho' \tag{5.37}$$

$$\rho' = r'/a \tag{5.38}$$

$$\delta_\rho = \frac{\delta}{a} = \sqrt{\rho^2 + \rho'^2 + 2\rho\rho' cos\theta} \tag{5.39}$$

This can't be solved analytically, thus, consider from other point of view. The following relationship between the j_0 and the Φ_p can be written approximately,

$$\begin{aligned} j(r,t) &= -\frac{1}{\mu_0}\frac{1}{r}\frac{\partial}{\partial r}\left(r\frac{\partial A}{\partial r}\right) \\ &= -\frac{1}{2\pi R\mu_0}\frac{1}{r}\frac{\partial}{\partial r}\left(r\frac{\partial \Phi}{\partial r}\right) \\ &= -\frac{1}{2\pi R\mu_0}\frac{1}{r}\frac{\partial}{\partial r}\left(r\frac{\partial \Phi_p}{\partial r}\right) \end{aligned} \tag{5.40}$$

and

$$j(\rho,t) = -\frac{1}{2\pi R_0\mu_0 a^2}\frac{1}{\rho}\frac{\partial}{\partial \rho}\left(\rho\frac{\partial \Phi_p}{\partial \rho}\right) \tag{5.41}$$

After integration, the following form can be written,

$$\Phi_p(\rho,t) = -2\pi R\mu_0 a^2 \left(\frac{c_{j1}}{36}\rho^6 + \frac{c_{j2}}{25}\rho^5 + \frac{c_{j3}}{16}\rho^4 + \frac{1}{4}\rho^2 + \alpha(t)\right) j_0(t) \quad (5.42)$$

where $\alpha(t)$ is integral constant. From this equation and eq. (5.36), the following form can be written,

$$\begin{aligned}\Phi_p(\rho,t) &= -2\pi R\mu_0 a^2 \left(\frac{c_{j1}}{36}\rho^6 + \frac{c_{j2}}{25}\rho^5 + \frac{c_{j3}}{16}\rho^4 + \frac{1}{4}\rho^2 + \alpha(t)\right) j_0(t) \\ &+ \mu_0 R_0 \left(ln\left(\frac{8R_0}{a}\right) - 2\right) I_p(t) \end{aligned} \quad (5.43)$$

and

$$\begin{aligned} I_p &= \int_0^a 2\pi\kappa r j(r) dr = 2\pi\kappa a^2 \int_0^1 \rho j(\rho) d\rho \\ &= 2\pi\kappa a^2 \left(\frac{c_{j1}}{6} + \frac{c_{j2}}{5} + \frac{c_{j3}}{4} + \frac{1}{2}\right) j_0(t) \end{aligned} \quad (5.44)$$

To estimate the $\alpha(t)$, the following boundary condition is used,

$$\Phi_p(1,t) = \mu_0 R_0 \left(ln\left(\frac{8R_0}{a}\right) - 2 + \frac{li}{2}\right) I_p \quad (5.45)$$

From this equation and eq. (5.43), the following relationship can be written,

$$\frac{\mu_0 R_0}{2} li I_p = -2\pi R\mu_0 a^2 \left(\frac{c_{j1}}{36} + \frac{c_{j2}}{25} + \frac{c_{j3}}{16} + \frac{1}{4} + \alpha(t)\right) j_0(t) \quad (5.46)$$

and

$$li = -\frac{2\left(\frac{c_{j1}}{36} + \frac{c_{j2}}{25} + \frac{c_{j3}}{16} + \frac{1}{4} + \alpha(t)\right)}{\kappa\left(\frac{c_{j1}}{6} + \frac{c_{j2}}{5} + \frac{c_{j3}}{4} + \frac{1}{2}\right)} \quad (5.47)$$

The internal inductance l_i can be written from the poloidal magnetic flux density B_p. B_p can be lead as follows,

$$j(r,t) = \frac{1}{\mu_0}\nabla \times B = \frac{1}{\mu_0}\frac{1}{r}\frac{\partial}{\partial r}(rB_p) \quad (5.48)$$

and

$$B_p(\rho,t) = \mu_0 a j_0(t) \left(\frac{c_{j1}}{6}\rho^5 + \frac{c_{j2}}{5}\rho^4 + \frac{c_{j3}}{4}\rho^3 + \frac{1}{2}\rho\right). \quad (5.49)$$

From B_p, l_i can be written as follows,

$$
\begin{aligned}
l_i &= \frac{2a^2 \int_0^1 \rho B_p^2(\rho) d\rho}{a^2 B_p^2(1)} \\
&= \frac{2 \int_0^1 \rho \left(\frac{c_{j1}}{6}\rho^5 + \frac{c_{j2}}{5}\rho^4 + \frac{c_{j3}}{4}\rho^3 + \frac{1}{2}\rho \right)^2 d\rho}{\left(\frac{c_{j1}}{6} + \frac{c_{j2}}{5} + \frac{c_{j3}}{4} + \frac{1}{2} \right)^2}
\end{aligned} \tag{5.50}
$$

Finally, with this equation and eq. (5.47), $\alpha(t)$ can be written as follows,

$$
\alpha(t) = -\left\{ \frac{\kappa \int_0^1 \rho \left(\frac{c_{j1}}{6}\rho^5 + \frac{c_{j2}}{5}\rho^4 + \frac{c_{j3}}{4}\rho^3 + \frac{1}{2}\rho \right)^2 d\rho}{\left(\frac{c_{j1}}{6} + \frac{c_{j2}}{5} + \frac{c_{j3}}{4} + \frac{1}{2} \right)} + \frac{c_{j1}}{36} + \frac{c_{j2}}{25} + \frac{c_{j3}}{16} + \frac{1}{4} \right\} \tag{5.51}
$$

In the case that the typical parameter $j_p = 2j_0, r_p = 0.5a$ are constant, $c_{j1} = 12, c_{j2} = -28, c_{j3} = 15$ and

$$
I_p(t)[MA] = 8.32\pi j_0(t) \tag{5.52}
$$

$$
\alpha(t) = -0.7987. \tag{5.53}
$$

To do the first method, this value is used later. To do the second method, $\alpha(t)$ is linearized around these values and written as follows,

$$
\begin{aligned}
\alpha(t) &\simeq \frac{\partial \alpha}{\partial c_{j1}}(c_{j1} - 12) + \frac{\partial \alpha}{\partial c_{j2}}(c_{j2} + 28) + \frac{\partial \alpha}{\partial c_{j3}}(c_{j3} - 15) - 0.7987 \\
&= -(0.00378 c_{j1} + 0.0258 c_{j2} + 0.0693 c_{j3} + 0.4346)
\end{aligned} \tag{5.54}
$$

Then, $\Phi_p(\rho, t)$ can be written as follows,

$$
\begin{aligned}
\frac{1}{2\pi R \mu_0 a^2}\Phi_p(\rho, t) &\simeq \left[-\frac{1}{36}\rho^6 + \frac{\kappa}{6}\left\{ ln\left(\frac{8R}{a}\right) - 2 \right\} + 0.00378 \right] c_{j1} j_0 \\
&+ \left[-\frac{1}{25}\rho^5 + \frac{\kappa}{5}\left\{ ln\left(\frac{8R}{a}\right) - 2 \right\} + 0.0258 \right] c_{j2} j_0 \\
&+ \left[-\frac{1}{16}\rho^4 + \frac{\kappa}{4}\left\{ ln\left(\frac{8R}{a}\right) - 2 \right\} + 0.0693 \right] c_{j3} j_0 \\
&+ \left[-\frac{1}{4}\rho^2 + \frac{\kappa}{2}\left\{ ln\left(\frac{8R}{a}\right) - 2 \right\} + 0.4363 \right] j_0 \\
&\equiv \begin{pmatrix} \alpha_1(\rho) & \alpha_2(\rho) & \alpha_3(\rho) \end{pmatrix} \begin{pmatrix} c_{j1} j_0 \\ c_{j2} j_0 \\ j_0 \end{pmatrix}
\end{aligned} \tag{5.55}
$$

Temperature, and density profile

To determine the plasma resistivity profile and the bootstrap current profile, the temperature and the density profile is needed. In this research, following assumption are used,

$$T_e = T_i = T_0(t)\left(1 - \frac{r^2}{a^2}\right)^{\alpha_T} \tag{5.56}$$

$$n_e = n_i = n_0(t)\left(1 - \frac{r^2}{a^2}\right)^{\alpha_n} \tag{5.57}$$

Using these, following relationship can be lead

$$< n >= \frac{1}{\pi\kappa a^2} 2\pi\kappa \int_0^a rn(r,t)dr = \frac{n_0}{\alpha_n + 1} \tag{5.58}$$

$$< T >= \frac{1}{\pi\kappa a^2} 2\pi\kappa \int_0^a rT(r,t)dr = \frac{T_0}{\alpha_T + 1} \tag{5.59}$$

$$N = 2\pi R \times 2\pi\kappa \int_0^a rn(r,t)dr = 2\pi^2\kappa R a^2 \frac{n_0}{\alpha_n + 1} \tag{5.60}$$

$$\begin{aligned} W[MJ] &= 2\pi R \times 1.6 \times 10^{-22} 2\pi\kappa \int_0^a r3n(r,t)T(r,t)dr \\ &= 9.6 \times 10^{-22}\pi^2\kappa R a^2 \frac{n_0 T_0}{1 + \alpha_n + \alpha_T} \end{aligned} \tag{5.61}$$

In addition, the plasma resistivity is determined as follows,

$$\eta = 1.65 \times 10^{-9} ln\Lambda Z_{eff}(T_e[kev])^{-1.5} = k_\eta T_e^{-1.5} \tag{5.62}$$

bootstrap current

In this research, the bootstrap current is formed as follows [2, 91]

$$j_{bs} = -4.71q(r)\left(\frac{R_0}{r}\right)^{0.5} \frac{T}{B_0}\left(\frac{\partial n}{\partial r} + 0.04\frac{n}{T}\frac{\partial T}{\partial r}\right) \tag{5.63}$$

and the safety factor profile is written as follows (the derivation is written later).

$$q(\rho,t) = \frac{\kappa B_t}{R\mu_0 j_0(t) \times 10^6} \times \left(\frac{c_{j1}}{6}\rho^4 + \frac{c_{j2}}{5}\rho^3 + \frac{c_{j3}}{4}\rho^2 + \frac{1}{2}\right)^{-1} \tag{5.64}$$

Finally, j_{bs} can be written as follows,

$$j_{bs}(r,t) = \frac{4.71R^{0.5}}{B_t} r^{0.5} q(r,t) \frac{2}{a^2}(\alpha_n + 0.04\alpha_T)\left(1 - \frac{r^2}{a^2}\right)^{\alpha_n+\alpha_T-1} n_0 T_0 \times 1.6 \times 10^{-22} \tag{5.65}$$

and the unit is MA/m^2.

NBI and RF current

The NBI and RF current profile is assumed as follows,

$$j_{nbi}(\rho,t) = j_{nbi0}(t) exp(-5\rho^{0.75}) \tag{5.66}$$

$$j_{RF} = -\frac{j_{RFp}}{0.3087}(\rho^4 + 0.4\rho^3 - 1.4\rho^2) \tag{5.67}$$

The NBI current is assumed to be peaked at $\rho = 0$, and RF current is assumed to be peaked at $\rho = 0.7$. The current drive efficient is assumed as follows,

$$I_{CD}[MA] = 0.11[A/W] P_{CD}[MW] \tag{5.68}$$

q profile

The safety factor can be derived from the following equations,

$$j(r,t) = \frac{\kappa B_t}{R\mu_0} \frac{1}{r} \frac{\partial}{\partial r}\left(\frac{r^2}{q(r,t)}\right) \tag{5.69}$$

and

$$j(\rho,t) = j_0(t)(c_{j1}\rho^4 + c_{j2}\rho^3 + c_{j3}\rho^2 + 1) \tag{5.70}$$

Finally, q profile can be written as follows,

$$q(\rho,t) = \frac{\kappa B_t}{R\mu_0 j_0(t) \times 10^6} \times \left(\frac{c_{j1}}{6}\rho^4 + \frac{c_{j2}}{5}\rho^3 + \frac{c_{j3}}{4}\rho^2 + \frac{1}{2}\right)^{-1} \tag{5.71}$$

In this case, the position of minimum safety factor can be written as follows ($0.54 < \rho_{min} < 0.74$),

$$\rho_{min} = \frac{3}{4c_{j1}}\left(-\frac{3}{5}c_{j2} - \sqrt{\frac{9}{25}c_{j2}^2 - \frac{4}{3}c_{j1}c_{j3}}\right) \tag{5.72}$$

5.4 The particle and the energy modeling

The differential equations of the plasma energy and the particle is written as the same form of previous chapters.

$$\frac{d}{dt}\begin{pmatrix} N \\ W \end{pmatrix} = \begin{pmatrix} -\frac{N}{\tau_p} - \frac{n^2}{2} < \sigma v > V + N_{puff} \\ -\frac{W}{\tau_e} + \frac{E_\alpha}{4} n^2 < \sigma v > V - C_B n_{20}^2 T_{10}^{1/2} V + P_{NBI} + P_{RF} \end{pmatrix} \tag{5.73}$$

5.5 First method controller design

5.5.1 The state equation

j_0 differential equation

Determining the typical parameter $j_p = 2j_0, r_p = 0.5a$ are constant, then $c_{j1} = 12, c_{j2} = -28, c_{j3} = 15$ and the diffusion equation can be written as follows,

$$\begin{aligned} f_0(\rho)\frac{d}{dt}j_0(t) &\simeq -2\pi R \left(T_0^{-1.5}(t) j_0(t) f_1(\rho) - \frac{n_0 T_0^{-0.5}}{j_0} f_2(\rho) \right. \\ &- \left. T_0^{-1.5}(t) P_{NBI}(t) f_3(\rho) - T_0^{-1.5}(t) P_{RF}(t) f_4(\rho) \right) \end{aligned} \tag{5.74}$$

where

$$\begin{aligned} f_0(\rho) &= -2\pi R \mu_0 a^2 \left(\frac{1}{3}\rho^6 - \frac{28}{25}\rho^5 + \frac{15}{16}\rho^4 + \frac{1}{4}\rho^2 - 0.7987 \right) \\ &+ 8.32\pi\mu_0 R_0 \left(ln\left(\frac{8R_0}{a}\right) - 2 \right) \end{aligned} \tag{5.75}$$

$$f_1(\rho) = k_\eta (1-\rho^2)^{-1.5\alpha_T} (12\rho^4 - 28\rho^3 + 15\rho^2 + 1) \tag{5.76}$$

$$f_2(\rho) = 1.6\times 10^{-28} (1-\rho^2)^{\alpha_n - 0.5\alpha_T - 1} (\alpha_n + 0.04\alpha_T) \frac{9.42\kappa k_\eta \rho^{0.5}}{R^{0.5}\mu_0 a^{1.5}} \left(2\rho^4 - \frac{28}{5}\rho^3 + \frac{15}{4}\rho^2 + \frac{1}{2} \right)^{-1} \tag{5.77}$$

$$f_3(\rho) = 0.11 k_\eta (1-\rho^2)^{-1.5\alpha_T} exp\left(-5\rho^{0.75}\right) \tag{5.78}$$

$$f_4(\rho) = -0.02676 k_\eta (1-\rho^2)^{-1.5\alpha_T} (\rho^4 + 0.4\rho^3 - 1.4\rho^2) \tag{5.79}$$

In this case, Φ_{CS} is assumed 0.

Integrating this equation with r, the approximated differential equation of j_0 can be lead. Defining the following coefficient,

$$C_1 = 2\pi R \frac{\int_0^{0.95} f_1(\rho)d\rho}{\int_0^{0.95} f_0(\rho)d\rho} \tag{5.80}$$

$$C_2 = 2\pi R \frac{\int_0^{0.95} f_2(\rho)d\rho}{\int_0^{0.95} f_0(\rho)d\rho} \tag{5.81}$$

$$C_3 = 2\pi R \frac{\int_0^{0.95} f_3(\rho)d\rho}{\int_0^{0.95} f_0(\rho)d\rho} \tag{5.82}$$

$$C_4 = 2\pi R \frac{\int_0^{0.95} f_4(\rho)d\rho}{\int_0^{0.95} f_0(\rho)d\rho} \tag{5.83}$$

the differential equation can be written as follows,

$$\begin{aligned} \frac{d}{dt}j_0(t) &\simeq -C_1 T_0^{-1.5}(t) j_0(t) + C_2 \frac{n_0 T_0^{-0.5}}{j_0} \\ &+ C_3 T_0^{-1.5}(t) P_{NBI}(t) + C_4 T_0^{-1.5}(t) P_{RF}(t) \end{aligned} \tag{5.84}$$

qmin

Using this assumption, the q_{min} can be written as follows,

$$r_{min} = 1.2876 \tag{5.85}$$

$$q_{min} = 1.1067 \frac{\kappa B_t}{R\mu_0} \times \frac{1}{j_0 \times 10^6} \tag{5.86}$$

P_{fus} **and** $< ne >$

The fusion power and the plasma density are defined as follows,

$$P_{fus} = \frac{5E_\alpha N^2}{4V} < \sigma v > \tag{5.87}$$

$$< ne >= \frac{N}{V} \tag{5.88}$$

The state equation of the first method

Finally, the state equation can be written as follows,

$$\frac{d}{dt}\begin{pmatrix} j_0 \\ N \\ W \end{pmatrix} = \mathbf{A_0}\begin{pmatrix} j_0 \\ N \\ W \end{pmatrix} + \mathbf{B_0}\begin{pmatrix} P_{nbi} \\ P_{RF} \\ N_{puff} \end{pmatrix} \tag{5.89}$$

$$\begin{pmatrix} q_{min} \\ P_{fus} \\ < ne > \end{pmatrix} = \mathbf{C_0}\begin{pmatrix} j_0 \\ N \\ W \end{pmatrix} \tag{5.90}$$

The equilibrium point is used as follows,

$$\mathbf{x_0} = \begin{pmatrix} 0.3488MA/m^2 \\ 6.0333 \times 10^{22} \\ 312.0219MJ \end{pmatrix},\ \mathbf{u_0} = \begin{pmatrix} 23.0219MW \\ 30.0219MW \\ 0.4503 \times 10^{22}/sec \end{pmatrix},\ \mathbf{y_0} = \begin{pmatrix} 3.8105 \\ 403.9781MW \\ 7.7028 \times 10^{19}/m^3 \end{pmatrix} \tag{5.91}$$

Other input parameter set is as follows [76],

$$\alpha_T = 3,\ \alpha_n = 0.1 \tag{5.92}$$

$$Z_{eff} = 2.07,\ ln\Lambda = 20,\ \kappa = 1.85 \tag{5.93}$$

$$R = 6.35m,\ a = 1.85m,\ B_t = 5.18T \tag{5.94}$$

$$HH = 1.57,\ \frac{\tau_p}{\tau_e} = 5 \tag{5.95}$$

5.5.2 Controller design and the result

Using the same method of the pole placement PI control in Chapter 3, the controller is designed. the pole is used as follows,

$$pole = (\ -1 \quad -1 \quad -1 \quad -0.1 \quad -0.1 \quad -0.1\ ) \tag{5.96}$$

In this case, $\mathbf{K_p}$ and $\mathbf{K_i}$ are determined as follows,

$$\mathbf{K_p} = 10^3 \times \begin{pmatrix} 2.2714 & 0.0013 & 0.0439 \\ -2.3579 & -0.0003 & -0.0118 \\ -0.0003 & 0.0000 & 0.0009 \end{pmatrix},\ \mathbf{K_i} = \begin{pmatrix} 218.7891 & 0.1413 & 3.1150 \\ -218.7891 & -0.0384 & -0.8461 \\ 0 & 0.0003 & 0.0844 \end{pmatrix} \tag{5.97}$$

The simulation result is shown in Fig. 5.2. The q_{min} follows the target value (the green dashed line), and the fusion power and the density are kept constant at the same time. To keep the fusion power constant with the change of the q_{min}, the ratio of the NBI power and the RF power are changed.
In chapter 3, chapter 4 and this case, the number of controlled parameters and that of actuators are same, i.e, the system is 3 inputs and 3 outputs. In next section, the case that they are different is discussed.

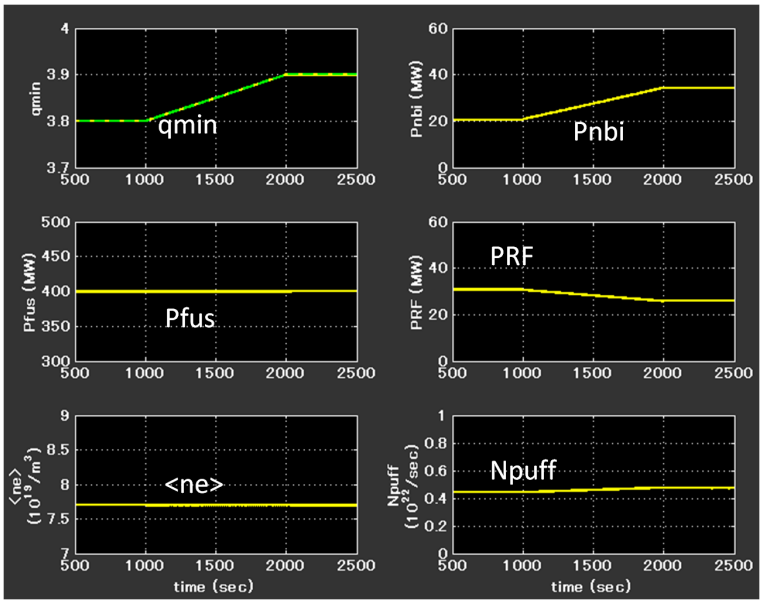

Figure 5.2: The result of the profile control simulation with first method

5.6 Second method controller design

The differential equation of Φ_p derived in previous section is formed as follows,

$$\frac{\partial \Phi_p(\rho, t)}{\partial t} = f(\rho, t) \tag{5.98}$$

This equation can be divided approximately with the basis function as Fig. 5.3

$$\sum_{k=0}^{2} \dot{\Phi}_p(0.33k, t)\phi_k(\rho) = \sum_{k=0}^{2} f(0.33k, t)\phi_k(\rho) \tag{5.99}$$

In this case, the number of the profile parameter is three (i.e. j_0, c_{j1} and c_{j2}), for this reason, it seems to be suitable to use three basis functions. The basis functions shown in Fig. 5.3 are not orthogonal function, but they are linearly independent.

Thus, the following differential equations can be written,

$$\frac{d}{dt}\Phi_p(0.33k, t) = f(0.33k, t) \ (k = 0 \cdots 2) \tag{5.100}$$

From eq. (5.55), the differential equations can be written as follows,

$$\begin{pmatrix} \alpha_1(0) & \alpha_2(0) & \alpha_3(0) \\ \alpha_1(0.33) & \alpha_2(0.33) & \alpha_3(0.33) \\ \alpha_1(0.66) & \alpha_2(0.66) & \alpha_3(0.66) \end{pmatrix} \frac{d}{dt} \begin{pmatrix} c_{j1} j_0 \\ c_{j2} j_0 \\ j_0 \end{pmatrix} \simeq \frac{1}{2\pi R \mu_0 a^2} \begin{pmatrix} f(0,t) \\ f(0.33,t) \\ f(0.66,t) \end{pmatrix} \tag{5.101}$$

From this equation, the following differential equation be written,

$$\frac{d}{dt} \begin{pmatrix} c_{j1} j_0 \\ c_{j2} j_0 \\ j_0 \end{pmatrix} = \frac{1}{2\pi R \mu_0 a^2} \begin{pmatrix} \alpha_1(0) & \alpha_2(0) & \alpha_3(0) \\ \alpha_1(0.33) & \alpha_2(0.33) & \alpha_3(0.33) \\ \alpha_1(0.66) & \alpha_2(0.66) & \alpha_3(0.66) \end{pmatrix}^{-1} \begin{pmatrix} f(0,t) \\ f(0.33,t) \\ f(0.66,t) \end{pmatrix} \tag{5.102}$$

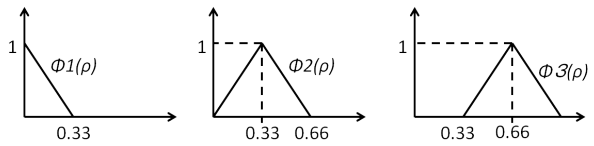

Figure 5.3: The basis function used to divide the equations

5.6.1 The state equation

From the second method, the following linear state equation can be written,

$$\frac{d}{dt} \begin{pmatrix} c_{j1} j_0 \\ c_{j2} j_0 \\ j_0 \\ N \\ W \end{pmatrix} = \mathbf{A_0} \begin{pmatrix} c_{j1} j_0 \\ c_{j2} j_0 \\ j_0 \\ N \\ W \end{pmatrix} + \mathbf{B_0} \begin{pmatrix} P_{nbi} \\ P_{RF} \\ N_{puff} \\ \dot{\Phi}_{CS} \end{pmatrix} \tag{5.103}$$

$$\begin{pmatrix} I_p \\ r_{min} \\ q_{min} \\ P_{fus} \\ n_e \end{pmatrix} = \mathbf{C_0} \begin{pmatrix} c_{j1} j_0 \\ c_{j2} j_0 \\ j_0 \\ N \\ W \end{pmatrix} \tag{5.104}$$

In this case, this state equation can be written as following state feedback form,

$$\frac{d}{dt}\mathbf{y} = \mathbf{C_0}\mathbf{A_0}{\mathbf{C_0}}^{-1}\mathbf{y} + \mathbf{C_0}\mathbf{B_0}\mathbf{u} \tag{5.105}$$

The equilibrium point is used as follows,

$$\mathbf{x_0} = \begin{pmatrix} -0.0317 \\ -1.8640 \\ 0.5278 \\ 5.5054 \times 10^{22} \\ 290.7816[MJ] \end{pmatrix}, \mathbf{u_0} = \begin{pmatrix} 4.425[MW] \\ 45.575[MW] \\ 0.4057 \times 10^{22}/sec \\ -0.0054 \times 10^{-7}[Wb/sec] \end{pmatrix}, \mathbf{y_0} = \begin{pmatrix} 9.0627[MA] \\ 0.6046 \\ 3.9269 \\ 337.0793[MW] \\ 6.9370 \times 10^{19}[m^{-3}] \end{pmatrix} \tag{5.106}$$

5.6.2 Controller design

In this case, the number of controlled parameters is larger than that of actuators. Thus, they are not controllable. In this research, optimum control theory is used. In the optimum control theory, the feedback gain is determined to minimize the evaluation function as follows,

$$J = \int_0^\infty [\mathbf{x}^t\mathbf{Q}\mathbf{x} + \mathbf{u}^t\mathbf{R}\mathbf{u}]dt \tag{5.107}$$

where $\mathbf{Q}and\mathbf{R}$ are weight functions. Then, the feedback gain $\mathbf{F}$ (i.e. the $\mathbf{F}$ used as $\mathbf{u} = -\mathbf{F}\mathbf{x}$) is determined as follows,

$$\mathbf{F} = \mathbf{R}^{-1}\mathbf{B}^t\mathbf{P} \tag{5.108}$$

where $\mathbf{P}$ is the answer of the following riccati equation,

$$\mathbf{P}\mathbf{A} + \mathbf{A}^t\mathbf{P} - \mathbf{P}\mathbf{B}\mathbf{R}^{-1}\mathbf{B}^t\mathbf{P} + \mathbf{Q} = 0 \tag{5.109}$$

In this simulation, the following 2 weight function and the feedback gain sets are used,

Case1

$$\mathbf{R} = diag(1, 1, 1, 10) \tag{5.110}$$

$$\mathbf{Q} = diag(1000, 10, 10, 0.001, 0.1) \tag{5.111}$$

and

$$\mathbf{F} = \begin{pmatrix} 5.0878 & -13.3675 & 3.8563 & 0.0023 & 0.0537 \\ 5.0616 & -2.5062 & 2.0369 & 0.0025 & 0.0572 \\ 4.7531 & 3.1651 & 0.4125 & 0.0056 & 0.9247 \\ -9.4882 & 1.3300 & 0.0540 & -0.0004 & -0.0113 \end{pmatrix} \tag{5.112}$$

Case2

$$\mathbf{R} = diag(1, 1, 1, 10) \tag{5.113}$$

$$\mathbf{Q} = diag(100, 10, 10, 0.001, 0.1) \tag{5.114}$$

and

$$\mathbf{F} = \begin{pmatrix} 2.2834 & -10.9948 & 3.1230 & 0.0023 & 0.0527 \\ 1.5119 & -1.6294 & 1.5686 & 0.0024 & 0.0556 \\ 3.7898 & 2.9066 & 0.3119 & 0.0055 & 0.9239 \\ -2.8173 & 0.3696 & 0.5176 & -0.0003 & -0.0085 \end{pmatrix} \tag{5.115}$$

5.6.3 Result

The simulation results are shown in Fig. 5.4 and Fig. 5.5. In Fig. 5.4, the target value of the q_{min} is changed, and the q_{min} follows to the target value. I_p and P_{fus} are kept nearly constant at the reference values. The reference error of the ρ_{min} and the $< ne >$ is larger than other three parameters. In Fig. 5.5, because of the change of the weight function, the reference error of the $< ne >$ becomes smaller. To find the suitable weight function is the future work.

5.7 Summary

In this chapter, the controller design for the current profile control is discussed, and the test simulation of the profile control is demonstrated. For the future reactor, the controller for the situation that the number of the controlled parameters are larger than that of the actuators will be needed. In this chapter, the example of the control simulation in such a situation is also demonstrated. The next issue is to check the effectivity of the method in this chapter with the experiment or the strictly simulation code.

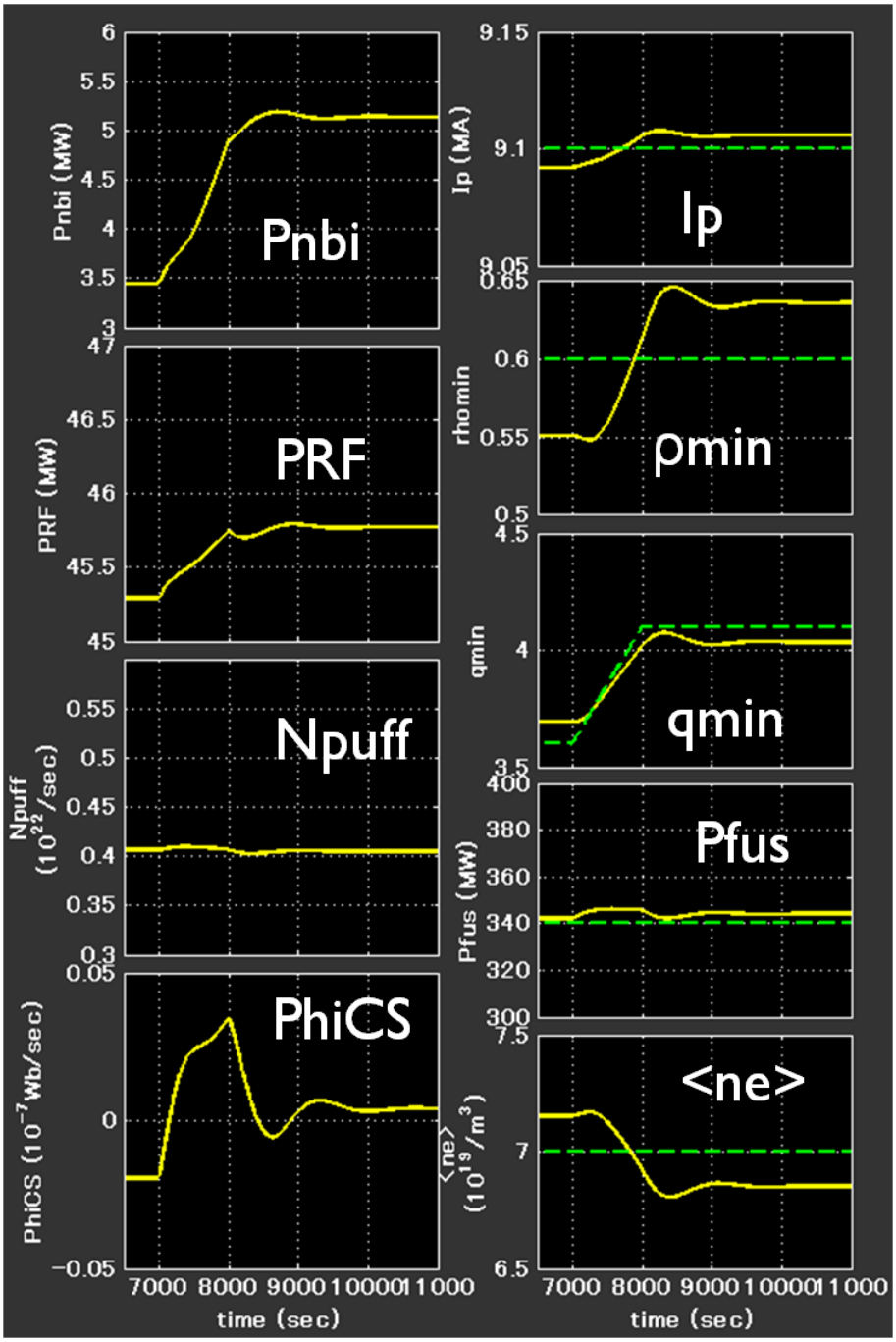

Figure 5.4: The profile control result with second method (case1)

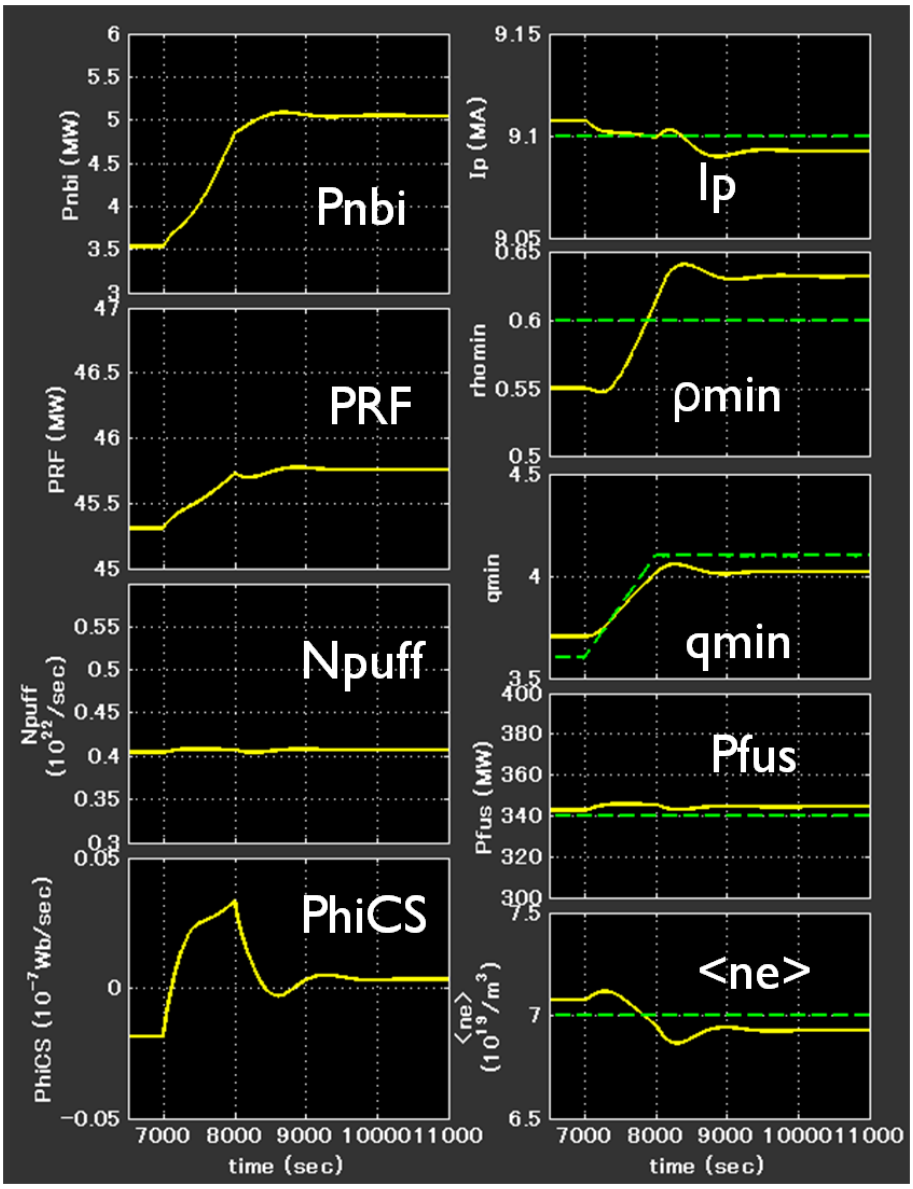

Figure 5.5: The profile control result with second method (case2)

Chapter 6

Conclusion

For the future fusion reactor operation, the core plasma control is one of the most important issue, and there are some subjects to be resolved. For example, multiple parameters have to be controlled simultaneously, and the actuators are not one-to-one correspondence to the parameters. In addition, the actuators and the diagnostics, which can be installed, will be limited because of the high neutron and heat flux. Thus, the discussion about what parameters have to be controlled, and what devices can be installed is quite important. While, since the future fusion reactor system is not fully established, flexible control system should be considered for various applications. The purpose of this research is to suggest the basic policy of the future reactor controller design which has the broad utility.

Chapter 2 discuss on the PID controller design based on the response characteristics of the fusion core plasma. In industrial world, the most broadly used controller is, in general, the PID controller which is designed from the response characteristics, and it is same in plasma experiments. In the PID theory, the actuator is defined as the linear sum of the proportional, integral and differential values of the difference between the target value and the controlled value. The controller is designed by adjusting the each coefficient. For PID controller design, the useful method of the adjusting from the response characteristics exists. In this method, the physical model of the controlled system is not necessary. This is the reason that the PID theory is popular. This method, however, is for SISO (Single-Input Single-Output) system. The future reactor plasma is MIMO (Multi-Input Multi-Output) system, thus, it is not clear that the method is suitable or not for the plasma control. In this research, it is examined that this method is suitable for the plasma control with the one-dimensional plasma simulation. In this simulation, the fusion power and the minimum q-value are controlled by the NBI and the gas-puff. In this case, 3 gain matrices$\in \mathbf{R}^{2\times 2}$ have to be adjusted. To control the

parameters, the adjustment requires the considerable try and error. In the future reactor, more parameters have to be controlled, thus, it seems to be unsuitable to design the PID controller from the response characteristics.

Chapter 3 shows the possibility that the multiple plasma parameters in the future reactor which have the large coupling effect can be controlled independently with the modern control theory. The modern control theory based on the physical model is applicable for the MIMO system. The physical model is, in general, expressed with the time differential equation, which is called state equation. In this chapter, the zero-dimensional plasma model is established from the plasma energy, momentum, and particle conservation law, and the 3-inputs 3-outputs control simulation with the model is demonstrated. In this simulation, the plasma current, the fusion power and the plasma density are controlled by the NBI, the ohmic current and the gas-puff. The control system is formed with PI controller, and each coefficient matrices are determined from the 0-D model with the pole placement method. The controller shows the high servo performance and the disturbance inhibiting performance. This result shows the effectiveness of the modern control theory.

Chapter 4 shows the applicability of the H-infinity control theory for the reactor control, especially paying attention to the possibility that the appropriate adjusted PI controller can have enough robust and servo performance. In the modern control theory, the physics model is needed but the plasma physics is quite complex. Thus, when the approximation model for the controller design is made, the effect of the difference between the real plasma and the model might be large. The post modern control theory or the robust control theory is made in 1980's for these situations. In the robust control theory, the effect of the model difference is dealt as the disturbance, and the controller is designed to minimize the effect of this. For these reasons, the robust control theory is expected to the most suitable method for the fusion reactor. In this chapter, the controller is designed with the H-infinity control theory which is one of the typical robust control theory. The control simulation with this controller shows the higher robust and servo performance than previous chapter. Next, the comparison of the H-infinity control and the PI control is demonstrated. In this case, the PI controller is re-adjusted to fit the diagonal low frequency band of the bode diagram of the PI controller to that of H-infinity controller. In this comparison, the PI controller and the H-infinity controller show the almost same performance. This result shows the possibility that the PI controller can show the enough robust performance. In this study, however, the concrete model difference or uncertainty of the system is not estimated. The controller design with the estimated model uncertainty is the future issue.

Chapter 5 suggests the basic policy for the plasma profile control. For the future reactor, plasma parameter profile should be controlled for the plasma stability. To use the modern or the post modern control method, the physical model have to be expressed as the time differential equation, but the model including the profile information is the time and space differential equation. In this study, two methods to make the state equation for the profile control have been suggested. The first method is to assume the parameter profile perfectly, and make the one profile parameter time differential equation. For example, assuming the current profile, and the time differential equation of the minimum q-value can be made. With this method, however, the multiple profile parameters can 't be controlled, for example, the minimum q-value and its location can 't be controlled simultaneously. The second method is to assume the parameter profile with some well-known function, and divide the equation with the base functions. For example, assuming the current profile as the 4th order polynomial and using the base functions, the time differential equation of each coefficient of the polynomial can be gotten. In the second method, the number of the controlled parameters is depend on the profile assumption and the choice of the base functions. Thus, in most case, the number of the controlled parameters is larger than the number of the actuators. In this case, the system is uncontrollable, i.e. the controller can 't make all parameters to the target values. Thus, in this study, the use of the optimal controller is suggested. The optimal control theory is one of the modern control theory, and the controller is designed to minimize the some evaluate function such as the summation of the reference errors. In this chapter, 4 inputs and 6 outputs simulation is demonstrated with the optimal control theory, and the possibility of the future profile control is shown.

In this research, the prototype control algorithms for the plasma MIMO control in the future reactor (i.e. MIMO PI controller, H-infinity controller and the profile controller) are designed and the benchmark of these controllers are carried out with the 0-D and 1-D plasma simulation. Although the controller design with the estimated model uncertainty, or the confirmation of the effectivity of this method with the 1-dimensional simulation or the experiment is the future issue, these simulations suggests the effectivity of the modern control theory and the robust control theory for the future reactor control. The controller design method used in this research is expected to be applied to the future reactor.

Reference

[1] Kenro MIYAMOTO, Plasma Physics and Controlled Nuclear Fusion, Univercity of Tokyo Press,（2004）(in Japanese)

[2] Jeffrey Freidberg, Plasma Physics and Fusion Energy, CAMBRIDGE (2007)

[3] J. Wesson, Tokamaks, third edn. Oxford (2004)

[4] Proc. Soc. B70 6, J. D. LAWSON (1957)

[5] W. R. Arnold, et al. Phys. REv. 93, 483 (1954)

[6] C. F. Wandel, et al. Nucl. Instr. and Methods 4, 249 (1959)

[7] J. C. Tuck, Nucl. Fusion 1, 201 (1961)

[8] JAEA web site, http://www.naka.jaea.go.jp/ITER/index.php

[9] A. S. Bishop Project Sherwood, Addison Wesley, Reading Mass (1958)

[10] R. S. Pease, Plasma Phys. Contr. Fusion 28, 397 (1986)

[11] L A Artsimovich, Sov. Phys. Usp. 10 117 (1967)

[12] PROGRESS IN THE ITER PHYSICS BASIS Nucl. Fusion 47 (2007)

[13] Text-Fusion reactors, Plasma Fusion Res, 87, Supplement (2011)

[14] R. Hiwatari et al., Nucl. Fusion 44, 106 (2004).

[15] R. Hiwatari et al., Nucl. Fusion 45, 96 (2005).

[16] 核融合実用炉経済性解析コードの改良 核融合動力炉経済性・環境負荷評価コード開発へ向けて

[17] N. Uckan and ITER Physics Group, ITER physics design guidelines, 1989 ITER Documentation Series No.10 (IAEA, Vienna)

[18] K. Okano, et al, Nucl Fusion, 40, 635 (2000)

[19] Z. Dragojlovic et al., Fusion Eng. Des. 85, 243 (2010).

[20] K. Tobita et al 2007 Nucl. Fusion 47 892

[21] S. Nishio et al, 19th IAEA Fusion Energy Conference, Lyon, IAEA-CN-FT/P1-21 (2002)

[22] H. Utho, et al, J. Plasma Fusion Res. SERIES, Vol. 9, 304 (2010)

[23] H. Fujieda et al., JAERI-M 08-256 (in Japanese) (1996).

[24] Y. Miyoshi, et al, Plasma, Fusion Res Volume 6, 2405110 (2011)

[25] T. Ihli et al, Fusion Eng. Design 75-79, 371 (2005)

[26] L. Giancarli et al, Fusion Eng. Design 75-79, 383 (2005)

[27] F. Najmabadi and A. R. Raffray, et al, Fusion Eng. Design 81, 2679 (2006)

[28] M. Nakamura, et al, J. Plasma Fusion Res. SERIES, Vol. 9 186, (2010)

[29] Y. Miyoshi, et al, Plasma Fusion Res, 9, 1405015 (2014)

[30] J.A. Snapes et al., Fusion Eng. Des. 85, 461 (2010).

[31] B. Goncalves et al., Energy Conversion and Management 51, 1751 (2010).

[32] Y. Kamada, J. Plasma Fusion Res. 86, 519 (2010) (in Japanese).

[33] NIFS-MEMO-68

[34] A.E. Costley, IEEE Transaction on Plasma Science 38, No10, OCTOBER (2010).

[35] K.M. Young, Fusion Sci. Technol. 57, 298 (2010).

[36] K. Shimomura, et al, Fusion Engineering and Design 82, 953 (2007)

[37] H. Takenaga, et al, Nucl Fusion 48 035011 (2008)

[38] T.Suzuki, JAERI Review 2009-045

[39] T. Suzuki, J. Plasma Fusion Res. 86, No9, 530 (2010) (in Japanese)

[40] H. Oualit et al, Fusion Engineering and Design 86 1018 (2011)

[41] R. V. Budny, Phys of Plasmas 17 042506 (2010)

[42] D.Moreau et al, Nucl Fusion 43 870-882 (2003)

[43] D.Moreau et al, Nucl Fusion 48 106001 (38pp) (2008)

[44] Atul S. Sharma et al, TRANSACTIONS ON CONTROL SYSTEMS TECHNOLOGY, VOL. 13, NO.3 356-369

[45] W.Z. Yu et al, Fusion Engineering and Design 88 3021-3027 (2013)

[46] O.Mitarai *et al.*, Fusion Science and tech Vol. **56** 1495 (2009)

[47] W. Hui et al ., Fusion Technol., 25, 318 (1994).

[48] J. C. Doyle et al., IEEE TRans. Automatic Control, 34, 8, 831 (1989)

[49] EUGENIO SCHUSTER, et al, Fusion Science and Tech 43, 18 (2003)

[50] Control System Design, Graham C. Goodwin .et,al, PHI (2001)

[51] H. Kimura, H Infinity Control, CORONA PUBLISHING CO., LTD (2000) (in Japanese)

[52] 堀　洋一、大西　公平、　制御工学の基礎、　丸善株式会社　(1994)

[53] J.C.Maxwell, Proc. Royal Society, vol. 16, 270-283 (1867)

[54] E.J. Routh, A Treatise on the Stability of a Given State of Motion, Mamillan (1877)

[55] A.Hurwits, Math. Ann., 46, 273 (1895)

[56] A.M.Lyapnov, The general problem of the stability of motion ,Tayor & Francis (1992)

[57] H.Nyquist, Bell system Tech. J., Vol.11, 126-147 (1932)

[58] H.M.Bode Network Analysis and Feedback Amplifier Design, D. VAN NORSTRAND COMPANY, (1945)

[59] N. Minorsky, J. Amer. soc. Naval Engineers, 34(2) , 280-309 (1922)

[60] A. Callender, et al. Phil. Trans. Roy. Soc. London, A235 (756) 415-444 (1936)

[61] J.G. Ziegler and N. B. Nichols, Trans. ASME, 64, 759-768, (1942)

[62] Y. Wakasa, 国立科学博物館 技術の系統化調査報告　第 11 集 95 (2008) (in Japanese)

[63] 須田信英 他、　PID 制御、　朝倉書店 (1992)

[64] R. E. Kalman, Proc, 1st IFAC Congress, Moscow, 405-410 (1960)

[65] W. Murray Wonham, Linear Multivariable Control, Springer (1985)

[66] 奥山佳史　他、制御工学　古典から現代まで、　朝倉書店　(2001)

[67] R. E. Kalman, Bol. Soc. Math. Maxicana Second Series, Vol 5, 102-119 (1960)

[68] 木村英気　LQG から H ∞へ　計測と制御 29 No.2 1990

[69] G. Zames, IEEE Trans. AC-26-2 585-601 (1981)

[70] J. C. Doyle and G. Stein, IEEE Trans. Auto. Control, AC-26-1. 4-16 (1981)

[71] MATLAB による制御機設計

[72] J. C. Doyle, IEE Proc., 129-D(6), 242-250 (1982)

[73] A. PAckard and J. C. Doyle Automatica, 29-1, 71-109 (1993)

[74] T. Mita, H_∞ Control, SHOKODO Co.,Ltd. (1995)

[75] Y. Miyoshi, et al, Plasma Fusion Res, 7, 2405135 (2012)

[76] プラズマ・核融合学会誌　第７８巻増刊「ITER 工学設計」2002

[77] MathWorks ウェブサイト http://jp.mathworks.com/products/matlab/

[78] JAERI-M 92-178

[79] 計測と制御　第４２巻　第７号　2003　７月号～　第４３巻　第７号　2004　７月号

[80] Geir E. Dullerud, Fernando Paganini 'A Course in Robust Control Theory' Springer (2000)

[81] Algebraic Riccati Equations, PETER LANCASTER and LEIBA RODMAN, OXFORD SCIENCE PUBLICATIONS 1995

[82] 美田勉　他 計測自動制御学会論文集 vol29, No11, 1320-1329 (1993)

[83] Tutomu Mita, et al, Proceedings of the 32nd Conference on Decision and Control, 650 (1993)

[84] Tutomu Mita, et al, Automatica 36 (2000)735-741

[85] Yu Feng, et al, Automatica 48 (2012)991-994

[86] S. Hara, et al Proceeding of the American Control Conference, 3166,(1994)

[87] Petter Lundstrom, et. al, Trans Inst MC Vol 13 No 5, 241 (1991)

[88] R. W. Beaven, et al, Control Eng. Practice, Vol. 4 No. 5 625-633 (1996)

[89] Jiankun Hu, et al, Control Eng. Practice Vol 8 241-252 (2000)

[90] D.C.Donha et al, International Journal of System Science vol 38, No 8

[91] M.N.Rosenbluth, R.D.Hazeltine, F.L.Hinton, Physics Fluids 15 116 (1972)

[92] 牛草健吉, プラズマ・核融合学会誌第 70 巻第 8 号 850 (1994)

Acknowledgment

I would like to express my deepest appreciation to my supervisor Professor Y. Ogawa. He has taught all about the research to me. Even though I'm not so good student, he hasn't abandoned me and advised to me and my research. Without his advise and encouragement, I couldn't complete this work. He is my master of research and life.

I would like to thank Mr. J. Morikawa. He invited me to go to lunch almost daily and talked to me about a lot of things. Even after his retire, He advised me in various chances.

Doctor S. Matsuda incited me to the conference about the nuclear fusion reactor control. This conference and the attendances gave me a lot of inspiration and the advise. I really appreciate them very much.

Doctor H. Fujimoto has advised me about the control engineering. Without his advise, I couldn't research about the reactor control. I also appreciate him.

I am deeply grateful to Dr. K. Uchijima and Mr. S. Togo. They are my precious friend. The discussion and the chat with them gave me a lot of fun time and the inspiration.

I also want to thank my juniors. Any time when I saw they researched or studied hard, I was encouraged. All the time of the discussion with them is my precious memory.

Finally, I'd like to express my gratitude to my family. They encourage my dream to be a nuclear fusion doctor.

Related Work

(1) 学術雑誌等
(査読あり、印刷済み)
1) Makoto NAKAMURA, Yuichi OGAWA, Naoki SHINJI, Yuya MIYOSHI, Ryoji HIWATARI, Kunihiko OKANO, and Youji SOMEYA, “ Development of the Integrated System Design Code for Fusion Power Plants ”, “ Journal of Plasma and Fusion Research SERIES ”, “ The Japan Society of Plasma Science and Nuclear Fusion Research ”, Volume 9, pp.186-189, (2010)

2) Yuya MIYOSHI, Makoto NAKAMURA, Yuichi OGAWA, “ Optimization of the Poloidal Field Coil System by Using an Integrated Design Code for Tokamak Fusion Reactors ”, “ Plasma and Fusion Research ”, “ The Japan Society of Plasma Science and Nuclear Fusion Research ” Volume 6, 2405110 (2011)

3) Yuya MIYOSHI, Yuichi OGAWA, Makoto NAKAMURA, “ Research on Burn Control of Core Plasma with the Transport Code ”, “ Plasma and Fusion Research ”,“ The Japan Society of Plasma Science and Nuclear Fusion Research ” Volume. 7, 2405135 (2012)

4) Yuya MIYOSHI, Yuichi OGAWA, “ Multi-Input Multi-Output (MIMO) Control System with a State Equation for Fusion Reactors ”, “ Plasma and Fusion Research ”,“ The Japan Society of Plasma Science and Nuclear Fusion Research ” Volume. 9, 1405015 (2014)

(2) 国際会議における発表
(査読無し、ポスター発表)
1) ○ Yuya MIYOSHI, Makoto NAKAMURA, Yuichi OGAWA, “ Automatic Optimization of Poloidal Field Coil System by Using Integrated Design Code of Tokamak Fusion Reactors ”,“ 20th International Toki Conference ”, P2-71, Ceratopia Toki, Toki-City, Gifu, Japan, (December, 2010)

2) ○ Yuya MIYOSHI, Makoto NAKAMURA, Yuichi OGAWA,“ Research on burn control of core plasma with the transport code ”,“ 21th International Toki Conference ”, P1-88, Ceratopia Toki, Toki-City, Gifu, Japan, (November, 2011)

3) ○ Yuya MIYOSHI, Yuichi OGAWA,“ Plasma control simulation using a robust control theory ”,“ 9th General Scientific Assembly of the Asia Plasma and Fusion Association in 2013 ”, TP-30, Gyeongju Hilton Hotel, Gyeongju City, Korea, (November, 2013)

(3) 国内学会・シンポジウム等における発表
（査読無し、ポスター発表）
1) ○三善悠矢、小川雄一、中村誠、宍道直樹、岡野邦彦、日渡良爾、染谷洋二、「トーラス型核融合炉の統合設計コードの開発と磁場コイル最適化に関する研究」、「第 8 回核融合エネルギー連合講演会」、11B-32p、高山市民文化会館、岐阜県高山市、6 月 2010 年

2) ○ Yuya Miyoshi, Yuichi Ogawa, Makoto Nakamura, ”Research on burn control of core plasma with the transport code ”, ”Plasma Conference 2011 ”, 24P111-P, 石川県立音楽堂、石川県金沢市、11 月 2011 年

3) ○三善悠矢、小川雄一、「核融合炉運転に向けた制御ロジック構築に関する研究」、「プラズマ・核融合学会第 29 回年会」、29E36P、クローバープラザ、福岡県春日市、11 月 2012 年

4) ○三善悠矢、小川雄一、「ロバスト制御理論の核融合炉への適用」、「プラズマ・核融合学会第 30 回年会」、05aD12P、東京工業大学大岡山キャンパス、東京都目黒区、12 月 2013 年

5) ○三善悠矢、小川雄一、「H ∞制御の核融合炉への適用」、「第一回制御部門マルチシンポジウム」、PS-25、電気通信大学、東京都調布市、3 月 2014 年

6) ○三善悠矢、小川雄一、「H ∞ロバストサーボ制御理論による炉心プラズマ制御シミュレーション」、「第 10 回核融合エネルギー連合講演会」、20-079、つくば国際会議場、茨城県つくば市、6 月 2014 年

7) ○三善悠矢、小川雄一、「核融合炉心プラズマ分布制御に向けた研究」、’Plasma Conference 2014’、20PB-074、朱鷺メッセ、新潟県新潟市、11 月 2014 年

（査読無し、口頭発表）
8) ○三善悠矢、小川雄一「輸送コードを用いたコアプラズマ燃焼制御に関す

る研究」、「第 15 回若手科学者によるプラズマ研究会」、日本原子力研究開発機構　那珂核融合研究所、茨城県那珂市、3 月 2012 年

9) ○ Yuya Miyoshi, Yuichi Ogawa “ Control of fusion reactor plasma ”, “ Japan-US Workshop on Power Plant Studies and Advanced Technologies ”, Kyoto University, Uji Japan, February 2013

10) ○三善悠矢、小川雄一「現代制御理論を用いた核融合プラズマ制御シミュレーション」、「第 16 回若手科学者によるプラズマ研究会」、日本原子力研究開発機構　那珂核融合研究所、茨城県那珂市、3 月 2013 年

11) ○三善悠矢、小川雄一　「原型炉制御の方式」、「第二回原型炉計装制御シンポジウム」、核融合科学研究所,　岐阜県土岐市、3 月 2013 年